Environmental Research 231 (2023) 116133

Contents lists available at ScienceDirect

Environmental Research

journal homepage: www.elsevier.com/locate/envres

Review article

Green and Sustainable Membranes: A review

Navid Rabiee [a,b,c,*,1], Rajni Sharma [a,1], Sahar Foorginezhad [a,d,1], Maryam Jouyandeh [e], Mohsen Asadnia [a,**], Mohammad Rabiee [f], Omid Akhavan [c], Eder C. Lima [g], Krzysztof Formela [h], Milad Ashrafizadeh [i,j], Zari Fallah [k], Mahnaz Hassanpour [l], Abbas Mohammadi [m], Mohammad Reza Saeb [h]

[a] School of Engineering, Macquarie University, Sydney, New South Wales, 2109, Australia
[b] Centre for Molecular Medicine and Innovative Therapeutics, Murdoch University, Perth, WA, 6150, Australia
[c] Department of Physics, Sharif University of Technology, Tehran, P.O. Box 11155-9161, Iran
[d] Lulea University of Technology, Department of Energy Science and Mathematics, Energy Science, 97187, Lulea, Sweden
[e] Center of Excellence in Electrochemistry, University of Tehran, Tehran, Iran
[f] Biomaterial Group, Department of Biomedical Engineering, Amirkabir University of Technology, Tehran, Iran
[g] Institute of Chemistry, Federal University of Rio Grande Do Sul (UFRGS), Porto Alegre, RS, Brazil
[h] Department of Polymer Technology, Faculty of Chemistry, Gdańsk University of Technology, G. Narutowicza 11/12, 80-233, Gdánsk, Poland
[i] Department of General Surgery and Institute of Precision Diagnosis and Treatment of Digestive System Tumors, Carson International Cancer Center, Shenzhen University General Hospital, Shenzhen University, Shenzhen, Guangdong, China
[j] Shanghai Institute of Cardiovascular Diseases, Zhongshan Hospital, Fudan University, Shanghai, China
[k] Faculty of Chemistry, University of Mazandaran, P. O. Box 47416, 95447, Babolsar, Iran
[l] Department of Chemistry, Institute for Advanced Studies in Basic Sciences (IASBS), Zanjan, 45137–66731, Iran
[m] Department of Chemistry, University of Isfahan, Isfahan, 81746-73441, Iran

ARTICLE INFO

Keywords:
Membrane
Green chemistry
Nanomaterials
Synthesis
Water purification
Sustainability

ABSTRACT

Membranes are ubiquitous tools for modern water treatment technology that critically eliminate hazardous materials such as organic, inorganic, heavy metals, and biomedical pollutants. Nowadays, nano-membranes are of particular interest for myriad applications such as water treatment, desalination, ion exchange, ion concentration control, and several kinds of biomedical applications. However, this state-of-the-art technology suffers from some drawbacks, e.g., toxicity and fouling of contaminants, which makes the synthesis of green and sustainable membranes indeed safety-threatening. Typically, sustainability, non-toxicity, performance optimization, and commercialization are concerns centered on manufacturing green synthesized membranes. Thus, critical issues related to toxicity, biosafety, and mechanistic aspects of green-synthesized nano-membranes have to be systematically and comprehensively reviewed and discussed. Herein we evaluate various aspects of green nano-membranes in terms of their synthesis, characterization, recycling, and commercialization aspects. Nanomaterials intended for nano-membrane development are classified in view of their chemistry/synthesis, advantages, and limitations. Indeed, attaining prominent adsorption capacity and selectivity in green-synthesized nano-membranes requires multi-objective optimization of a number of materials and manufacturing parameters. In addition, the efficacy and removal performance of green nano-membranes are analyzed theoretically and experimentally to provide researchers and manufacturers with a comprehensive image of green nano-membrane efficiency under real environmental conditions.

1. Introduction

Population growth and worldwide industrialization from one side and the unavoidable contamination of water resources by penetration of pollutants of different types with individual and interactive harms on both the human beings and the environment from the other side

* Corresponding author. School of Engineering, Macquarie University, Sydney, New South Wales, 2109, Australia.
** Corresponding author.
E-mail addresses: nrabiee94@gmail.com, navid.rabiee@mq.edu.au (N. Rabiee), Mohsen.asadnia@mq.edu.au (M. Asadnia).
[1] These authors contributed to writing this article equally.

https://doi.org/10.1016/j.envres.2023.116133
Received 1 February 2023; Received in revised form 21 April 2023; Accepted 12 May 2023
Available online 19 May 2023

underline the need for water treatment (Taghizadeh et al., 2020; Rabiee et al., 2021a). The contamination of water resources has become more challenging since December 2019 by the SARS-CoV-2 or COVID-19 pandemic, followed by mutation-induced infections worldwide, person-to-person and country-to-country. Membrane-based water purification has been at the core of attention over the past two decades. However, serious challenges such as fouling hinder their practical applications. New technologies such as nanofabrication and nanoparticles are proven to be appropriate solutions to such problems in membrane technology (Vatanpour et al., 2021). In recent years, nano-membranes have found a solid position in this technological field, but membrane-based water purification plants are expensive, exclusive and not environmental-friendly. In this sense, from a sustainability angle, green chemistry/synthesis should be merged with nanotechnology to rely on the aforementioned needs (Nasrollahzadeh et al., 2021).

Applying green chemistry to nano-membrane fabrication serves as a promising way to limit the usage of petroleum-based membranes with their hazardous features and expense (Rethinam et al., 2020). Moreover, disposal and recycling of synthetic nano-membranes are inevitably additional concerns of membrane manufacturers (Amir Razmjou et al., 2019; Razmjou et al., 2019; Landaburu-Aguirre et al., 2016; Lawler et al., 2012). Over the last two decades, much more attention and investments have been directed toward green membranes and green synthesized components applying nanomaterials of different classes (Wang et al., 2023; Tabani et al., 2023). In recent studies, several attempts have been carried out in order to technically develop innovative sustainable nano-membranes. In this regard, natural or bio-based materials such as tannic acid and premises has been used more frequently. In a typical study, green and sustainable membranes have been designed by using polymer waste and tannic acid, synthesized, and characterized (Park et al., 2021a). Normally, these types of green membranes are prepared through a routine chemical reaction not favorable from sustainability angle, but still superior to some extent to commercial chemicals. Although green synthesis approaches and green-synthesized nanomaterials aimed at membrane development are experiencing a rapid progressive period of manufacturing, mechanisms behind the properties and performance of green nano-membranes used in water treatment have not been comprehensively reviewed and discussed.

This review seeks to address and summarize the latest advancements in green synthesis of nanomaterials intended for membrane applications

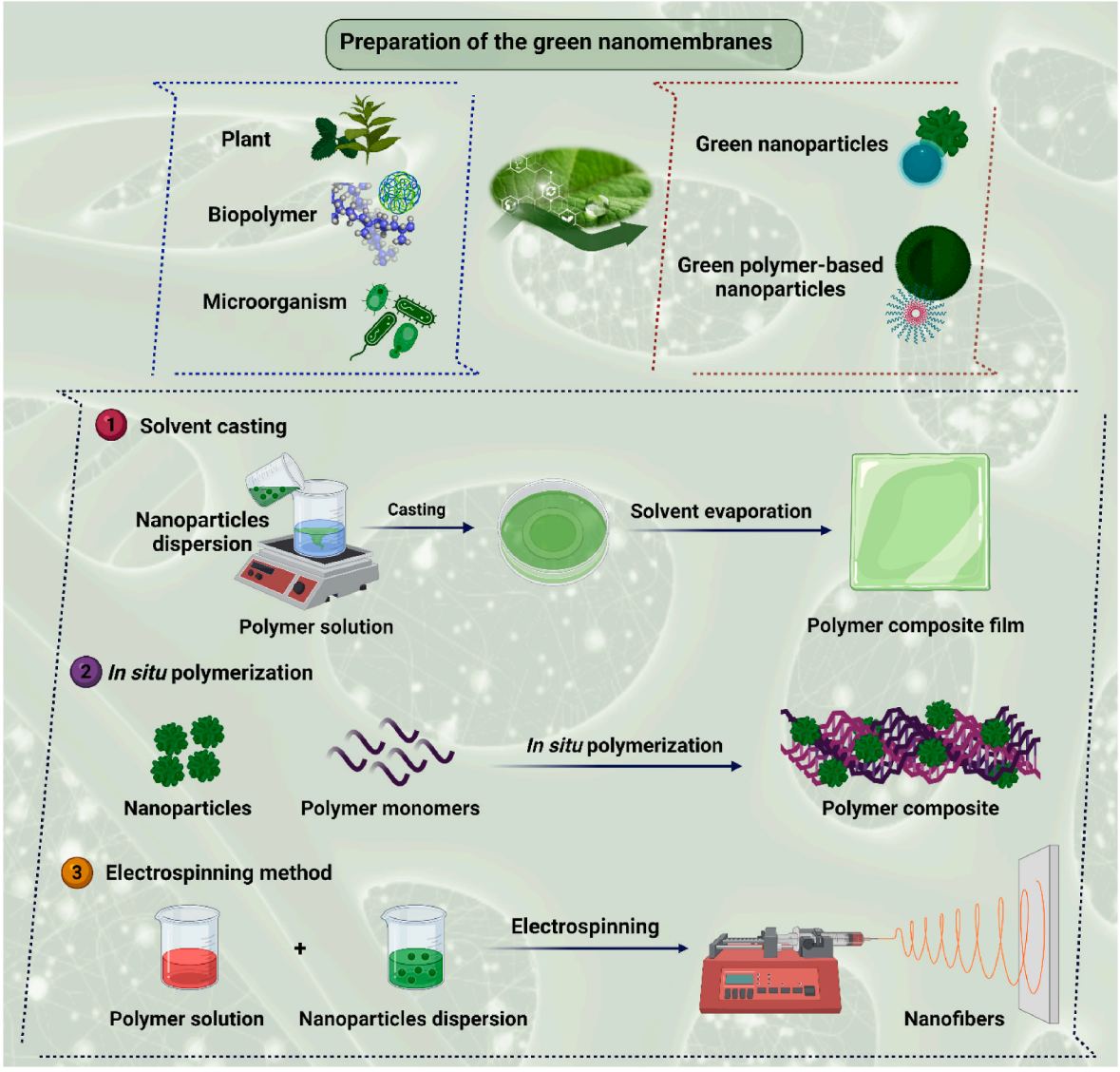

Fig. 1. Schematic representation of the most frequently green materials and methods examined in preparation of green (nano)membranes, which showed different green precursors for the synthesis of green (nano)materials and (nano)membranes, and also three different methods for preparation, modification, and synthesis of them.

as well as preparation and characterization of green nano-membranes. First, we need to generally classify green nanomaterials (naturally green or chemically synthesized in green media), to provide readers with a full image of the advantages and disadvantages of using such nano-scale devices. Fig. 1 summarizes schematically green approaches and materials in preparation of sustainable nanomembranes. Herein we also review and discuss some challenging aspects of the synthesis and application of green nano-membranes in view of their poor mechanical properties, biodegradability, and biocompatibility.

2. Green synthesized nano-membranes

2.1. Green nanoparticles

The majority of green membranes nowadays are green nanoparticles. They are available in a wide variety of size, shape, porosity and reactivity. In this regard, careful selection of the source and the green reaction medium comes with the prime importance. Choudhury et al. (2018) have fabricated ceramic ultrafiltration membranes for Cr(IV) removal from aqueous solutions. The CuO nanoparticles were synthesized through a green method using *Catharanthus Roseus* leaf extract. According to X-ray diffraction (XRD) analysis, size of CuO crystals was ≈1 nm. In tandem with this, field-emission scanning electron microscopy (FE-SEM) micrographs illustrated the formation of uniform spherical particles, while transmission electron microscopy (TEM) analysis verified that the average size of CuO nanoparticles was ca. 5–10 nm. In terms of membrane fabrication, silica-alumina microfiltration ceramic support was commercially provided. Then, a suspension of the synthesized CuO nanoparticles was coated onto the support *via* dip-coating technique. Pore size distribution curves indicated that the pore size of the as-prepared membrane was 3.2 nm. Furthermore, it was observed that the support porosity (≈34.9%) was plummeted by 16%, attributed to pore size reduction caused by CuO nanoparticles. Moreover, FE-SEM micrographs delineated the formation of crack-free coating over the support. Besides, aggregation of CuO nanoparticles over the surface and smaller pore size of the coated layer resulted in a decline in pure water permeability. Almost 88.08% Cr (IV) removal was observed at the pressure of 3 bar.

In another study, Mondal et al. (Mondal and Purkait, 2018) synthesized iron nanoparticles using clove extract and immobilized the synthesized nanoparticles onto a pH-responsive poly(vinylidene) fluoride (PVDF)-*co*-hexafluoropropylene (HFP) membrane prepared through polyethylene glycol methyl ether and humic acid blending. FE-SEM micrographs revealed that iron nanoparticles were synthesized in a spherical shape and 13.5 nm size. A close view provided by TEM images supported by XRD diffractogram suggested the size of synthesized nanoparticles in the range of 10–20 nm and 15–20 nm, respectively. Moreover, FE-SEM images delineated that (Fig. 2) the addition of iron nanoparticles above 1 wt% to the membrane matrix led to pore blockage and aggregation, while lower blockage and agglomeration was observed upon 0.01 wt% nanoparticles addition. The aforementioned iron nanoparticles were added to the membrane matrix with various concentrations, resulting in a catalytic effect on nitrobenzene to aniline reduction and fluoride rejection enhancement through dead-end filtration. The

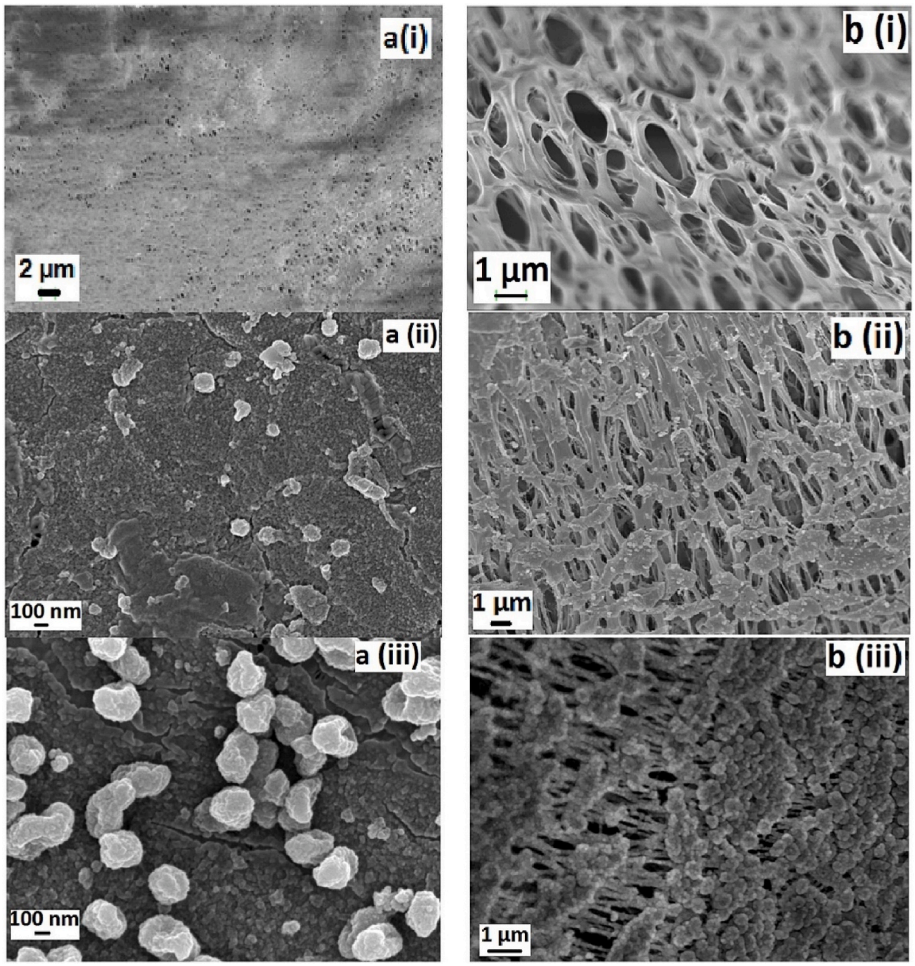

Fig. 2. (a) The surface and (b) cross-sectional FESEM images of the PVDF-*co*-HFP membranes with different magnifications. Reproduced with permission from Ref (Mondal and Purkait, 2018). Copyright 2018 Elsevier.

highest nitrobenzene reduction (89.92%) was achieved using the membranes comprised of 0.01 wt% of iron nanoparticles, related to the superior contact between the nanoparticles and reactant species originating from less aggregation and more homogeneity of iron nanoparticles throughout the membrane matrix. In terms of fluoride rejection (at solution pH 4), 84.4, 78.56, and 65.8% rejection were obtained for 20, 10, and 5 mg L^{-1} solutions, respectively.

Having one eye on the future, the use of iron nanoparticles in green nanomembranes should bring about significant potential for a wide range of applications. Further studies may investigate the optimization of the concentration and size of iron nanoparticles to maximize their contribution to catalytic and filtration efficiencies. Additionally, research would explore the role of the green synthesis method in production of iron nanoparticles with unique characteristics and properties to be utilized in the development of novel nanomembranes. Overall, the incorporation of iron nanoparticles into green nanomembranes holds promise for the development of more efficient and effective water treatment and purification technologies, with potential applications in interdisciplinary fields such as medicine, environmental science, and industrial processes.

Hamid et al. (2020), synthesized PbO nanoparticles using *Datura Sternum* plants leaf extract and utilized them to fabricate nanocomposite membranes. To this end, as filler, polyvinyl chloride (PVC) was filled with various amounts of PbO nanoparticles in the 5–35 wt% range. According to XRD results, the PbO particle size was 60 nm. The porosity and water uptake of the as-prepared membranes containing various PbO nanoparticles were in the range of 0.5–0.87 and 72.01–141.3%, respectively. They explained improved water uptake in relation to more void fractions at higher nanoparticle concentration and nanoparticles hydrogen bonding with water molecules. Nthunya et al. (2019a) synthesized silver nanoparticles (AgNPs) using apple extract through thermally-assisted one-pot and microwave-assisted techniques. Nanofiber membranes were fabricated through electrospinning, while synthesized nanoparticles were immobilized on PVDF nanofiber membranes at 2 wt% concentration. The morphology of silver nanoparticle was verified using TEM analysis, illustrating that elongated and spherical-shaped domains were formed with 28.24 nm (thermally-assisted) and 22.05 nm (microwave-assisted) diameters. SEM images depicted that initial membrane and silver nanoparticle incorporated membranes were close to 345 nm and 448 nm, respectively. Antibacterial activity of as-prepared membrane against various bacteria, including mesophile *P. aeruginosa, S. Aureus, K. pneumoniae,* and thermophile *G. stearothermophilus,* was estimated using a modified disk-diffusion technique. Results delineated a minimum inhibition concentration in the 0.06–0.11 g.L^{-1} range. The as-prepared membranes were supposed to be considered a prominent candidate for water purification because no biofilm was formed over the membrane surface.

In recent years, there has been a growing interest in research on the synthesis and utilization of nanoparticles for various applications, including in the fabrication of composite membranes. The above-mentioned studies conducted by Hamid et al. and Nthunya et al. demonstrated the potential of natural extracts for the synthesis of nanoparticles for incorporation into membrane materials. Hamid et al. used leaf extract from *Datura Sternum* plants to synthesize PbO nanoparticles, which were subsequently incorporated into PVC polymeric matrix to create nanocomposite membranes. Higher concentrations of PbO nanoparticles led to higher water uptake capacity of the resulting membranes. This suggests that there may be potential for the development of highly porous, water-absorbing membranes for use in water treatment or filtration applications. Similarly, Nthunya et al. utilized apple extract to synthesize silver nanoparticles, which were then incorporated into PVDF nanofiber membranes through electrospinning. The resulting membrane showed promising antibacterial activity against various bacteria, a potential candidate for water purification applications, but pertinent to optimization of properties of nanocomposite membranes per application. Further research may focus on the synthesis of nanoparticles using a wider range of natural extracts or alternative methods, as well as incorporation of these nanoparticles into other membrane materials. The potential toxicity of these nanoparticles and their impact on the environment should additionally be studied. Overall, the use of natural extracts for nanoparticle synthesis and incorporation into membrane materials opens wider avenues for the development of sustainable and effective filtration technologies. Future research programs may need to place focus on optimizing the parameters involved in the synthesis and fabrication of nanocomposite membranes. For example, in the study by Hamid et al., the authors used PVC polymer as a filler and synthesized PbO nanoparticles using *Datura Sternum* plants leaf extract. However, they only investigated the effect of the number of nanoparticles on membrane properties. Future studies may unveil the effect of other parameters such as the type and concentration of polymer, extraction method, and synthesis conditions on the properties of the resulting nanocomposite membranes. Likewise, in the study by Nthunya et al., the authors used apple extract to synthesize AgNPs and fabricated nanofiber membranes through electrospinning. They evaluated the antibacterial activity of the as-prepared membranes against various bacteria. However, they did not investigate the effect of other parameters such as the concentration of nanoparticles or the electrospinning conditions on membrane properties. Future studies can take into account the studied parameters to optimize the properties of the resulting nanocomposite membranes and to achieve a higher antibacterial activity. Moreover, future studies may also explore the potential applications of these nanocomposite membranes in other fields such as energy, biomedicine, and environmental remediation. For instance, nanocomposite membranes can be used as electrodes in energy storage devices such as supercapacitors due to their high surface area and excellent conductivity. They can also be utilized in drug delivery systems (DDS) due to their biocompatibility and controlled release features. Furthermore, nanocomposite membranes can be employed in wastewater treatment applications for the removal of heavy metals, dyes, and organic pollutants due to their high adsorption capacity and selectivity.

In another study, Nthunya et al. (2019b) synthesized silica nanoparticles using apple extract and modified them with octadecyltrimethoxysilane (OTMS), N-octadecyltrichlorosilane (ODTS), and chlorodimethyl-octadecyl silane (CI-MOS). Synthesized nanoparticles were incorporated into the PVDF nanofiber membranes with 1 wt% concentration *via* electrospinning technique. TEM analysis revealed nanoparticles' mean sizes of 17.4, 24.5, 23.7, and 24.9 nm for initial, ODTS, OTMS, and CI-DMOS modified particles, respectively. According to the results, membrane porosity and pore size were ≈80% and 1.24–1.41 μm, respectively. Moreover, >99% of salt rejection was obtained for the as-prepared membranes. SEM micrographs revealed the formation of a smooth and non-beaded structure through the addition of initial SiO_2 nanoparticles, while the membrane morphology turned to a beaded structure upon the addition of modified SiO_2 nanoparticles. Hubadillah et al. (2018) prepared crystalline and amorphous silica extracted from rice husk and fabricated a hollow fiber membrane. To this end, rice husk was burned in an oven at 600–1000 °C individually, followed by milling and sieving the as-prepared powder. In terms of membrane fabrication, ceramic suspensions were prepared using the produced silica powders in various concentrations (35, 37.5, and 40 wt %), dispersant, and solvent. After ball milling and adding polyethersulfone (PES) to the mixture (5 wt%), it was extruded and immersed in water for the phase-inversion process. Then, they were sintered at temperatures in the range of 1200–1400 °C. TEM images of the as-prepared silica revealed that silica particles sintered at 600 °C were amorphous with ≈2 μm size, while silica particles sintered at 1000 °C were produced in a crystalline rod shape with an average diameter of 1 μm. The rod-shaped particles consisted of nanoparticles with an average size of 200 nm. Brunauer–Emmett–Teller (BET) analysis of porosity delineated that the surface area of amorphous silica was 43.5 $m^2\ g^{-1}$, while the crystalline structure exhibited a lower surface area (7.7 $m^2\ g^{-1}$), which was attributed to the sintering temperature. SEM

micrographs of the as-prepared hollow fiber membranes revealed that membranes incorporated by amorphous silica particles were fabricated in symmetric and sponge-like structures. Increasing the silica content up to >40 wt% led to the appearance of imperfections. On the other hand, the addition of crystalline silica particles to the membrane matrix resulted in a denser structure. Moreover, it was conspicuous that increasing the silica amount led to an escalation in the membrane thickness (the thickness enhanced from 305 to 902 μm when the silica content increased from 35 to 40 wt%) (Fig. 3). Meanwhile, increasing silica content from 35 to 40 wt% resulted in the mechanical strength enhancement from 40.08 to 58.83 MPa and ≈53–311.9 MPa in terms of the addition of amorphous and crystalline silica, respectively. Pure water flux of the fabricated membranes was performed through 150 min, and it was observed that pure water flux plummeted from ≈480 L $m^{-2}.h^{-1}$ for membranes sintered at 1200 °C to ≈330 L $m^{-2}.h^{-1}$ for membranes sintered at 1400 °C. Results showed that the optimum membrane was fabricated using 37.5 wt% crystalline silica sintered at 1200 °C, which exhibited pore size in the range of 0.55–2.3 μm, 43.1% porosity, 71.21 MPa mechanical strength, and 303 L $m^{-2}.h^{-1}$ stable pure water flux.

In the future, researchers can report further about the use of natural extracts, such as apple extract, to synthesize nanoparticles and modify them for various applications. They can investigate the potential of these modified nanoparticles in improving membrane performance, such as enhancing salt rejection and increasing mechanical strength. Additionally, they can continue to study the effect of sintering temperature and

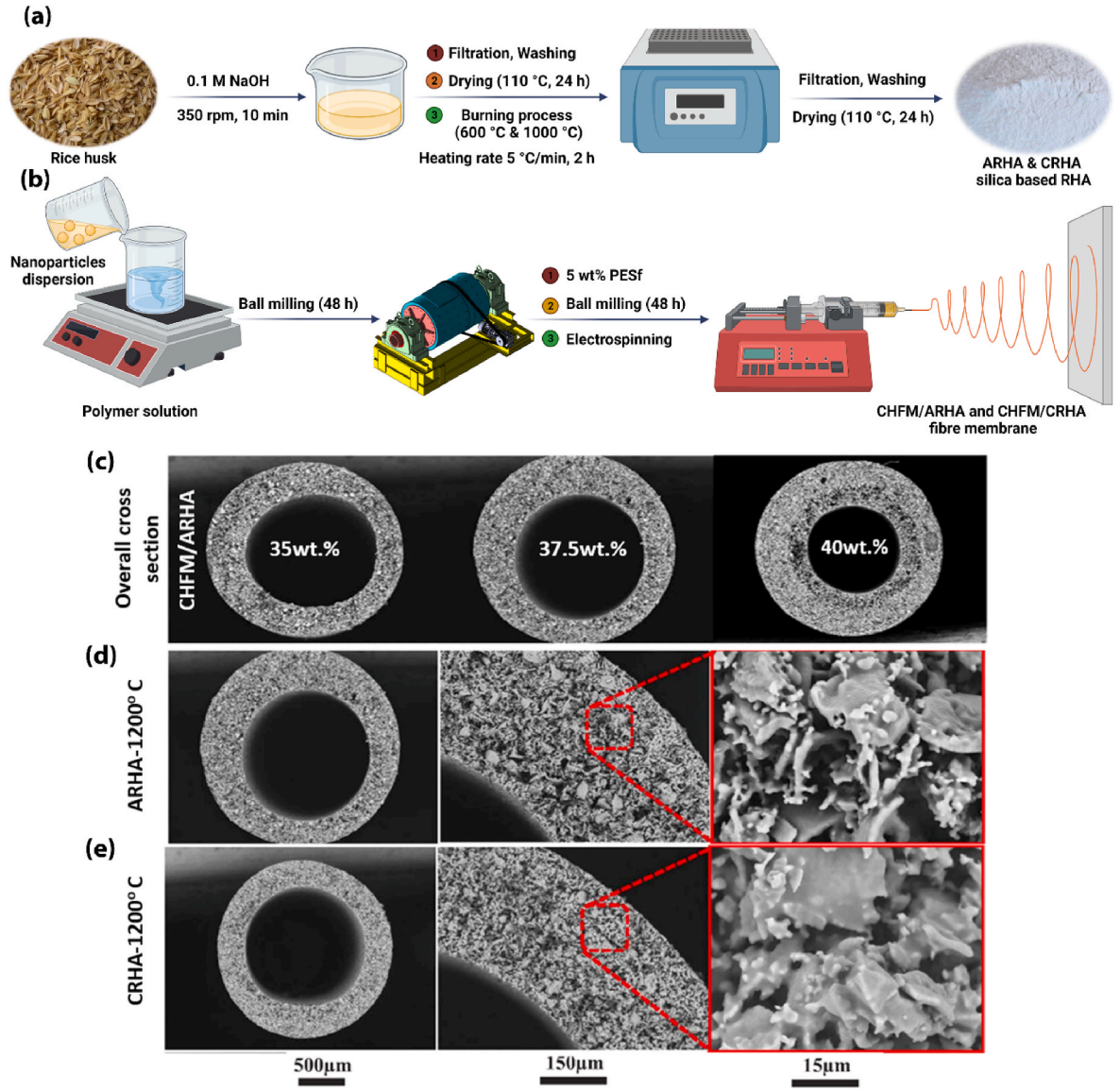

Fig. 3. **(a)** Preparation of the silica based rice husk ash: I) Washing the rice husk with NaOH solution, rinsing with distilled water, and drying in oven. II) Burning the dried rice husk in a furnace at 600 °C and 1000 °C for formation of amorphous and crystalline silica based rice husk (ARHA and CRHA), respectively. **(b)** The preparation of silica based ceramic hollow fibre membranes (CHFM/ARHA and CHFM/CRHA) using phase inversion and sintering technique: I) The formation of ceramic suspensions by dissolving the dispersant (Arlacel P135; polyethyleneglycol 30-dipolyhydroxystearate) in solvent and then adding the ARHA and CRHA silica powders to the mixture at different contents. II) Ball milling the mixture with zirconia milling balls. III) Adding 5 wt% polyethersulfone (PESf) followed by further ball milling. IV) Degassing, transferring the prepared suspension into stainless steel syringes, and extruding the ceramic suspension through the spinneret. V) Immersing the membrane precursors in water overnight and washing with water. VI) Cutting the precursor fibers, drying at ambient temperature for 24 h, and sintering the dried hollow fibers in a high-temperature tubular furnace at ranging from 1200 °C to 1400 °C for 3 h. **(c)** Cross-sectional SEM images of the CHFM/ARHA at different dope composition. **(d)** Surface and cross-sectional SEM images of CHFM/ARHA-37.5 wt% and CHFM/CRHA-37.5 wt% sintered at 1200 °C. Reprinted with permission from Ref (Hubadillah et al., 2018). Copyright 2018 Elsevier.

silica content on membrane morphology, thickness, and pure water flux to optimize membrane fabrication. Furthermore, the use of other natural resources, like rice husk, in membrane fabrication can be explored, and their properties can be characterized to determine their potential in improving membrane performance. To improve the stability of the prepared membranes, researchers could focus on optimizing the membrane fabrication process and modifying the surface properties of membranes. For example, researchers could investigate the effects of different sintering temperatures, particle sizes, and concentration of the silica nanoparticles on the stability of membranes. Furthermore, surface modification techniques such as plasma treatment, grafting, or coating with other materials could also enhance the membrane stability by improving the surface hydrophilicity, chemical resistance, and mechanical strength. Another approach to improving membrane stability would be the development of novel membrane materials with improved chemical and physical properties. For instance, more may be reported in the future about the use of nanomaterials, such as carbon nanotubes (CNTs) or graphenic derivatives, which have superior mechanical strength and chemical stability compared to the conventional materials. Additionally, the use of advanced membrane fabrication techniques, such as 3D printing or electrospinning, could also lead to the development of highly stable and efficient membranes.

Research on the utilization of AgNPs has recently boomed due to unique properties such as chemical stability, antimicrobial and antiviral activity, surface-enhanced Raman scattering, and elevated thermal and electrical conductivity (Brown, 2017). AgNPs have been widely used for water disinfection against viruses, bacteria, pathogens, and fungi (Singh et al., 2019). Moreover, they can attach to the bacterial cell membranes and improve the membrane permeability through the free radical generation and damage the cell membrane and apoptosis (Le et al., 2012). The addition of AgNPs has been shown to improve the mechanical strength, thermal stability, and water resistance of nanocomposites, while also providing effective antibacterial and antifungal properties. In nanocomposites, the incorporation of AgNPs has been shown to improve the mechanical properties and thermal stability of the material. This was due to the strong interaction between the AgNPs and the polymer matrix, which results in the formation of a uniform and homogeneous dispersion of nanoparticles within the matrix. The AgNPs act as reinforcing agents, which enhance the mechanical properties of the nanocomposite, including tensile strength, elastic modulus, and fracture toughness. The thermal stability of the nanocomposite was also improved due to the thermal stability of the AgNPs themselves, which can withstand high temperatures without degradation. In membranes, the addition of AgNPs has been shown to improve both the physical and chemical stability of the membrane. The AgNPs act as a barrier against the growth of bacteria and fungi, preventing the development of biofilms and maintaining the integrity of the membrane structure. The antibacterial properties of AgNPs are due to their ability to interact with the cell membrane of bacteria, leading to the disruption of cell function and ultimately cell death. This property is particularly useful in water treatment membranes, where the growth of bacteria can lead to fouling and reduced membrane performance. Furthermore, the addition of AgNPs has also been shown to improve the water-resistance of membranes, allowing them to maintain their performance in the presence of water or other liquids. The hydrophobic nature of AgNPs allows them to repel water and other liquids, preventing them from adhering to the surface of the membrane and reducing membrane fouling. Additionally, the presence of AgNPs can also improve the permeability of the membrane, allowing for more efficient filtration (Vazquez-Muñoz et al., 2019; Zodrow et al., 2009; Sureshkumar et al., 2010; Pandey et al., 2012).

In terms of antimicrobial activity, silver nanoparticle dissolution leads to Ag^{+} ions release followed by incapacitation of enzymes and interruption of the life functions (Aziz et al., 2019). For example, AgNPs have been synthesized using *fenugreek* leaves, and their antibacterial activity against *Staphylococcus aureus* (*S. aureus*) and gram *Escherichia coli* (*E. coli*) bacteria was evaluated (Senthil et al., 2017). To this end, ethanolic fenugreek extract was prepared and used as a reducing agent for silver nanoparticle synthesis. UV-VIS analysis verified the formation of nanoparticles through an increase in absorbance. The crystallite size of the synthesized nanoparticles was measured using the Debye-Scherrer equation (≈18 nm). According to HRTEM images, AgNPs were formed in monodispersed and spherical shapes with 20–30 nm diameter. Also, crystalline morphology without the presence of agglomerations can be seen from the HRTEM micrographs. In terms of antibacterial activity, 1 μL of nanoparticles was incubated into the related cells. After incubation, the AgNPs inhibition zone was 16.27 mm and 12.47 mm for *E. coli* and *S. aureus*, respectively, which was higher than *streptomycin* inhibition zone amounts (10.12 mm and 9.41 mm in *E. coli* and *S. aureus*, respectively). In the meantime, to evaluate the lowest concentration for bacterial cell growth inhibition, the plate count technique estimated minimal concentration incubation (MIC) of silver nanoparticles. Results delineated that the MIC amount was 12.5 (*S. aureus*) and 6.25 μg/mL (*E. coli*). Also, superior bactericidal activity was observed for *E. coli*, which could be attributed to variation in the peptidoglycan layer thickness. Results depicted that the *S. aureus* cells exhibited a thicker layer than *E. coli* cells. Overall, synthesized AgNPs can be considered an effective ad non-toxic antibacterial substance immobilized in membranes for water purification applications. The AgNPs have been found to interact with the bacterial cell wall and cell membrane, leading to the disruption of cell membrane integrity and the leakage of cellular contents. The surface charge and size of AgNPs play a significant role in determining their interaction with bacterial membranes. It has been reported that the positively charged AgNPs are more effective in disrupting the cell membrane than negatively charged particles. The size of the nanoparticles is also critical, with smaller nanoparticles being more effective in penetrating the cell membrane and inducing cellular damage. Another mechanism proposed for the action of AgNPs was the generation of reactive oxygen species (ROS), which could explain oxidative damage of bacterial cells. It has been suggested that AgNPs can generate ROS by interacting with bacterial DNA, proteins, and lipids, leading to oxidative stress and cell death. Moreover, AgNPs have been shown to affect the electron transport chain of bacterial cells, leading to the production of ROS and cellular damage. AgNPs also affect the bacterial cell's enzymatic activity, leading to cell death. For example, AgNPs can inhibit the activity of respiratory enzymes, such as cytochrome *c* oxidase and succinate dehydrogenase, leading to a reduction in bacterial energy production and cellular damage. Furthermore, AgNPs can interfere with the bacterial cell's replication and transcription processes, leading to bacterial cell death. AgNPs have been found to bind to bacterial DNA and inhibit DNA replication and transcription, leading to the accumulation of DNA damage and the inability of the bacterial cell to carry out its normal functions. The mode of action of AgNPs against bacterial cells is multifaceted, and the exact mechanism of action may depend on the size, shape, concentration, and surface chemistry of the nanoparticles. The antibacterial mechanism of AgNPs involves the interaction of nanoparticles with the bacterial cell membrane, the generation of ROS, the inhibition of enzymatic activity, and interference with the bacterial cell's replication and transcription processes (Yin et al., 2020a; Tang and Zheng, 2018).

In another study, nanocomposite of reduced graphene oxide (rGO) and AgNPs, namely (Ag-rGO) nanocomposite, was synthesized using carbogenic quantum dots and ultrasonic shock (Ganguly et al., 2017). To this end, water-dispersible graphite oxide (GO) and gelatin-derived carbogenic quantum dots were prepared. Then, Ag-rGO nanocomposite was prepared through *in situ* sonochemical routes and GO and gelatin-derived carbon dots. According to XRD results, the initial interlayer spacing of GO plummeted from 0.82 nm to 0.44 nm in terms of Ag-rGO nanocomposite, which can be attributed to a partial reduction of GO through the ultrasonication process. TEM analysis revealed the stacked structure of the initial GO. Moreover, incorporation of AgNPs onto the GO surface could be seen in TEM images, and restacking of

nanosheets was avoided through the agglomeration of AgNPs on the surface of the layers. Moreover, FE-SEM micrographs approved successful synthesis of AgNPs in the 20–40 nm range, which was spread over the surface. EDAX analysis depicted that almost 4.69% of the silver atoms were formed over the surface. Furthermore, the average hydrodynamic diameter of GO was ≈322 nm, which was reduced to ≈122 nm after GO reduction (i.e., when rGO was used) and incorporation by AgNPs. The catalytic activity of the as-prepared nanocomposite over 4-nitrophenol was evaluated in aqueous borohydride and the as-prepared nanocomposite in the 0.5–2 $g.L^{-1}$ concentration. Results inferred that the time reduction of 4-nitrophenol was 7 min, which was considerably less than previous studies with reusability of 5 cycles. Antibacterial activity of Ag-rGO nanocomposite was evaluated against *E. coli,* and inhibition zone was measured using disk-shaped filter paper immersed in the aqueous solution of 1 mg mL^{-1} sample concentration, and 200 μl of *E. coli* was spread over agar plate, and incubation was performed during at 37 °C during 24 h in the 1 $g.L^{-1}$ of nanocomposite concentration, the inhibition zone related to *E. coli* reached to 2.1 cm.

Despite the promising advantages, the accumulation of AgNPs in liquid media reduces their effectiveness, which can be solved by incorporating them into the membrane matrix. On the other hand, nanoparticles' high surface/volume ratio makes them more prone to toxicity than the bulk form. Recent studies have been extensively focused on the utilization of AgNPs for wastewater treatment. AgNPs have been demonstrated to be effective in removal of organic and inorganic contaminants, as well as in inhibiting bacterial growth within the water. The antibacterial mechanism of AgNPs has been widely studied, and was primarily attributed to their ability to release silver ions (Ag^{+}) into the surrounding medium, which can then bind to bacterial cells and disrupt their metabolic processes. The Ag^{+} ions can cause damage to the bacterial cell membrane and DNA, leading to cell death. The release of Ag^{+} ions is influenced by several factors, including the size, concentration, and surface properties of the AgNPs. Several studies have shown that AgNPs are effective in inhibiting the growth of both Gram-negative and Gram-positive bacteria, including *E. coli*, *P. aeruginosa*, *S. aureus*, *and B. subtilis*. The antibacterial activity of AgNPs is dependent on the size and concentration of the particles, where smaller particles and higher concentrations appear more effective. Additionally, the surface properties of AgNPs, such as their charge and coating, can affect their antibacterial activity. In water treatment and desalination, AgNPs can be used in various forms, including coatings, membranes, and filters. AgNPs can be incorporated into the surface of materials to create antimicrobial coatings, which can be applied to water treatment equipment to prevent bacterial growth and biofilm formation. Membranes and filters can also be modified with AgNPs to improve their antibacterial properties and extend their lifespan. One of the key advantages of using AgNPs in water treatment and desalination is their ability to remove contaminants, including heavy metals, organic compounds, and pathogens. AgNPs have been shown to be effective in removing organic pollutants, such as phenols, pesticides, and dyes, from water. They can also remove heavy metals, such as lead and mercury, by binding to the metal ions and forming stable complexes. In addition to their antibacterial and contaminant removal properties, AgNPs can also improve the stability and performance of water treatment equipment. For example, AgNPs can be incorporated into the surface of reverse osmosis (RO) membranes to improve their fouling resistance and extend their lifespan. The use of AgNPs in RO membranes has been shown to reduce fouling caused by bacterial growth and improve water flux. Despite the promising results, some concerns have been raised regarding the potential environmental and health impacts of AgNPs. The release of Ag^{+} ions into the environment can lead to the accumulation of AgNPs in water and soil, which pose toxic effects on aquatic organisms and plants. Additionally, the potential toxicity of AgNPs to human health is still not fully understood, and further studies are needed to determine their long-term effects (Dankovich and Gray, 2011; Yusuf, 2019; Khan et al., 2022).

The use of nanoparticles in water treatment and desalination has gained significant attention in recent years. Zinc oxide nanoparticles (ZnONPs) are among the promising nanomaterials that have been explored for their potential in water treatment applications. ZnONPs have several properties that make them suitable for water treatment applications. One of the most significant advantages of ZnONPs is their strong antibacterial properties. Bacteria are known to grow and multiply in water, leading to the contamination of water sources. The use of ZnONPs can effectively inhibit the growth and proliferation of bacteria in water, making it safe for human consumption. The utilization of zinc nanoparticles results in a higher contamination degradation rate than zerovalent iron nanoparticles (Singh et al., 2019). In terms of the characteristics, ZnONPs benefit from a wide bandgap, great binding energy, and elevated piezoelectric properties (Fortunato et al., 2005). In the meantime, although bulk ZnONPs cannot effectively remove arsenic and sulfur, ZnONPs have successfully been used for their efficient removal as well as the great potential to be synthesized in the presence of leaf extracts to be the potential nano-architecture for pathogens/microorganisms culture/livings (Fig. 4) (Ishwarya et al., 2018). Besides, ZnONPs have exhibited excellent antibacterial (Applerot et al., 2009) and antifungal (Sharma et al., 2010) properties.

Another advantage of ZnONPs is their high surface area to volume ratio, which enables them to effectively adsorb and remove impurities from water. ZnONPs can remove heavy metals, organic compounds, and other pollutants from water, making them safe for use. Furthermore, ZnONPs are relatively inexpensive and readily available, making them a practical option for water treatment applications. They are also easy to synthesize, making them a viable alternative to other nanomaterials with difficult synthesis routes. Several studies have demonstrated the effectiveness of ZnONPs in water treatment applications. For example, scientists investigated the effectiveness of ZnONPs in removing lead ions from water. The study found that ZnONPs could effectively remove lead ions from water with an efficiency of up to 99%. The researchers attributed this to the high surface area to volume ratio of ZnONPs, which facilitated the adsorption of lead ions. Another scientist investigated the use of ZnONPs in the removal of organic pollutants from water. The study found that ZnONPs could effectively remove a wide range of organic pollutants from water, including phenols, polycyclic aromatic hydrocarbons, and dyes. The researchers attributed this to the strong adsorption capacity of ZnONPs, which facilitated the removal of organic pollutants from water. In addition to their effectiveness in water treatment applications, ZnONPs have also been explored for their potential in desalination processes. Desalination is the process of removing salt and other minerals from seawater to make it safe for human consumption. One of the most significant challenges in desalination processes is the fouling of membranes, which significantly reduces their effectiveness. Several studies have investigated the use of ZnONPs in desalination processes to overcome membrane fouling. For example, researchers investigated the use of ZnONPs in the fabrication of composite membranes for desalination applications. The study found that the incorporation of ZnONPs into the membrane matrix could effectively reduce membrane fouling, leading to improved water flux and salt rejection. Moreover, the use of ZnONPs in the modification of forward osmosis membranes for desalination applications has been studied. The study found that the incorporation of ZnONPs into the membrane matrix could effectively reduce membrane fouling, leading to improved water flux and salt rejection (Klink et al., 2022; Al Jabri et al., 2022; Punia et al., 2021; Raghavendra et al., 2022; Shivalingam et al., 2022; Al Mayyahi, 2018; Rajakumaran et al., 2019).

Vijayakumar et al. (2018) synthesized ZnONPs using *Atalantia monophylla* leaf extracts through a green route. According to XRD spectra, ZnONPs were synthesized in a hexagonal wurtzite structure. Also, the sharp peaks revealed the highly crystalline and pure nature of the synthesized particles. Meanwhile, the crystallite size was evaluated using Debye Scherrer's formula. The result depicted that the average particle size of the nanoparticles was 33.01 nm, which was in good accordance with TEM micrographs. Furthermore, SEM images revealed

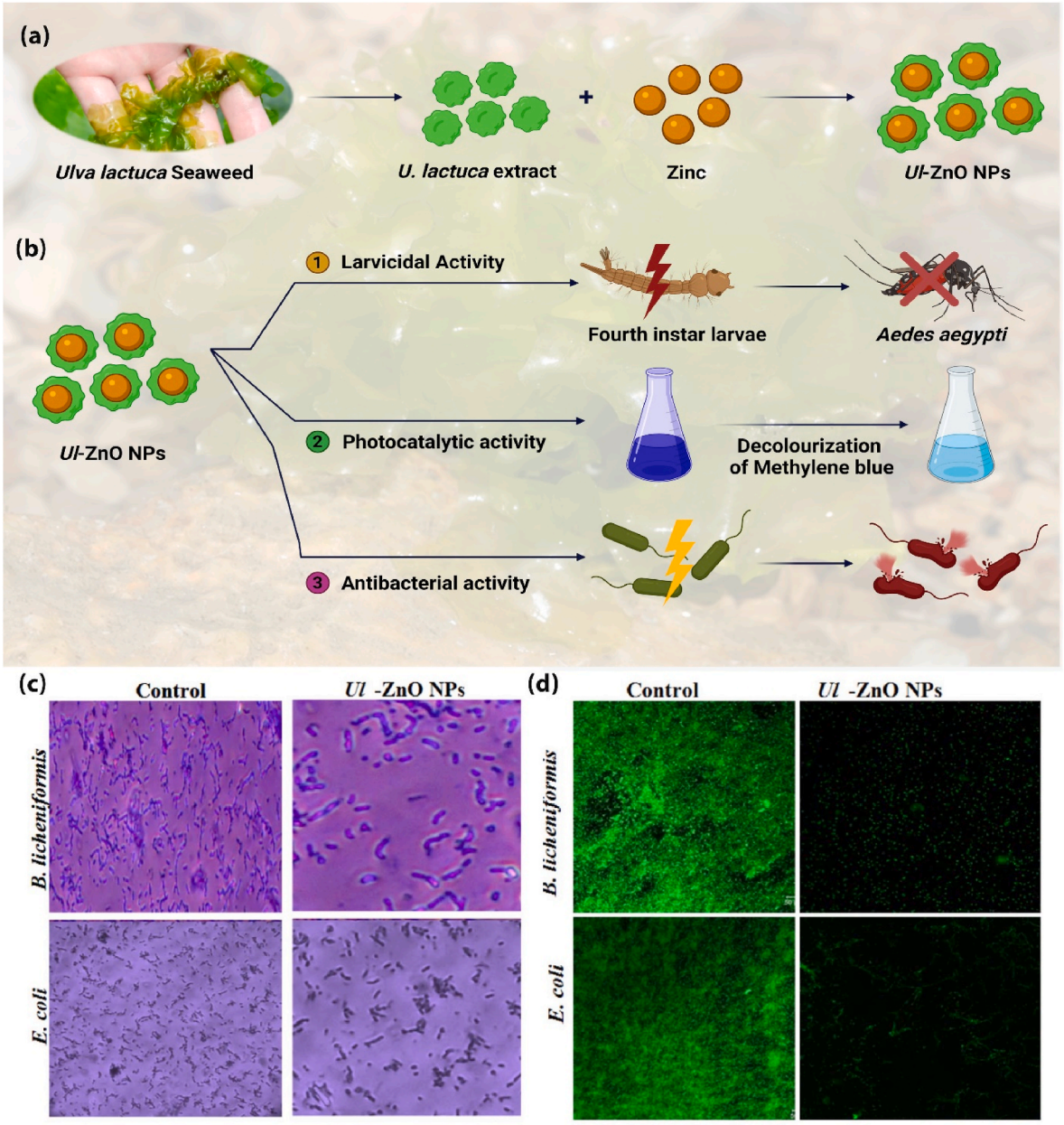

Fig. 4. **(a)** Synthesis of the *Ulva lactuca*-fabricated zinc oxide nanoparticles (*Ul*-ZnONPs); The preparation of *U. lactuca* extract: I) Rinsing the *U. lactuca* seaweeds with distilled water, cutting them into little pieces, and drying in air. II) Adding the seaweed powder into a double distilled water, boiling for 20 min, filtering the seaweed extract by filter paper, and storing in refrigerator at 4 °C. The fabrication of *Ul*-ZnONPs: I) Adding the *U. lactuca* extract into an aqueous solution of zinc acetate, stirring the reaction mixture for 3–4 h at 70 °C. II) Centrifuging, collecting the solid product, and rinsing with distilled water. III) Heating the ZnO-extract mixture in air oven at 450 °C for 4 h. **(b)** The *Ul*-ZnONPs performances: 1. Larvicidal activity against Aedes aegypti larvae, 2. Photodegradation action against methylene blue, and 3. Antibiofilm effect. **(c)** Light microscopic images and **(d)** confocal laser scanning microscopy of bacterial biofilms (Gram positive: *B. licheniformis* and Gram negative: *E. coli*) in the presence of *Ul*-ZnONPs. Reprinted with permission from Ref (Ishwarya et al., 2018). Copyright 2018 Elsevier.

that the ZnONPs were synthesized in a spherical shape, while TEM images illustrated the formation of hexagonal and spherical particles. As per energy dispersive X-ray analysis (EDAX) patterns, ZnONPs were formed in 48.81 wt%. The antibacterial activity of as-prepared ZnONPs was evaluated using the agar well diffusion technique through the incubation time in the 24–48 h range at ≈30 °C and ≈37 °C for bacteria and fungi, respectively. The results indicated 28, 23, 21, 22, 20, and 19 mm inhibition zone for *S. aureus, E. coli, B. cereus, P. aeruginosa, B. subtilis,* and *K. pneumoniae*, respectively.

In terms of fungi, the inhibition zone was 24 and 18 mm for *C. albicans* and *A. niger*, respectively. More susceptibility to ZnONPs was observed for the bacterial strains compared to fungi was observed. Overall, it was concluded that the non-toxic and inexpensive synthesized ZnONPs significantly reduced the infections resulted from microorganisms. Different kinds of nanoparticles have been synthesized through a green and cost-effective method in order to use in water treatment applications (Table 1).

2.2. Green polymer-based nanomaterials

Celebioglu et al. (2019) have fabricated antibacterial nanofibers using cyclodextrin (CD) and AgNPs employing electrospinning. They used N,N-dimethylformamide (DMF), and an aqueous consisted of various amounts of silver nanoparticles. Typically,

Table 1
A comprehensive analysis of nanoparticles synthesized through green synthetic procedures and utilized for water treatment, in terms of greenness, size, application, and removal efficiency.

Type	Green additive	Size (nm)	Application	Removal (%, inhibition zone, or adsorption capacity)	Refs.
Iron oxide	Leaf extract: Magnolia champaca (MC), Azadiracta indica (AI), Murraya Koenigii (MK), Magnifera Indica (MI)	99-129, 96-110, 100–150	Domestic wastewater treatment	Phosphate: (MC) 98.84, (AI) 98.08, (MI) 91.89 (MK) 97.68 Nitrate: (MI) 54.42, (AI) 84.32	Devatha et al. (2016)
Iron oxide	eucalyptus leaf extracts	70 ± 20 (SEM), 71.5 ± 2 (DLS)	Cr(VI) removal from aqueous solutions	98.6%	Jin et al. (2018)
Iron oxide	Dolichos lablab L. extract	13 (XRD), 8-60 (FE-SEM), 4-30 (TEM)	Crystal violet (CV) removal from aqueous solutions	93%	Basavaiah et al. (2018)
Iron oxide	Lantana camera leaf extract	10–20	Antibacterial activity against Pseudomonas sp., Klebsiella sp., Staphylococcus sp., and Salmonella sp. Seed germination of Vigna mungo	Inhibition zone: (Pseudomonas sp.) ≈20.1 mm, (Klebsiella sp.) ≈18 mm, (Staphylococcus sp.) ≈19 mm, (Salmonella sp.) ≈17 mm, (seed germination) 87%	Rajiv et al. (2017)
Iron oxide	Citrus reticulum peels extract	57.59 (XRD), 20-63 (SEM, TEM)	Degradation of Basic Blue 41, Acid Blue 158, 2,6-dichlorophenol	(Basic Blue 41) 77.3%, (Acid Blue 158) 82.5%, (2,6-dichlorophenol) 81.5%	Ali et al. (2017)
Iron oxide	pomegranate (Punica granatum) extracts, and green tea (Camellia sinensis)	(Pomegranate extract) 43.8, (Green tea extract) 10.1	Color removal, Dissolved organic carbon removal	(Color removal) 95%, (Dissolved organic carbon removal) 80%	Ozkan et al. (2018)
Cobalt oxide	Latex of Calotropis procera	3-5 (XRD), <20 (TEM)	Antibacterial activity against E. coli, Pseudomonas sp., Alcaligenes sp., Enterococcus sp.	Inhibition zone: (E. coli) 17 mm, (Pseudomonas sp.) 12 mm, (Alcaligenes sp.) 13 mm, (Enterococcus sp.) 14 mm	Dubey et al. (2018)
Cobalt oxide	Neem (Azadirachta indica) leaf	0.24 (XRD), 1-7 (HRTEM)	Antibacterial activity against S. aureus, B. subtilis, P. aeruginosa, E. coli	Inhibition zone: (S. aureus) 16.3 mm, (B. subtilis) 22.2 mm, (P. aeruginosa) 34.5 mm, (E. coli) 16.4 mm	Sivachidambaram et al. (2017)
Cobalt oxide & Cobalt–Silver oxide	Helianthus annuus extract	1–20 μm (87% of particles are in the 2–5 μm)	Methyl orange degradation from aqueous solution	(Cobalt oxide) 53%, (Cobalt–Silver oxide) 87%	Saeed et al. (2019)
Silver oxide	Helichrysum graveolens extract	11	Methyl orange	85.39	Yazdi et al. (2020a)
Silver nanoparticles	Artemisia vulgaris leaf extract	27-53 (SEM), 25 (TEM)	Antimicrobial activity against K. pneumonia, H. influenza, P. aeruginosa, E. coli, S. aureus	Inhibition zone: (K. pneumonia) ≈11 mm, (H. influenza) 12 mm, (P. aeruginosa) ≈9 mm, (E. coli) 10 mm, (S. aureus) 8 mm	Rasheed et al. (2017)
Silver nanoparticles	Xerophytic plant extract (Neurada procumbens)	20-50 (SEM, TEM)	Inhibition zone against K. pneumoniae, A. baumannii, E. coli	Inhibition zone: (K. pneumoniae) >17 mm, (A.baumannii) 12–14 mm, (E. coli) >17 mm	Alharbi and Alarfaj (2020)
Silver nanoparticles	Gelidium amansii	27-54 (SEM)	Antimicrobial activity against parahaemolyticus, E. coli, P. aeruginosa V., S. aureus, A. hydrophila, and B. pumilus, biofilm-forming bacteria	Up to ≈99% micro-fouling formation reduction	Pugazhendhi et al. (2018)
Silver nanoparticles	Aqueous extract of Aerva lanata	5-50 (SEM, TEM, AFM), 24.36–141.8 (DLS)	Antibacterial activity and minimum inhibitory concentration (MIC) against wound associated bacteria: P. aeruginosa, E. coli,	Inhibition zone (mm) & (MIC) (μg. ml^{-1}): (P. aeruginosa) 21, 5, (E. coli) 22, 5, (M. morgani)	Appapalam and Panchamoorthy (2017)

(*continued on next page*)

Table 1 (*continued*)

Type	Green additive	Size (nm)	Application	Removal (%, inhibition zone, or adsorption capacity)	Refs.
			M. morgani, S. aureus, B. subtilis, E. faecalis, S. agalactiae, C. striatum	41, 5, (S. aureus) 21, 15, (B. subtilis) 15, 10, (E. faecalis) 23, 5, (S. agalactiae) 15, 10, (C. striatum) 16, 10	
Silver nanoparticles	Capparis zeylanica L. leaf extract	28 (FE-SEM), 23 (TEM)	Antimicrobial activity against Aspergillus niger, Enterococcus faecalis, Candida albicans, Staphylococcus epidermidis, Shigella dysenteriae, Salmonella paratyphi,	Inhibition zone: (Staphylococcus epidermidis) 30 mm, (Enterococcus faecalis) 26 mm, (Salmonella paratyphi) 23 mm, (Shigella dysenteriae) 20 mm, (Candida albicans) 25 mm, (Aspergillus niger) 23 mm	Nilavukkarasi et al. (2020)
Silver nanoparticles	Annona reticulata leaves aqueous extract	6–8	Minimum inhibitory concentration (MIC) and inhibition zone against Bacillus cereus, Staphylococcus aureus, Pseudomonas aeruginosa, Escherichia coli, Candida albicans	Inhibition zone (mm) and (MIC) (μg ml^{-1}): (Bacillus cereus) 17, 125, (Staphylococcus aureus) 18, 31.2, (Pseudomonas aeruginosa) 22, 62.5, (Escherichia coli) 12, 62.5, (Candida albicans) 21, 62.5	Parthiban et al. (2019)
Silver oxide	Aspergillus brasiliensis	6-21 (FE-SEM, HRTEM) 35.8 (DLS)	Minimum inhibitory concentration (MIC) and minimum inhibitory lethal (MLC) against C. albicans, B. subtilis, E. coli, P. aeruginosa and S. aureus	(MIC), (MLC) (μg. ml^{-1}): (C. albicans) 300, 400, (B. subtilis) 300, 600, (E. coli) 500, 700, (P. aeruginosa) 600, 600, and (S. aureus) 400, 600	Omran et al. (2018)
Silver nanoparticles	Escherichia coli	118 (Scherrer), 5-25 (SEM)	Antibacterial activity against human pathogens, including Klebsiella pneumoniae, Bacillus subtilis, Salmonella typhi, Vibrio cholerae	(Inhibition zone) 7–13 mm	Divya et al. (2016)
Silver nanoparticles	corn of Z. mays L.		Antibacterial activity and against B. cereus ATCC 13061, E. coli ATCC 43890, L. monocytogenes ATCC 19115, S. aureus ATCC 49444, S. Typhimurium ATCC 43174	Inhibition zone (mm) & minimum inhibitory concentration (MIC) (μg. ml^{-1}): (B. cereus ATCC 13061) ≈11.39, 25, (E. coli ATCC 43890) ≈10.55, 50, (L. monocytogenes ATCC, 19115) ≈9.26, 25 (S. aureus ATCC 49444) ≈11.57, 12.5 (S. Typhimurium ATCC 43174) ≈11.22, 50	
Silver nanoparticles	Lippia nodiflora aerial extract	78 (XRD), 143.7 (DLS), 30-60 (TEM)	Antibacterial activity against S. aureus, S. mutans, S. pneumonia, E. coli, K. pneumonia	Inhibition zone: (S. aureus) ≈20.3 mm, (S. mutans) ≈18.2 mm, (S. pneumonia) ≈24.1 mm, (E. coli) ≈22 mm, (K. pneumonia) ≈20.4 mm	Sudha et al. (2017)
Silver nanoparticles	Ocimum Sanctum (Tulsi) leaf extract and its derivative quercetin	10–20	Antibacterial activity against E-Coli gram-negative bacterial strains	Inhibition zone: 14 mm	Jain and Mehata (2017)

(*continued on next page*)

Table 1 (*continued*)

Type	Green additive	Size (nm)	Application	Removal (%, inhibition zone, or adsorption capacity)	Refs.
Silver nanoparticles	Carya illinoinensis leaf extract	12-30 (TEM)	Antibacterial activity and minimum inhibitory concentration (MIC) against S. aureus, L. monocytogenes, E. coli, P. aeruginosa	Inhibition zone (mm) & (MIC) (μg. ml^{-1}): (S. aureus) 11, 128, (L. monocytogenes) 12, 64, (E. coli) 15, 16, (P. aeruginosa) 13, 32	bakht Dalir et al. (2020)
Silver nanoparticles	Rosa canina plant	13-21 (TEM), 19.75 (XRD)	Minimum inhibition concentration (MIC) against P. aeruginosa E. hirae, B. cereus, E. coli, S. aureus, Candida albicans, L. pneumophila	(MIC) (μg. ml^{-1}): (P. aeruginosa) 128, (E. hirae) 256, (B. cereus) 32, (E. coli) 256, (S. aureus) 256, (Candida albicans) 128, (L. pneumophila) 16	Gulbagca et al. (2019)
Silver nanoparticles	Psidium guajava L. leaf	20–35 (SEM), 25 (TEM), 25-35 (Zetasizer)	Antimicrobial activity against A. niger, S. cerevisiae, Escherichia coli, Alcaligenes faecalis, R. oryzae	Inhibition zone: 13.24–14.41 mm (Gram-positive bacteria), 16.92 ± 0.18 mm (E. coli), 18.13 ± 0.02 mm (A. faecalis)	Wang et al. (2018)
$MgFeCrO_4$ spinel	Tragacanth gum	20–22	Direct black 122 dye	96	Moradnia et al. (2020)
Nickel oxide	Andrographis paniculata leaf extract	24 (Scherrer)	Evans blue (EB) dye	88.13	Karthik et al. (2019)
Titania	leaf extracts of Jatropha curcas L.	10–120	Tannery wastewater	Cr: 76.48 COD: 82.26	Goutam et al. (2018)
Titania	Leaf extract of Trigonella foenum-graecum	20-90 (HR-SEM)	Antimicrobial activity against: S. aureus, S. faecalis, E. coli, P. vulgaris, E. faecalis, P. aeruginosa, Y. enterocolitica, B. subtilis, and fungus C. albicans.	Inhibition zone: (S. aureus) 11.2 mm, (S. faecalis) 11.6 mm, (E. coli) 10.8 mm, (E. faecalis) 11.4 mm, (Y. enterocolitica) 10.6 mm	Subhapriya and Gomathipriya (2018)
$NaEuTi_2O_6$	Carbohydrates such as glucose, galactose, lactose and starch	11-15 (Scherrer)	Decolonization of methyl orange azo dye	90	Hosseinpour-Mashkani and Sobhani-Nasab (2017)
Ginger powder loaded by: Copper-silver (Cu–Ag/GP), Copper-nickel (Cu–Ni/GP), Nickel-silver (Ni–Ag/GP)	Ginger rhizome powder	Scherrer: (Cu–Ag) 59, (Cu–Ni) 68, (Cu–Ag/GP) 0.2, 0.5 and 1 M treated: 59, 88, 106	2-nitrophenol (2-NP), 4-nitrophenol (4-NP), Methyl orange (MO), Congo red (CR), Rhodamine B (RhB)	Cu–Ag/GP: (4-NP & 2-NP) 96, (Rhodamine B) 97, (Congo Red) 98, Cu–Ni/GP: (4-P & 2-NP) 98, (Rhodamine B) 97, (Congo red) 98, Cu–Ag/GP & Cu–Ni/GP: (MO & 4-NP) 97, (RhB and CR) ≈100, (CR and MO) 96,	Ismail et al. (2018a)
Copper nanoparticles	Syzygium aromaticum bud extract	≈12 (XRD), ≈20 (FESEM)	Antimicrobial activity against E. coli A. niger Penicillium spp, Pseudomonas spp. Bacillus spp. A. flavus Staphylococcus spp.	Inhibition zone: (E. coli) ≈6 mm, (Pseudomonas spp.) ≈7 mm, (Penicillium spp.) ≈6 mm (Bacillus spp.) ≈8 mm, (Staphylococcus spp.) ≈5 mm, 1. niger) ≈5 mm A. flavus) ≈5 mm	Rajesh et al. (2018)
Copper nanoparticles	Impatiens balsamina leaf extract	5-10 (TEM)	Degradation of methylene blue (MB) and congo red (CR) dye	(MB) ≈90%, (CR) ≈85%	Roy et al. (2017)
Copper nanoparticles	Ripened Duranta erecta fruits	70 (FE-SEM), 76 (XRD)	Degradation of congo red (CR) and methyl orange (MO)	(CR) 90.35%, (MO) 96%	Ismail et al. (2019)
Copper oxide	fruit extract of Ziziphus spina-christi (L.) Willd.	8-15 (XRD), 5-20 (FE-SEM), 9 (TEM)	Crystal violet (CV) removal from aqueous solution, Antibacterial activity against: E. coli, S. aureus	(CV) 95%, Inhibition zone: (E. coli) 1.7 mm, (S. aureus) 1.8 mm	Khani et al. (2018)

(*continued on next page*)

Table 1 (*continued*)

Type	Green additive	Size (nm)	Application	Removal (%, inhibition zone, or adsorption capacity)	Refs.
Ag incorporated carbopol–alginate beads	Mukia maderaspatna plant	Ag nanoparticles: 19 (TEM, XRD)	Methylene blue	Adsorption capacity: 213.7 (mg/g)	Karthiga Devi et al. (2016)
Zinc Oxide	Camellia Sinensis extract	9.04 (XRD)	Methylene blue	84	Nava et al. (2017a)
Zinc oxide	Fruit peel extract	9-20 (XRD)	Methylene blue	97	Nava et al. (2017b)
Zinc oxide	Garcinia mangostana fruit pericarp	23.56 (XRD), 5-45 (TEM)	The degradation of malachite green dye under solar irradiation	99% degradation	Aminuzzaman et al. (2018)
Zinc oxide	Costus pictus D. Don plant	20-80 (SEM, TEM, XRD)	Antibacterial activity against B. subtilis, E. coli, S. aureus, S. paratyphi, C. albicans, A. niger	Inhibition zone: (S. aureus) 10 mm, (B. subtilis) 17 mm, (E. coli) 10 mm, (S. paratyphi) 12 mm, (C. albicans) 12 mm, (A. niger) 16 mm	Suresh et al. (2018)
Zinc oxide	Phoenix dactylifera waste	30	Methylene blue (MB), Eosin yellow (EY), Gram-positive (Staphylococcus aureus and Streptococcus pyogenes) and gram-negative (Pseudomonas aeruginosa and Proteus mirabilis) bacterial strains	MB & EY: 90, Inhibition zone: (Proteus mirabilis) 18.7 mm, (Pseudomonas aeruginosa) 18.4 mm, (Staphylococcus aureus) 15.9 mm, (Streptococcus pyogenes) 14.5 mm	Rambabu et al. (2021)
Zinc oxide	Passiflora caerulea fresh leaf extract	70 (SEM), 37.67 (XRD)	Antimicrobial activity against E. coli, Streptococcus sp., Enterococcus sp., Klebsiella sp.	Inhibition zone: (E. coli) ≈13 mm, (Streptococcus sp.) ≈11.67 mm, (Enterococcus sp.) ≈9.33 mm, (Klebsiella sp.) ≈11 mm	Santhoshkumar et al. (2017)
Zinc oxide	Ulva lactuca seaweed extract	5-15 (XRD), 10-50 (TEM)	Antibacterial activity against Bacillus licheniformis, Bacillus pumilus, E. coli, Proteus vulgaris	Inhibition zone: (Bacillus licheniformis) ≈26.3 mm, (Bacillus pumilus) ≈21.2 mm, (E. coli) 24 mm, (Proteus vulgaris) 20.3 mm	Ishwarya et al. (2018)
Zinc oxide	Parthenium hysterophorus Leaf Extract	16-45 (SEM-TEM)	Antimicrobial activity against Enterobacter aerogenes, Staphylococcus aureus, Bacillus subtilis, Klebsiella pneumonia, Escherichia Coli	Inhibition zone: (Enterobacter aerogenes) 36 mm, (Staphylococcus aureus) ≈11 mm, (Bacillus subtilis) ≈10 mm, (Klebsiella pneumonia) ≈14 mm, (Escherichia Coli) ≈20 mm	Datta et al. (2017)
Cobalt oxide	Grape jumbo Muscadine (Vitis rotundifolia)	–	Acid Blue-74	98	Samuel et al. (2020)
Biomaterial supported zero-valent iron oxide	Calotropis gigantea (CG) flower extract, Pithecellobium dulce seeds	Zero-valent iron oxide: 30 (XRD), 50-90 (SEM)	Methylene blue (MB)	(MB) 85.5, (Aniline) 74.8	Sravanthi et al. (2018)
Iron-based nanoparticles	Nephrolepis auriculata	40-70 (TEM)	Cr(VI) removal	90.93	Yi et al. (2019)
Iron hexacyanoferrate nanoparticles	sapindus-mukorossi	10-60 (TEM)	PAHs (anthracene, phenanthrene, chrysene, fluorene, and benzo (a) pyrene) removal from water and soil	(Anthracene & phenanthrene) 80–90, (Fluorene, Chrysene & Benzo (a) pyrene) ≈70-80	Shanker et al. (2017)
Fe/Ni nanoparticles	eucalyptus leaf extracts	20-50 (SEM)	Methyl orange (MO)	99.6	Weng et al. (2017)
Carbon encapsulated zerovalent iron	Olive mill wastewater	(iron nanoparticles: ≈4, Thin carbon layer: <1	Cu, Zn, Cr, Ni and Cd removal from aqueous solutions	(Zn, Cd, Cu & Cr) 99, (Ni) 97	Calderon et al. (2018)
Nickle oxide	Aegle marmelos leaf extract	8-10 (HR-SEM),	Cytotoxic activity against A549 cell culture, Antibacterial activity/photocatalytic	(A549 cell Viability) 64.6 Inhibition zone: (Staphylococcus Aureus)	Ezhilarasi et al. (2018)

(*continued on next page*)

Table 1 (*continued*)

Type	Green additive	Size (nm)	Application	Removal (%, inhibition zone, or adsorption capacity)	Refs.
			degradation of 4-chlorophenol (4-CP),	16 mm, (Streptococcus Pnemoniae) 12 mm, (Escherichia Coli) 12 mm, (Escherichia Hermannii) 6 mm, (Photocatalytic degradation of 4-CP) ≈98 (Photocatalytic mineralization of 4-CP) complete,	
Bimetallic mixed copper-nickel (Cu–Ni/TP), silver copper (Ag–Cu/TP), and nickel silver (Ni–Ag/TP) nanoparticles	Turmeric Curcuma longa powder	Ag–Cu/TP: 40-55 (FE-SEM), 45 (XRD)	Antibacterial activity against Escherichia coli, Reduction of: Fluoroquinolone antibiotics Levofloxacin (LVO) ciprofloxacin (CIP) Rhodamine B (RhB) Congo red (CR), methylene blue (MB), Methyl orange (MO),	Antibacterial activity: (Ag–Ni/TP) 77, (Ag–Cu/TP) 45, (Cu–Ni/TP) 7, MO: (Ag–Cu/TP & Ag–Ni/TP) 90, (Cu–Ni/TP) 95, Ag–Cu/TP: (CIP) 67, (LVO) 64, (CR) 90, (MB) 100, (RhB) 90	Ismail et al. (2018b)
Gold nanoparticles	Crescentia cujete L.	32.89 (TEM), 30 (XRD), 100 (DLS)	Antibacterial activity against E. Coli, S. Typhi, S. Flexneri, V. Colerae, P. Aurogens, B. Subtilis	Inhibition zone: (E. Coli) ≈20 mm, (S. Typhi) ≈17.5 mm, (S. Flexneri) ≈22 mm, (V. Colerae) ≈12 mm, (P. Aurogens) ≈16 mm, (B.Subtilis) ≈13 mm	Seetharaman et al. (2017)

hydroxypropyl-β-cyclodextrin (HP-β-CD) was dissolved in either DMF or water, followed by silver nitrate with different ratios. After adjusting the solution pH and homogeneous mixing for AgNPs formation, the as-prepared solutions were electrospun. The antibacterial activity of the as-prepared nanofibers was evaluated against *E. coli* and *Staphylococcus aureus* through the agar-diffusion method, and 150 μL of each bacteria was poured onto the agar plate. It was inferred that AgNPs formed in DMF depicted a bigger size than nanoparticles synthesized in aqueous solutions. Results revealed that nanofibers fabricated from DMF solution exhibited smaller diameters compared to those prepared from aqueous solutions. Therefore, the size of nanofibers formed in DMF and aqueous solutions escalated from ≈184 nm to ≈280 nm and ≈207 nm up to ≈440 nm, increasing the silver content from 1 wt% to 2 wt%., respectively. Besides, increasing the silver loading enhanced the silver nanoparticle's average size formed in DMF and aqueous solutions from ≈3.5 nm to ≈4.8 nm and ≈1.9 nm to ≈2.3 nm, respectively. It was proposed that the creation of larger nanoparticles of silver in DMF can be originated from the reducing effect of DMF. SEM micrographs illustrated that the as-prepared nanofibers were formed in a bead-free structure. According to TEM and STEM images, AgNPs were homogeneously distributed over the surface of the fibers. Also, solid-state UV–Vis spectra revealed the presence of AgNPs in the 2–5 nm range. In terms of antibacterial activity, the inhibition zone of nanofibers incorporated with 1 wt% of AgNPs was ≈1.07 cm (*E. coli*) and 1.16 cm (*S. aureus)*.

Water scarcity is a growing problem worldwide, and water desalination and treatment have become essential processes to ensure access to clean and safe water. However, traditional methods of water treatment and desalination are often energy-intensive and costly, making them unfeasible for many regions. Nanotechnology has emerged as a promising alternative to traditional methods of water treatment and desalination. In particular, the use of nanofibers and natural polymeric structures has been the focus of extensive research due to their unique physical and chemical properties. Nanofibers are materials with a diameter of less than 100 nm and a high surface area to volume ratio. This high surface area makes them effective at adsorbing pollutants and contaminants from water. Natural polymers, such as chitosan, alginate, and cellulose, have also been studied extensively for their ability to remove heavy metals, organic pollutants, and microorganisms from water. These materials are abundant, renewable, biodegradable, and non-toxic, making them a sustainable alternative to synthetic materials. One of the most promising applications of nanofibers and natural polymeric structures is in membrane technology for water desalination and treatment. Membrane technology uses a semipermeable barrier to separate contaminants from water, allowing for the production of clean and safe water. Traditional membrane materials, such as polyamide and polypropylene, have limitations in terms of pore size and selectivity, leading to lower efficiency and fouling issues. The use of nanofibers and natural polymeric structures has the potential to overcome these limitations and improve the efficiency and selectivity of membranes. Research has shown that nanofiber-based membranes can remove a wide range of contaminants from water, including heavy metals, organic compounds, and microorganisms. For example, electrospun polyacrylonitrile (PAN) nanofiber membranes have been shown to effectively remove heavy metals, such as lead and chromium, from contaminated water. Similarly, nanofiber membranes made from chitosan and cellulose have been shown to remove organic pollutants and microorganisms from water.

Natural polymeric structures have also been studied extensively for their ability to remove contaminants from water. Chitosan, for example, has been shown to effectively remove heavy metals, such as copper and cadmium, from water. Alginate, a natural polysaccharide derived from seaweed, has been used to develop membranes that can remove organic compounds and heavy metals from water. Cellulose, the most abundant biopolymer on earth, has been used to develop membranes that can remove bacteria and viruses from water. In addition to their ability to remove contaminants from water, nanofibers and natural polymeric

structures also have the potential to improve the stability and durability of membranes. Nanofibers can be used to reinforce traditional membrane materials, improving their mechanical strength and resistance to fouling. Natural polymeric structures can also be used to enhance the stability and durability of membranes, particularly in harsh environments. While the use of nanofibers and natural polymeric structures in water desalination and treatment shows great promise, there are also challenges and limitations that need to be addressed. One of the biggest challenges is the scalability of these materials. Many of the methods used to produce nanofibers and natural polymeric structures are still in the research and development phase, making it difficult to produce these materials in large quantities at an affordable cost. There is also a need for more research on the long-term stability and durability of these materials, particularly in real-world applications (Saleem et al., 2020; Kugarajah et al., 2021; Agrawal et al., 2021; Lee et al., 2016).

Fu et al. (2019) synthesized chitosan functionalized activated coke to incorporate Au nanoparticles in which chitosan acted as a promising reductant, linker activated carbon and Au nanoparticles, and stabilizer for Au nanoparticle to prevent them from agglomeration. It was inferred that the surface amino and hydroxyl groups make chitosan a great candidate for stabilizer, reductant, and linker. The as-prepared catalyst was utilized for the hydrogenation of 4-nitrophenol. According to TEM images, activated carbon initially consisted of thin porous layers, and chitosan incorporation resulted in smooth and transparent layers over the surface. Also, almost uniform dispersion of Au nanoparticles can be observed in the TEM images. Fourier Transform Infrared (FTIR) spectrum delineated that the surface amino and hydroxyl groups of chitosan-coated activate carbon make them an excellent Au anchoring substrate. EDAX analysis depicted the presence of Au nanoparticles over the surface. Besides, XRD depicted the crystalline structure of activated carbon, chitosan incorporated activated carbon, and Au anchored substrate. In terms of the catalytic hydrogenation of 4-nitrophenol, activated carbon and chitosan incorporated activated carbon exhibited 14% and 7% of adsorption, respectively, while hydrogenation significantly escalated up to 98% using the as-prepared catalyst.

Moreover, increasing the Au loading from 0.0014 to 2.5033 wt% led to increased catalytic activity, which could be related to the active site improvement. On the other hand, further increase in the Au amount resulted in the agglomeration and drop in the catalytic activity. Synthesized catalysts were also utilized for 6 cycles, and no significant deactivation was observed after the 6th cycle.

Alippilakkotte et al. (2017) fabricated Polylactide/Ag nanofibers through the electrospinning method. To this end, AgNPs were synthesized using bitter gourd extract as a reducing agent and silver nitrate in a diphase environment consisting of polylactide as a capping agent. First, nanosilver colloidal sol and polylactide/Ag nanocomposite were prepared by dissolution of silver nitrate in dichloromethane (DCM) and polylactide followed by the addition of *M. charantia* extract. Next, the as-prepared nanocomposite was dissolved in 2,2,2-trifluoroethanol, and after the homogeneous mixing, the as-prepared mixture was electrospun by the electrospinning process.

The antibacterial activity of the nanofibers against *E. coli* and *S. aureus* was estimated using the disk diffusion method through inhibition zone measurement. AT-IR analysis revealed the characteristic peaks of AgNPs present in the polylactide matrix. Also, UV-VIS spectrum and Surface Plasmon Resonance (SPR) delineated the creation of colloidal sol of nanoparticles of silver. SEM analysis indicated that AgNPs were distributed over the fiber's surface with ≈30 nm diameter, and TEM micrographs depicted the creation of spherical nanoparticles of silver in the 5–20 nm interval, which was in good accordance with XRD results. Also, the mean diameter of the polylactide/Ag nanocomposite with various silver content was in the ≈150–271 nm range. Besides, the presence of AgNPs on the polylactide fibers surface was verified using EDAX.

In terms of antibacterial activity, the inhibition zone reached 7.57 mm and 6.75 mm for E. coli and S. aureus, respectively. Due to an escalation in particle size, an enhancement in the silver nitrate concentration led to a decrease in antibacterial activity. Dynamic light scattering analysis showed that the nanoparticles of silver were in the 50–200 nm and average mean size of 80 nm. Moreover, tensile strength was enhanced from ≈0.32 to 0.82 MPa through increasing the silver content up to 2 wt%.

Qasim et al. (2018) synthesized various poly-N-isopropylacrylamide (pNIPAM) nanoparticles in the 100–500 nm range through the radical polymerization of N-isopropylacrylamide. To this end, Sodium dodecyl sulfate was utilized as a surfactant, and ammonium persulfate (APS) was added to initiate the polymerization. Next, the amine group was introduced to the polymeric particles by adding N-(3-aminopropyl) methacrylamide hydrochloride (APMAAHC) to the reaction mixture. Then, they encapsulated AgNPs inside the as-prepared polymeric particles by adding $AgNO_3$ after incubating the as-prepared polymeric nanoparticles in $NaBH_4$ solution. In terms of liquid culture, the antimicrobial activity on the as-prepared nanoparticles was evaluated against *S. aureus and E. coli* by adding 40 μL of the nanoparticles to 160 μL of the bacterial suspension. Pure culture and culture media without cells were utilized as positive and negative controls, respectively. Moreover, different encapsulation methods have been done so far in order to increase and improve the filtration of different analytes. In this regard, a well-defined molecular architecture based on polyethyleneimine and decorated nanocapsules have been emerged (Fig. 5) (Xia et al., 2020). This new technology leads to controlled release of carbon dioxides and other types of gases by a predictable manner. Nanofibers and natural polymeric structures have attracted significant attention in recent years for their potential use as antibacterial agents. The unique properties of these materials, including their high surface area-to-volume ratio and biocompatibility, make them promising candidates for a variety of biomedical and environmental applications. One of the primary mechanisms by which nanofibers and natural polymers exhibit antibacterial activity is through physical interactions between the material and the bacterial cell. The high surface area-to-volume ratio of nanofibers allows for a large number of contact points between the material and the bacterial cell, leading to the disruption of the bacterial membrane and subsequent cell death. In addition, natural polymeric structures such as chitosan and cellulose contain functional groups that can interact with the bacterial cell wall, leading to structural changes and permeability alterations that inhibit bacterial growth and replication. Several studies have demonstrated the antibacterial efficacy of nanofibers and natural polymeric structures. For example, electrospun nanofibers of polyvinyl alcohol (PVA) and polyvinylpyrrolidone (PVP) were shown to have strong antibacterial activity against both Gram-positive and Gram-negative bacteria. The antibacterial activity was attributed to the high surface area-to-volume ratio of the nanofibers, which allowed for increased contact with the bacterial cells. Similarly, nanofibers of chitosan and its derivatives have been shown to have potent antibacterial activity, with the mechanism of action likely involving interactions with the bacterial cell wall and subsequent damage to the cell membrane. In addition to their direct antibacterial activity, nanofibers and natural polymeric structures can also be used to deliver antibacterial agents. For example, AgNPs can be incorporated into nanofibers and natural polymers to create antibacterial composites that release silver ions over time, leading to sustained antibacterial activity. This approach has been shown to be effective in inhibiting bacterial growth and reducing bacterial adhesion on surfaces. While the use of nanofibers and natural polymeric structures as antibacterial agents holds great promise, there are also potential drawbacks and challenges that must be addressed. One concern is the potential for these materials to induce inflammation or toxicity *in vivo*. In addition, the long-term stability and degradation of these materials in the environment is not well understood, and their impact on natural ecosystems requires further investigation (Ulubayram et al., 2015; Homaeigohar and Boccaccini, 2020; Qiu et al., 2020).

In terms of AgNPs encapsulated in nanogels, the plate diffusion method evaluated the antimicrobial activity on solid media. First, 1 mg/

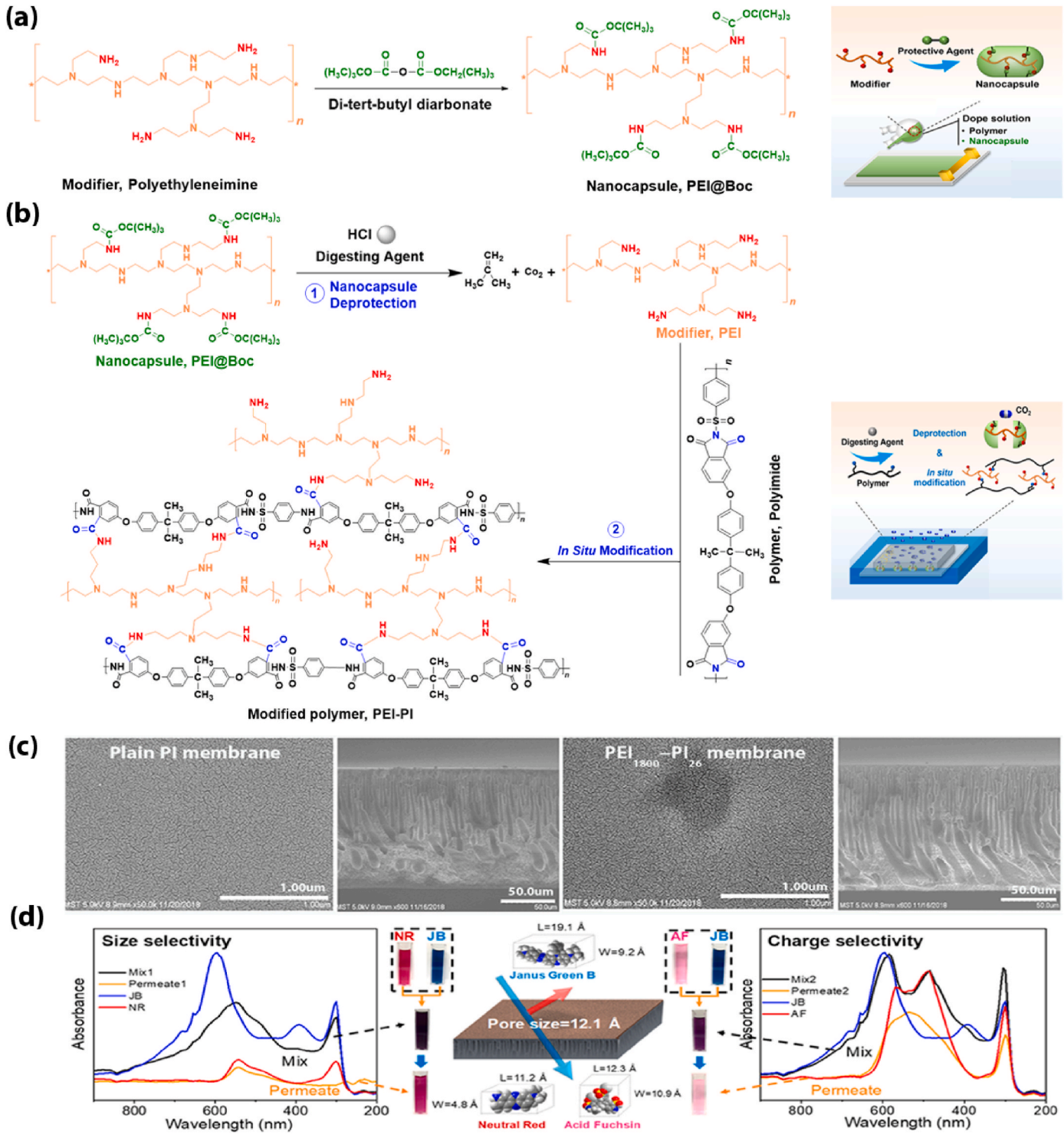

Fig. 5. **(a)** Construction of the PEI@Boc nanocapsules: I) Preparation of the 20 wt% polyetherimide (PEI) and 20 wt% di-tert-butyl dicarbonate $(Boc)_2O$ solutions from dissolving the PEI1800 and $(Boc)_2O$ in dichloromethane. II) Adding the $(Boc)_2O$ solution into PEI solution, collecting the milky dispersion after stirring for 12 h at 25 °C, centrifuging, and washing by dimethylacetamide (DMAc). **(b)** Construction of the polyetherimide-polyimide (PEI-PI) membranes: I) Formation of the PI/DMAc solution under stirring at 65 °C for 8 h, then cooling to 25 °C. II) Adding the PEI@Boc nanocapsules into polymer solution under stirring at 25 °C for 8 h. III) Degassing the resultant dope solution, casting on nonwoven fabric, immersing into the special coagulation bath containing a certain concentration of HCl, transferring into the water bath at 70 °C for 10 min, and transferring and storing into distilled water. **(c)** The surface and cross-sectional SEM images of membrane surface. **(d)** Membrane selectivity for dyes separation through the size sieving or Donnan effects; Ultraviolet absorption spectra of mixed dyes (NR: neutral red, JB: Janus green B and AF: acid fuchsin) before and after filtration. Reprinted with permission from Ref (Xia et al., 2020). Copyright 2020 American Chemical Society.

ml of nanogels were dissolved in water. Then, 0.5 ml of the solutions were applied to the plates' surface, and the zone of inhibition was measured after 24 h. According to the DLS technique, the average size of the pNIPAM nanoparticles synthesized in various NIPAM: N,N-methylenebisacrylamide (BIS) ratios were 131 ± 78, 312 ± 71, and 483 ± 35 nm. It was observed that the average pNIPAM-NH_2 nanoparticles sizes were slightly higher (135 ± 59, 174 ± 10, and 532 ± 48 nm). The UV-VIS spectra revealed the encapsulation of AgNPs in nanoparticles.

TEM images depicted the morphology and size of each particle. The pNIPAM and silver encapsulated pNIPAM-NH_2 nanoparticles were spherical, and AgNPs were in the 1–35 nm range. Moreover, it was observed that silver encapsulated pNIPAM-NH_2 nanoparticles consisted of larger silver particles compared with silver encapsulated pNIPAM nanoparticles, which can be related to the extra positive charge of amine groups. The amine groups available on the PNIPAM surface were also verified using the XPS technique. In terms of liquid culture, for particles synthesized in various NIPAM: BIS ratios of 131 ± 78, 312 ± 71, and 483 ± 35 nm, the average inhibition zones of silver incorporated pNIPAM nanoparticles were 48 ± 2, 36 ± 6.08, and 28 ± 2 mm against *E. coli* and 24 ± 2.64, 20 ± 4.58, 16 ± 2.64 mm against *S. aureus*, respectively. On the other hand, silver incorporated pNIPAM-NH_2 particles exhibited the inhibition zone of 58 ± 8.71, 50 ± 4.35, and 30 ± 1 mm against *E. coli* and 27 ± 2, 22 ± 1, and 20 ± 4.35 mm against *S. aureus*. Results verified that the addition of NH_2 resulted in the improvement of antimicrobial activity.

Wongpreecha et al. (2018) synthesized AgNPs, which were stabilized with chitosan through a green procedure. To this end, chitosan was dissolved in acetic acid and mixed with $AgNO_3$ solution. Then, a 15 psi pressure was applied to the as-prepared mixture. Besides, the experiment was performed without applying pressure. Agar disk diffusion technique was utilized to assess the activity of antibacterial of the synthesized nanoparticles. 40 μl of the as-prepared nanoparticle suspension was placed on a plate and exposed to the surface of Mueller-Hinton Agar. After 24 h of incubation, the inhibition zone diameter was measured.

Moreover, the minimum bactericidal concentration (MBC) was evaluated using a broth dilution method. Typically, dilutions of 0.4 wt% solutions of the synthesized nanoparticles in tryptic soy broth were put on 48-well plates and incubated with E. coli and S. aureus. Surface plasmon resonance (SPR) analysis indicated the creation of nanoparticles of silver. According to the XRD pattern, the crystallite size of the silver-chitosan nanoparticles was 12.7 nm. TEM analysis revealed that the nanoparticles were spherical with >20 nm size, and no significant agglomeration was observed. Results depicted that the MBC value for silver-chitosan nanoparticles was 39.1 μg/ml and 312.5 μg/ml against *E. coli* and *S. aureus*, respectively. Moreover, the inhibition zone was estimated at 37.2 ± 16.4 nm.

2.3. Green metal-organic frameworks (MOFs)

MOF structures are also utilized in the matrix membranes to enhance water filtration and removal (Abdollahzadeh et al., 2021; Ahmadi et al., 2020; M Izzah Binti Mohammad et al., 2019). Yin et al. (2020b) synthesized three types of MOFs, including MWMIL-101(Cr), MW-UiO-66, and MW-ZIF-8, and incorporated the particles into the PVDF membranes. Particles were synthesized through the microwaved-assisted solve-hydrothermal technique. MOF/PVDF mixed matrix membranes (MMMs) were fabricated using the phase inversion method. Typically, MOF structures were dispersed in N,N-dimethylformamide (DMF), followed by the addition of PVDF and casting the as-prepared solution onto a glass plate. Then, the plate was immersed in deionized water, and the as-prepared membrane was separated. According to SEM micrographs, MW-MIL-101(Cr) and MW-UiO-66 structures exhibited octahedron shapes with 95 nm and 820 nm sizes, respectively. Besides, regular rhombic dodecahedron morphology of 4.2 μm was observed for MW-ZIF-8 particles. The incorporation of MOF particles into the membrane matrix was also verified by XRD analysis. No aggregation was observed in terms of the addition of 10–20 wt% MOF onto the MW-MIL-101(Cr)/PVDF membrane. In terms of MW-UiO-66/PVDF and MW-ZIF-8/PVDF membranes, the addition of 10–20 wt% of MOF particles resulted in the formation of regular octahedral and rhombohedral polyhedral shaped structures, respectively as well as the uniform dispersion. Results depicted <5% of NaCl rejection for MW-MIL-101 (Cr)/PVDF MMMs membranes, which can be attributed to the large pore size of the membrane in the 0.86–2.65 nm range, while >94% of NaCl rejection was observed for MW-UiO-66/PVDF or MW-ZIF-8/PVDF membranes.

One of the most promising applications of MOF-based membranes is in gas separation. MOFs can be incorporated into the polymer matrix of membranes to increase their selectivity and permeability. In particular, MOFs have shown great potential in the separation of CO_2 from flue gases and natural gas. For example, the incorporation of ZIF-8 (zeolitic imidazolate framework-8) into a polymeric membrane resulted in a significant increase in CO_2 permeability, while maintaining high selectivity over other gases. Similarly, a composite membrane made from a PVA matrix and MIL-101(Cr) MOF showed high CO2 permeability and selectivity, making it a promising candidate for CO_2 capture.

In addition to gas separation, MOFs have also been incorporated into membranes for water purification. The high surface area and tunable properties of MOFs make them ideal candidates for removing contaminants from water. For example, a composite membrane made from PVA and MIL-101(Cr) was shown to effectively remove heavy metal ions such as lead and cadmium from water. Similarly, a MOF-based membrane made from UiO-66-NH_2 and PVA was found to be highly effective at removing dyes from water. Another potential application of MOF-based membranes is in drug delivery. MOFs have high loading capacities and can be designed to release drugs in a controlled manner. For example, a MOF-based membrane made from MIL-101(Cr) was shown to effectively deliver the anticancer drug doxorubicin to cancer cells. The MOF membrane was able to control the release of the drug, resulting in a significant increase in the drug's efficacy compared to the free drug. Recent advances in MOF-based membranes have focused on improving their stability and scalability. One approach to improving stability is the use of post-synthetic modification (PSM) techniques. PSM involves modifying the surface of MOFs after their synthesis to improve their stability and performance. For example, the incorporation of hydrophilic groups onto the surface of MOFs can improve their stability in aqueous environments, making them more suitable for water purification applications. Another approach to improving MOF-based membranes is through the use of scalable fabrication techniques. One promising technique is the use of electrospinning, which involves the use of an electric field to spin a polymer solution into nanofibers. MOFs can be incorporated into the polymer solution to create MOF-based nanofibrous membranes. These membranes have high surface area and can be easily scaled up for industrial applications (Adatoz et al., 2015; Aguado et al., 2011; Qian et al., 2020; Jun et al., 2020).

Fu et al. (2021) coated a hybrid selective layer comprised of polyvinyl alcohol/polydopamine and ZIF-8 onto commercial membranes to enhance the fouling resistance of the membrane as well as the transport property. ZIF-8 nanostructures were synthesized through the dissolution of $Zn(NO_3)_2$–$6H_2O$ in methanol, followed by the addition of 2-methylimidazole. Polydopamine@ZIF-8 nanocomposite was synthesized through the dispersion of ZIF-8 nanoparticles in methanol and the addition of dopamine to the suspension. Membranes were prepared by mixing polyvinyl alcohol, glutaraldehyde, and H_2SO_4 with polydopamine@ZIF-8 suspension and coating the as-prepared mixture onto a commercial PES membrane.

According to SEM images, the size of ZIF-8 nanostructures was ≈80 nm, while it escalated up to ≈100 nm after modification with polydopamine. Moreover, it was depicted that, after dopamine modification, the surface charge of ZIF-8 nanoparticles was altered from positive to negative. Furthermore, BET analysis delineated that dopamine

modification resulted in a decrease in the surface area of ZIF-8 nanostructures from 1464 to 1168 m^2/g. In terms of the fabricated membranes, SEM micrographs revealed that adding 0.05–0.1 wt% of ZIF-8 nanostructures led to a uniform distribution over the surface with no surface cracks. Therefore, the as-prepared membrane was utilized as a forward osmosis membrane with improved water flux (pristine −8.7 and coated membrane- 14.2 L. m^{-2}. h^{-1}). Moreover, up to 93.8 ± 0.9 of $MgCl_2$ rejection was obtained using the fabricated membranes.

Parkerson et al. (2020) have fabricated membranes using commercial nanofiltration membranes comprised of a polyamide and a PES layer and modified MOF for dye removal from the aqueous solution. They successfully synthesized Cu-MOF and modified them with dopamine which acted as binder, functionalizing agent, and stabilizer to incorporate onto a thin-film composite (TFC). Typically, Cu-MOF nanostructure was synthesized through the ultrasonication of 1,3,5-benzenetricarboxylic acid (BTC) and copper nitrate hemipentahydrate in water. Then, membrane functionalization was performed via dynamic filtration-assisted coating and static dip-coating.

Commercial membranes were immersed in the dip-coating procedure in the Cu-MOF/dopamine solution followed by sonication. On the other hand, for filtration-assisted coating, surface functionalization was achieved using pristine membrane through cross-flow filtration of Cu-MOF/dopamine solution. According to SEM and TEM micrographs, Cu-MOF nanoparticles were synthesized in a crystalline structure and 32 nm size. Moreover, the XRD spectrum revealed that the size of the Cu-MOF nanostructure was ≈32.2 nm. Furthermore, SEM images of membranes delineated the formation of a Cu-MOF/polydopamine layer over the surface. Besides, it was depicted that the addition of MOF to the membrane surface increased the surface roughness. Meanwhile, membranes fabricated through the filtration-assisted method exhibited a higher surface roughness than membranes prepared through the dip-coating procedure, related to the agglomeration and nonuniform polymerization caused by filtration shear stress.

On the other hand, membranes fabricated using the dip-coating method depicted more negative surface area compared to the filtration-assisted technique, which can be related to MOF agglomeration and nonuniform polymerization through the filtration method. Regarding the membranes' performance, membranes fabricated via filtration-assisted method exhibited ≈15% lower water flux than membranes fabricated using the dip-coating method. Moreover, 46% and 62% methylene blue and 79% and 85% methyl orange rejection rates were observed for membranes fabricated using filtration-assisted and dip-coating methods.

Li et al. (2018) synthesized Zr-based MOF (UiO-66-$(COOH)_2$) nanostructures and incorporated them polyurethanes foam (PUF) membrane through the in-situ hydrothermal synthesis and hot-pressing technique. The Zr-MOF nanostructure was synthesized by the dissolution of $ZrCl_4$ and 1,2,4,5-benzenetetracarboxylic acid (H_4BTEC) in deionized water followed by heating at 100 °C. The membrane was fabricated via the addition of synthesized nanostructures to the PUF membranes using a hydrothermal synthesis procedure followed by the hot-pressing method. SEM micrographs of the membrane revealed the distribution of Zr-MOF structures to the internal structure. Moreover, no significant agglomeration was observed in the SEM images. Besides, BET analysis delineated that the membrane surface area and pore sizes were 1.451 m^2/g and 5.682 nm, respectively.

The experimental kinetic data for dye removal followed the pseudo-second-order model (PSO). Moreover, it was verified that the addition of NaCl to the dye solution improved the Congo red removal, but it reduced the methylene blue removal and showed no effect on rhodamine B removal rates. The as-prepared membrane removed rhodamine B, methylene blue, and Congo red dyes from aqueous solutions. According to results, 98.8%, 97.57%, and 87.39% removal efficiency was obtained for rhodamine B, methylene blue, and Congo red, respectively.

Yang et al. (2018) synthesized Zn/Co-ZIF nanostructure on a flexible substrate and utilized the as-prepared membrane for heavy metal removal from aqueous solutions. To this end, a cloth was immersed in Carboxymethylcellulose sodium (CMC) solution through a dip-coating method. On the other hand, $Co(NO_3)_2{\cdot}6H_2O$ and $Zn(NO_3)_2{\cdot}6H_2O$ were dissolved in methyl alcohol (solution A), and 2-methylimidazole was dissolved in methyl alcohol (solution B). Then, CMC-cloth was treated with the prepared solutions. According to SEM images, the addition of CMC to the cloth surface resulted in the surface roughness improvement. Moreover, a more uniform and compact distribution of Zn/Co-ZIF nanostructures was observed for membranes treated with CMC. Moreover, it was delineated that the Zn/Co-ZIF particles were synthesized in rhombic dodecahedral shape in the 500–600 nm range. Results showed Pb(II) adsorption capacity was 862.44 mg/g with the removal efficiency of >80%, which declined to 79.12% after the 5th cycle of utilization.

Sun et al. (2018) synthesized hydrophilic hollow ZIF-8 through surface-functionalization-assisted etching technique. To this end, ZIF-8 particles were synthesized by dissolution $Zn(NO_3){\cdot}6H_2O$ and 2-methylimidazole in methanol, followed by mixing. Then, to modify the synthesized particles, they were dispersed in tannic acid solution. Membranes were fabricated through the phase-inversion procedure. Modified ZIF-8 particles were dispersed in N-Methyl-2-pyrrolidone, and PES was added to the mixture after the sonication. The solution was cast onto a glass surface and immersed in deionized water. Membranes were fabricated through phase separation and solidification. TEM images depicted the polyhedral shape of ZIF-8 particles with ≈400 nm size. Moreover, it was illustrated that the treatment of ZIF-8 with tannic acid led to forming a hollow structure with 25 nm shell thickness. Based on N_2 adsorption and desorption curves, the average pore size and surface area of ZIF-8 particles were ≈0.86 nm and 1368 m^2/g, respectively. Furthermore, it was verified that modification of ZIF-8 particles resulted in a plummet in surface area (957 m^2/g), which can be related to partial amorphization through acid treatment. FE-SEM images of the as-prepared membranes exhibited the formation of finger-like pores with the porosity up to 71.4%. Besides, the surface pore diameter average of the membranes was in the 3.5–17.5 nm range. In terms of membrane performance, water flux and bovine serum albumin (BSA) rejection rate were estimated at 597 L m^{-2} h^{-1} and >98%, respectively. Meanwhile, it was delineated that the addition of ZIF-8 structures improved the fouling resistance of the membrane. Moreover, a comparison between different membranes based on green additives in terms of their surface area, application, and biohazardous removal has been conducted (Table 2).

2.4. Green nanocomposite membranes

Several studies have focused on synthesizing nanocomposites using green additives and utilizing them in membrane matrix for water purification. For example, Liu et al. (2019a) fabricated a thin-film nanocomposite membrane through the incorporation of 2,2,6,6-tetramethylpiperidine-1-oxyl radical (TEMPO)-oxidized cellulose nanofibers (CNF) as an environmentally friendly agent into the membrane polyamide layer. To this end, CNF was synthesized through the dispersion of wood pulp in deionized water followed by the addition of sodium bromide and 2,2,6,6-tetramethyl-1-piperidinyloxy. Then, a polyamide layer was coated onto a polysulfone (PS) membrane surface via interfacial polymerization. Various chemicals such as phenylenediamine, triethylamine, caprolactam, surfactant, and CNF were utilized to prepare the aqueous phase, and the PS membrane was immersed in the as-prepared solution. Finally, the organic solution of trimesoyl chloride was poured oner the surface, and the treated membrane was rinsed with water.

According to TEM images, CNF structures were synthesized in rod shape in the 250–550 nm length and 3–10 nm diameter ranges. The surface morphology of the as-prepared membrane was evaluated using SEM micrographs, and it was depicted that the addition of CNF did not significantly change the morphology. Furthermore, TEM images depicted that the addition of CNF particles resulted in reducing top layer

Table 2
A comparison between different membranes based on green additives in terms of their surface area, application as well as the biohazardous removal.

Type	Green additive	Size area (m^2/g)	Application	Removal (%, inhibition zone, or adsorption capacity)	Refs.
Fe_2O_3 nanofiber supported ZIF8	Methanol	–	Photocatalytic degradation of Reactive Red 198 (RR198)	94.27%	Mahmoodi et al. (2019a)
Activated carbon-MIL 101 (Cr)	Cucumber peels	2412.1	Acid Green 25 (AG25) and Reactive Yellow 186 (RY186) dyes removal from the binary systems	Up to ≈90%	Mahmoodi et al. (2019b)
COOH/TA-$Ni_{50}Co_{50}$-Layered double hydroxide (LDH)/UiO-66(Zr)-$(COOH)_2$ nanocomposite	Water	69	Heavy metal removal from aquatic environments	Hg (II) 509.8 mg/g, Ni (II) 441 mg/g	Soltani et al. (2021a)
$Ni_{50}Co_{50}$-Layered double hydroxide (LDH)/UiO-66(Zr)-$(COOH)_2$ nanocomposite	Water, Ethylene glycol, Ethanol	–	Cd(II) and Pb(II) removal	Cd(II) 415.3 mg/g, Pb(II) 301.4 mg/g	Soltani et al. (2021b)
Co-MOF and ZIF-67	Anhydrous methanol, Water	(Co-MOF) 10.44, (ZIF-67) 1208.87	Congo red removal from aqueous solution	(Co-MOF) 1019.06 mg/g, (ZIF-67) 1044.58 mg/g	Guo et al. (2020)
Sn(II)-Benzene-1,4-dicarboxylic acid (BDC) MOF	Distilled water	17	Toxic anionic dyes including Congo Red (CR), Erichrome Black T (EBT), and Eosin Yellow (EY) removal from aqueous solution	(CR) 95.2 mg/g, (EBT) 125 mg/g, (EY) 208.3 mg/g	Ghosh and Das (2020)
Titania nanofiber-Fe based MIL 100	Water	1194.48	Methylene Blue (MB) photocatalytic degradation	99.4%	Oveisi et al. (2019)
Aluminum-succinic based MOF	Water	358.03	Azo dye Acid Black 1 removal from aqueous	739.3 mg/g	Jung et al. (2018a)
(NH2-CNT/Fe2O3)-ZIF8	Water, Methanol, Ethanol	1659	Malachite Green (MG) and Rhodamine B (RhB) removal from binary system	>95%	Mahmoodi et al. (2019c)
Polypyrrole/aluminum fumarate-MOF	Water	809	Pb(II) removal from aqueous solutions	600 mg/g, ≈92%	Zayan et al. (2020)
Al-MOF/Fe3O4/PDA@Ag	Water	54.31	Ciprofloxacin, Norfloxacin, Methyl orange	(Ciprofloxacin) 81.7%, (Norfloxacin) 80.1%, (Methyl orange) 98.2%	Wang et al. (2020a)
MIL-100(Fe) immobilized onto bacterial cellulose (BC) nanofibers	Water	47.13 ± 0.15	Arsenic and Rhodamine B removal from aqueous solution	(Rhodamine B) 2.77 mg/g, (Arsenic) 4.81 mg/g	Ashour et al. (2020)
BUC-21/titanate nanotube	Water	–	Cr (VI) reduction and Cr (III) removal	(Cr(VI) reduction) 100%, (Cr(III) removal) 97.6%	Wang et al. (2019a)
MOF-Fe, MOF-Al, MOF-Cu	Water	–	Silicic acid removal from aqueous solutions	(MOF-Al) 182.2 mg/g, (MOF-Fe) 157.7 mg/g, (MOF-Cu) 201.4 mg/g	Ni and Fox (2020)
Biomass-C@MIL-53-C Carbon Aerogels	Aqueous solution	–	Oils and organic solvents adsorption	(adsorption capacity) 35–119 times higher than the adsorbent weight	Chen et al. (2020)
ZIF-8 membrane	Aqueous solution	–	NaCl and Na_2SO_4 rejections	(NaCl) 64.7%, (Na_2SO_4) 92.2%	Xu et al. (2021)
Al@Fe-MOF	Water	1368	Selenite adsorption	75.33 mg/g	Ye et al. (2019)

thickness. Furthermore, NaCl rejection of the membrane reached up to 96.2% using the as-prepared membrane. Besides, the addition of CNF improved the eater flux compared to the initial membrane.

Hubadillah et al. (2018) have fabricated ceramic hollow fiber membranes using green silica synthesized from waste rice husk and utilized them for water treatment. To this end, rice husk was burned in a furnace, and the obtained silica was milled and sieved. Membranes were fabricated via phase inversion followed by sintering. Suspensions were prepared through the dissolution of dispersant insolvent and the addition of certain amounts of silica. After ball milling the mixture, PES was added and homogeneously mixed. The final suspension was extruded, and the as-prepared membrane was immersed in water for inversion of the phase. Then, membranes were sintered at the 1200°-1400 °C range.

According to TEM images, the size of synthesized amorphous and crystalline silica particles was 2 μm and 1 μm, respectively. Furthermore, BET analysis illustrated that the surface area of amorphous silica (43.5 m^2/g) was higher than the crystalline one (7.7 m^2/g). SEM images of the as-prepared membranes illustrated that the addition of amorphous silica resulted in finger-like pores, while no finger-like pores were formed in terms of the addition of crystalline silica to the membrane matrix, which can be attributed to an increase in the viscosity of the membrane suspension. Besides, it was delineated that the incorporation of silica particles led to an increment in the membrane mechanical strength.

In terms of pore size distribution, membranes fabricated using amorphous silica particles exhibited sponge-like pores in the 1.63–3.41 μm range, while a broader range (0.55–2.3 μm) was observed for membranes fabricated using crystalline silica particles. In addition, the initial water flux of the membranes was measured in the ≈500 L m^{-2} h^{-1} range.

Chang et al. (2017) utilized triethyl phosphate (TEP) as a non-toxic and green solvent to fabricate PVDF hollow fiber membranes. To this end, dope solutions were synthesized by adding certain amounts of PVDF to the N-methyl-2-pyrrolidone (NMP) and triethyl phosphate (TEP) solvents. After homogeneous mixing, solutions were spun, while water/isopropanol or water/TEP were used as a coagulant. The as-prepared fibers were then immersed in water for 3 days. According to FE-SEM images, membranes fabricated using 88% NMP and 88% TEP exhibited the densest and the most porous (89.7%) structure, respectively. Furthermore, the surface porosity of membranes prepared using 88% TEP was significantly higher (20–30 times) than membranes fabricated using 88% NMP, which can be related to the solvent viscosity. At an optimum point, the membrane permeation flux was reached up to 20 kg $m^{-2}.h^{-1}$ at 1.8 bar in addition to great mechanical strength ≈99.99% NaCl rejection was observed at 60 °C (Table 3).

Table 3
Different types of nano-membranes based on the used green additives for high-efficiency water treatment applications.

Type	Green additive	Size (nm)	Application	Removal (%, inhibition zone, or adsorption capacity)	Refs.
Cobalt ferrite silica magnetic	Salix alba bark extract	15.41 ± 0.65 (TEM), 15-51 (XRD)	Malachite green dye removal from water	75.5 ± 1.21 mg/g	Amiri et al. (2017)
Expanded graphite/layered double hydroxides	Deionized water	42-31(XRD)	Cr(VI) removal from aqueous solutions	13.44 mg/g	Hu et al. (2019)
EDTA modified Fe_3O_4/sawdust carbon	Water	638 (DLS)	Cadmium removal from water	63.3 mg/g	Kataria and Garg (2018)
Poly(vinylimidazole) grafted xanthan gum/montmorillonite	Water	–	Antibacterial activity against *S. aureus*, and *E. coli* Malachite green (MG) dye removal	(MG adsorption) 909.1 mg/g, Inhibition zone diameter (mm): (E. coli) 24.0 ± 0.81, (S. aureus) 26.0 ± 0.25	Elella et al. (2021)
Curcumin based Fe_3O_4 nanoparticles	Water	Fe_3O_4: 20–30 (SEM)	Hg(II) removal from aqueous solution	144.9 mg/g	Naushad et al. (2019)
Layered double hydroxide/UiO-66-(Zr)-$(COOH)_2$	Water, Ethylene glycol, Ethanol	Average pore diameter: 1.9 (BET)	Cd(II) and Pb(II) removal from water	Cd (II) 415.3 mg/g, Pb (II) 301.4 mg/g	Soltani et al. (2021b)
TiO_2/Graphene oxide (GO)	*Chlorella pyrenoidosa* green alga, Water	TiO_2: 50 (SEM)	Crystal violet removal from aqueous solution under visible light	63%	Sharma et al. (2018a)
ZnO–Ag	*Thymus vulgaris* leaf extract	Ag nanoparticles: 5 (TEM)	Antimicrobial activity against E. coli and S. aureus, Photocatalytic activity against phenol	Inhibition zone: 15 ± 0.21 (E. coli), 18 ± 0.24 (S. aureus), 97.2% (maximum photocatalytic activity against phenol)	Zare et al. (2019)
Functionalized mesoporous fibrous silica KCC-1, oleic acid, and chitosan	Water, Ethanol	300-400 (FESEM, TEM)	Pb(II) removal from aqueous solution	168 mg/g	Zarei et al. (2019)
g-Fe_3O_4/rGO	*Averrhoa carambola* leaf extract	TEM: 46 ± 2 (Fe_3O_4), 32 ± 2 (g-Fe_3O_4),	Cr(VI) reduction, Phenol degradation, Antibacterial activity against S. aureus, B. Subtilis, And E. coli	97% Cr(VI) reduction, 76% (Phenol degradation), Inhibition zone (mm), 16 (S. aureus), 10 (B. subtilis), 11.2 (E. coli)	Padhi et al. (2017)
Rhodium/GO	Ethanol, Water	TEM, HRTEM: 1.8 ± 0.4 (Rhodium nanoparticles)	4-nitrophenol reduction in presence of NaBH4	≈99%	Liu et al. (2019b)
Ag/Fe_3O_4/rGO	Punica Granatum peel extract, Ethanol, Water	FE-SEM: 31 (Ag), 33 (Fe_3O_4), TEM: 25 (Ag/Fe_3O_4), XRD: 21 (Ag/Fe_3O_4/rGO)	4-nitrophenol (4-NP), methylene blue (MB), methyl green (MG), and methyl orange (MO) reduction from water	Complete reduction	Adyani and Soleimani (2019)
Fungus hyphae/Fe_3O_4/GO	Water	–	Methyl violet and uranium removal from water	117.35 mg/g (methyl violet), 219.71 mg/g (uranium)	Zhu et al. (2019a)
Ag–Cr-Activated carbon	*Azadirachta indica* leaf extract	40-150 (SEM)	Reactive Red (RR) and Crystal Violet (CV) removal from water	64.92% (RR), 82.47% (CV)	Saad et al. (2017)
CuO/ZnO	Melissa Officinalis L. leaf extract	TEM: 10-20 (CuO)	4-nitrophenol (4-NP) and Rhodamine B (RhB) reduction from water	Complete reduction	Bordbar et al. (2018)
Ag–Cu_2O/glucose rGO	Water, Glucose	SEM, TEM: <200 (Cu_2O), 60 (Ag)	Methyl orange photodegradation	90	Sharma et al. (2018b)

3. Mechanistic aspects of green synthesis of nano-membranes

There are a variety of techniques for the treatment of wastewater based on nano-membranes. Typically, the physical, chemical, and biological methods can be named, applied conventionally based on sedimentation, flocculation, advanced oxidation process (AOPs), adsorption, ion exchange, reverse osmosis, membrane-based filtration, ultra-filtration. However, understanding the mechanisms controlling the removal of pollutants by green nano-membranes would support further developments. Among the classical approaches, AOPs, photocatalysis, ozonation, Fenton reaction, and combinations of the aforementioned methods are used worldwide to degrade organic contaminants. These methods can be applied simply with acceptable reproducibility and usually end with inadequate purification efficiency (Chong et al., 2010; Bremner et al., 2009). AOP is grounded on an in-situ generation of non-selective yet highly reactive chemical oxidants such as radicals of hydroxyl and oxygen or H_2O_2 and O_3, which promisingly facilitates the degradation of highly resistant non-biodegradable contaminants. Undeniably, Fenton reaction based on radicals of hydroxyl seems an efficient, inexpensive, and sustainable technique to treat wastewater. When applying nanomaterials to remove pollutants, we have ample space to choose the pathway through which photolysis of photocatalysis takes place under UV light (Fig. 6). Other phenomena such as surface sorption (adsorption) and photodegradation can degrade the organic and

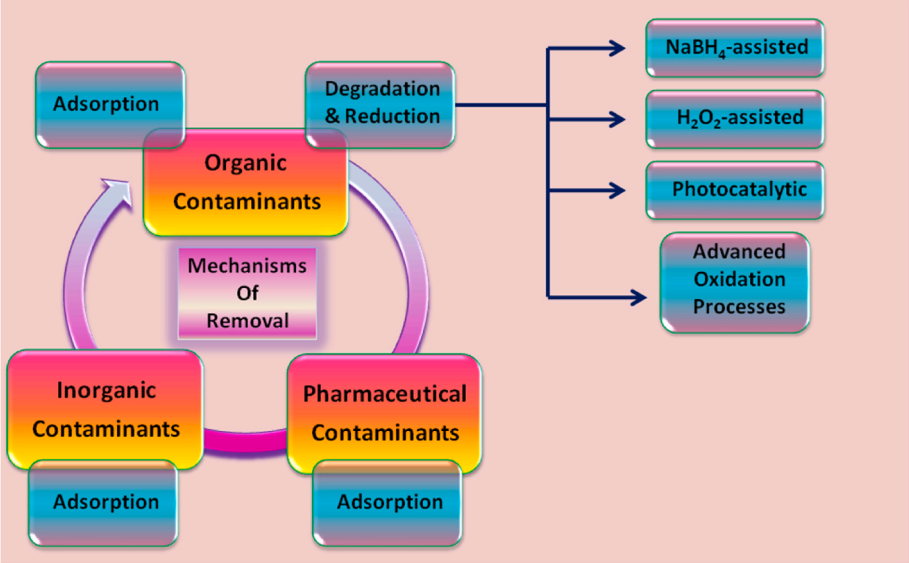

Fig. 6. A general view of the removal of pollutants by applying nanomaterials, which showed different types of contaminants and their removal mechanisms.

inorganic pollutants in the groundwater and freshwater sediments (Eskandarloo et al., 2017).

3.1. Adsorption of pollutants

Nanoparticles fabricated through green routes are promising candidates for the removal of very toxic chemicals. Typically, some mechanisms are straightforward to understand, but the complexity arises from complexation and/or chemical multiple interactions. The carcinogenic arsenic (As) present in the aqueous sources can be named a highly hazardous contaminant. For example, iron nanoparticles can accept As through the formation of FeOAs linkage (Wu et al., 2019a). The formation of such bonds is proved by Fourier-transform infrared spectroscopy (FTIR); moreover, X-ray photoelectron spectroscopy (XPS) was probed into arsenate anchored to the surfaces of iron nanoparticles. It was inferred that As removal proceeds with forming a monodentate chelating ligand followed by complexation of a bidentate binuclear. At best, an As adsorption capacity of nearly 14.617 mg g^{-1} onto iron nanoparticles was detected by changing pH between 4 and 6, such that anionic arsenate was adsorption in an optimal pH (Wu et al., 2019a). The facile synthesis of iron oxide nanoparticles for removing As(V) is an example of chemically adsorbed contaminants using green adsorbents.

3.2. Adsorption and photodegradation of organic contaminants

The adsorption of pollutants is not the only objective of researchers and developers of green adsorbents. The blend of conventional water treatment techniques such as oxidation and adsorption with photodegradation and/or Fenton-like mechanisms is more efficient and has been receiving much more attention in view of being combinatorial. In this strategy, both adsorption and in-situ degradation of pollutants into cleaner products take place simultaneously, and a wide range of pollutants are eliminated using a photodegradation treatment (Huang et al., 2017; Khodadadi et al., 2017). On the other hand, low efficiency or activity, low rate of oxidation, and very acidic nature of such decontaminations are shortcomings associated with the use of combinatorial processes. Indeed, individual approaches are economically more reasonable in the decontamination of water resources. For instance, biomimetic photocatalytic decontamination of pollutants by combining g–C_3N_4–imidazole-hemin and H_2O_2 was liable for very high photocatalytic oxidation activity once underwent solar irradiation (Chen et al., 2017). The exceptional structural and chemical properties of MOFs make them an attractive candidate for a wide range of applications, particularly as adsorbents for pollutants. MOFs are crystalline materials consisting of metal ions or clusters that are linked by organic ligands to form a three-dimensional (3D) porous structure with high surface area and tunable pore sizes. The unique properties of MOFs, such as high porosity, large surface area, and tunable pore sizes, make them excellent adsorbents for pollutants. Adsorption is a process in which a solid or liquid substance adheres to the surface of another substance. MOFs can act as an adsorbent for different types of pollutants, including heavy metals, organic pollutants, and gases. The high porosity of MOFs enables them to adsorb pollutants in large quantities, while the functional groups on their surface can interact with the pollutants through various chemical interactions, such as electrostatic attraction, hydrogen bonding, and van der Waals forces. Heavy metals are one of the most harmful pollutants found in wastewater, as they are toxic to both humans and the environment. MOFs have been shown to be effective in the removal of heavy metals from wastewater. For example, researchers demonstrated the use of a MOF-based membrane for the removal of cadmium from wastewater. The MOF membrane exhibited high adsorption capacity and selectivity for cadmium ions, with a removal efficiency of up to 99%. Organic pollutants, such as dyes and pesticides, are another major class of pollutants that pose a serious threat to the environment. MOFs have been shown to be effective for the removal of organic pollutants from wastewater. For example, scientists demonstrated the use of a MOF-based membrane for the removal of methylene blue, a common dye pollutant. The MOF membrane exhibited high adsorption capacity and selectivity for methylene blue, with a removal efficiency of up to 95%. Gaseous pollutants, such as carbon dioxide and methane, are also a major concern due to their impact on climate change. MOFs have been shown to be effective for the adsorption of gaseous pollutants. For example, a groupd of scientists demonstrated the use of a MOF-based membrane for the adsorption of carbon dioxide from flue gas. The MOF membrane exhibited high adsorption capacity and selectivity for carbon dioxide, with a separation efficiency of up to 90%. MOFs have also been used as green membranes for the removal of pollutants from the air. For example, researchers demonstrated the use of a MOF-based membrane for the removal of volatile organic compounds (VOCs) from indoor air. The MOF membrane exhibited high adsorption capacity and selectivity for VOCs, with a removal efficiency of up to 90%. In addition to their high adsorption capacity and selectivity, MOFs have other advantages as green membranes for the removal of pollutants. MOFs can be easily synthesized using green and sustainable

methods, such as microwave-assisted synthesis and solvent-free synthesis. Moreover, MOFs can be easily modified to enhance their adsorption properties, such as increasing their surface area, adding functional groups, and tuning their pore size (Peng et al., 2018; Gargiulo et al., 2020; Wang et al., 2016; Lee et al., 2018; Policicchio et al., 2017).

3.3. Reduction of pollutants and dyes

$NaBH_4$ is broadly used in the removal of pollutants because of being a highly water-soluble reductant among a wide range of reducing agents. It has the edge over hydrogen sources used as a reductant for poisonous nitro compounds. It is a powerful adsorbent of amino compounds in aqueous media. Activation of $NaBH_4$ is the critical process, which needs a metal substrate playing the role of the active site because metal

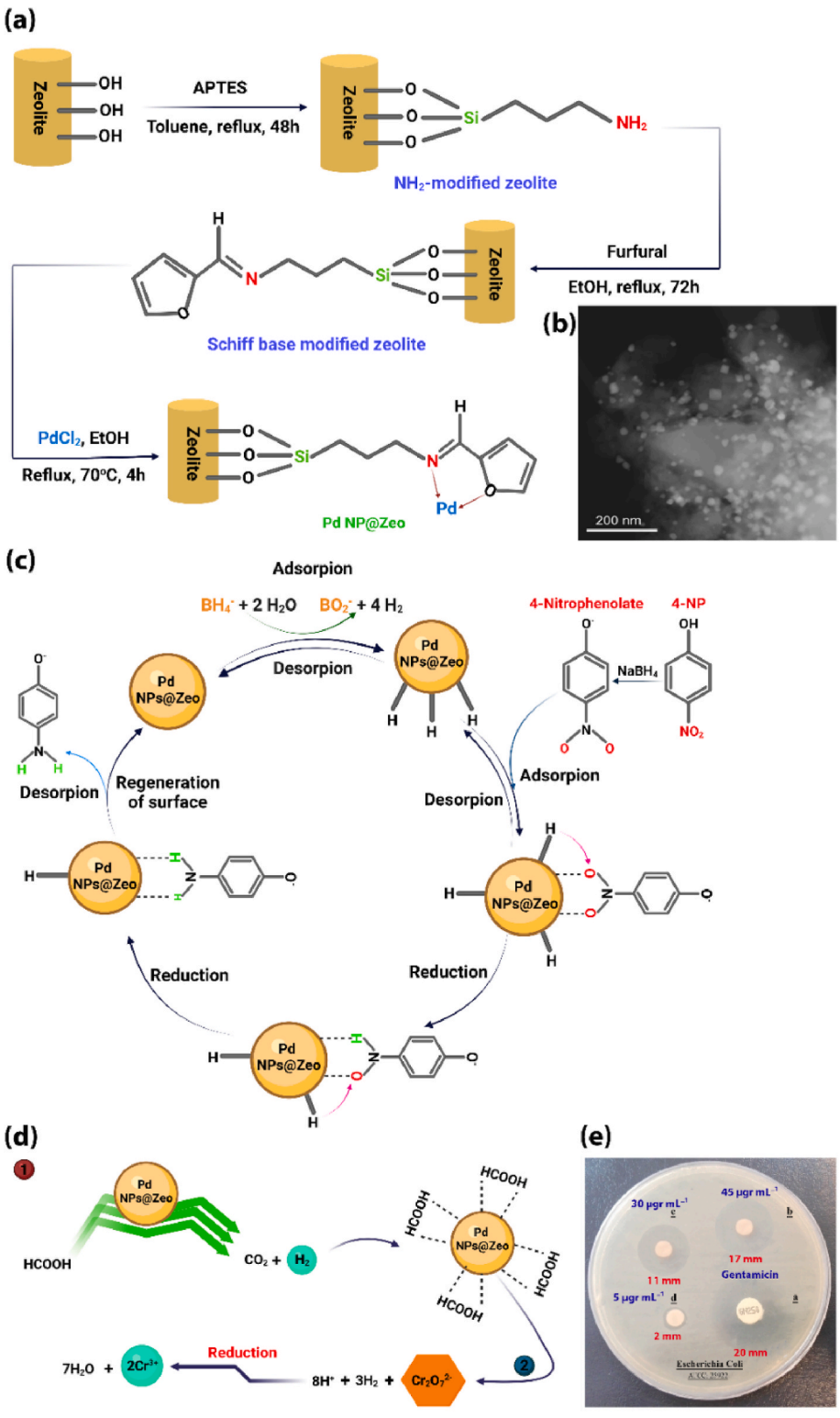

Fig. 7. **(a)** The fabrication of palladium nanocatalyst stabilized on amine-modified zeolite (PdNPs@Zeo); Synthesis of the NH_2 modified zeolite (Zeo-NH_2): Refluxing the mixture of zeolite and (3-aminopropyl) triethoxysilane (APTES) in anhydrous toluene for 48 h. Preparation of the Schiff base modified zeolite (Zeo-Sch): Adding the Zeo-NH_2 into furfural, transferring the resultant mixture into EtOH, and refluxing for 72 h. Construction of the PdNPs@Zeo: I) Stirring the Zeo-Sch and Palladium chloride ($PdCl_2$) in EtOH at 70 °C for 4 h. II) Filtration, rinsing with EtOH, and drying the nanocatalyst. **(b)** The PdNPs@Zeo SEM image. **(c)** The plausible mechanism for reduction of 4-nitrophenol (4-NP) using the PdNPs@Zeo. **(d)** The reduction of hexavalent chromium by using the PdNPs@Zeo. **(e)** The antibacterial activity of PdNPs@Zeo at different concentrations against *E. coli*. Reprinted with permission from Ref (Nasrollahzadeh et al., 2020). Copyright 2020 Elsevier.

hydride complexes formed by BH_4^- ions through π-π interactions are mechanistically explained to be intermediates for reduction (Nasrollahzadeh et al., 2020). For example, $NaBH_4$ was used as a reductant of the toxic 4-NP, where the Pd nano-catalyst was used to stabilize amine-modified Pd nanoparticles onto zeolite (PdNPs@Zeo) *via* π-π interactions (Fig. 7) (Nasrollahzadeh et al., 2020). The PdNPs@Zeo reductant facilitates the conversion of $NaBH_4$ into molecular H_2 along with BO_2^- anions dissociated on the surface of the nano-catalyst. At that locus, the adsorbed 4-NP forms interaction with the H_2 gas dissociated, leading to a stepwise 4-NP reduction to form 4-aminophenol. The resulting aminophenol will eventually be detached from the nano-catalyst surface to put the subsequent catalytic into action. Nano-catalyst imparts to adsorption of molecular H_2 as well as 4-NP to expedite reduction.

3.4. Photocatalytic degradation of organic pollutants

Regardless of the action of nanomaterials in adsorption of pollutants or catalytic degradation by the aid of photocatalysis, $NaBH_4$, and H_2O_2, green nanoparticles are exceptional aids of photocatalytic water purification (Fig. 7). Toxic organic pollutants can be disintegrated (Yaqoob et al., 2020) or completely mineralize to harvest water, carbon dioxide, or inorganic ions. Normally, a semiconducting nanoparticle like TiO_2 can absorb the light with band gaps wider or even equal to semiconductors, creating electron-hole pairs (e^--h^+). As a result of the reduction-oxidation (redox) reaction, the nano-catalyst surface strongly interacts with the species adsorbed onto the catalyst's surface. Moreover, h^+_{vb} will react with the surface-bound water molecules and assists the formation of %OH, and concurrently photo-reduction proceeds between the e^-_{cb} and the selected oxygen leading to the generation of a superoxide radical anion. There has been continued attempt to develop green photocatalytic moieties on the bedrock of metal-organic frameworks (MOFs). MOFs are well-known for their potential application to degrade toxic organic micropollutants (Lin and Maggard, 2008; Toyao et al., 2013).

4. Applications of green membranes

The precipitous industrialization and stipulation of recycling and recovering valuable materials urged an efficient development of separation tools and increased utilization. As a result, for the last few decades, membrane usage has been growing by leaps and bounds in a broad field of applications, compared to other purification and separation methods, due to low energy consumption and high-quality effluent, in addition to the compact designs and installation (Xie et al., 2020; Nunes et al., 2020; Wang et al., 2019b). Further, in the era of increased environmental awareness, more research is focused on making the membrane industry 'green' to attain sustainable development.

Remarkably, the 'green' membrane technology involves numerous approaches such as the use of biodegradable polymers and non-toxic solvents for membrane coating/casting instead of non-biodegradable petroleum-based products and hazardous solvents; recycling of useful membrane components; minimum number of preparatory steps to reduce energy consumption and waste generation; recycling of waste brine or sludge; waste reduction by antifouling characteristics; and energy generation from wastes (Xie et al., 2020; Jiang and Ladewig, 2020; Aburabie et al., 2020; Carner et al., 2020).

Nowadays, membrane separation systems are progressively being used as a promising tool to address environmental health and energy crisis. Though the list of their applications is interminable, some applications of such eco-friendly membranes have been portrayed in the following sections for water treatment, organic solvent recovery, removal of therapeutics and pharmaceutical contaminants, and other applications.

4.1. Water treatment

The diminishing amount of potable water is becoming a formidable challenge worldwide, especially to developing countries. In the existing situation, desalination and wastewater treatment are the most appropriate resolutions that can ensure the safe and adequate amount of water supply to the ever-growing population perpetually, as the tremendous amount of water resides in the oceans and abundant wastewater is generated from day-to-day activities (Sharma et al., 2021). Although several approaches have been executed, the membrane separation systems have become one of the most popular technologies for water purification, desalination, and wastewater treatment (Cheng et al., 2019; Sargazi et al., 2019; Karim et al., 2019). Desalination mainly requires removing inorganic salts to purify water; on the other hand, wastewater treatment needs to get rid of heavy metals, organic dyes, pesticides, and oily substances in addition to the inorganic salts.

At first sight, it may not seem like a realistic and economical approach to treat a vast amount of water with membranes, but thanks to all cost-effective, efficient, and easily scalable technologies, it was feasible to execute the idea into actual practice fabricating high-performance membranes.

For instance, Han and his team (Han et al., 2013) developed ultrathin (22–53 nm) graphene nanofiltration membranes on microporous substrates, which presented 20–60% retention of ionic salts (0.02 M) with retention order, i.e., Na_2SO_4 > NaCl > $MgSO_4$> $MgCl_2$ according to Donnan exclusion principle in addition to complete rejection of organic dyes. Here, only 34 mg of rGO was used to fabricate a square meter of the membrane, which inferred the new generation of cost-effective and resource-saving technology for water purification.

Typically, microfiltration, ultrafiltration, nanofiltration, reverse osmosis, pervaporation, membrane distillation, and electrodialysis account for the most regularly employed membrane operations for water purification. Usually, as the separation efficiency of membranes increases, the matrix pore size keeps on decreasing, necessitating increased pressure application. Therefore, the mechanically stable, flexible, and thermal resistance synthetic polymers are most frequently used, including PVDF, PAN, polytetrafluoroethylene (PTFE), PS, PES, polyetherimide (PEI), and polyethylene; or inorganic materials such as ceramics or metals. Although these fossil-based polymers endow the membranes with improved performance, their harmful impacts on the environment and health cannot be overlooked. Therefore, the synthetic polymers are being replaced by biodegradable polymers such as polylactic acid (PLA), polyhydroxyalkanoates (PHA), polybutylene succinate (PBS), alginate, cellulose, chitin, chitosan, collagen, lignin, and sericin (Xie et al., 2020; Jiang and Ladewig, 2020; Aburabie et al., 2020; Abdellah et al., 2018; Wu et al., 2019b; Sagle and Freeman, 2004; Galiano et al., 2018).

Albeit, the use of biocompatible membrane technology can be traced back to 1960 when cellulose acetate-based polymer membranes were first commercialized to produce potable water *via* RO desalination (Loeb, 1965). However, at that time, the use of natural polymer was superseded by synthetic polymers attributed to the difficult production of functionalized cellulose acetate.

Currently, the environmental awareness and depletion of fossil fuels have again aroused attention towards the use of green membrane technology, and their suitability has been progressively examined for different fields of application. Furthermore, the membrane systems have been studied to have the excessive potential for selective removal of contaminants and recovery of value-added products.

4.1.1. Removal of solid waste

Introducing inexpensive, efficient, and green technologies for membranes fabrication has surmounted the concerns like membrane fouling, high expenses, and low permeate flux and justified the efficient separation via adsorption, electrostatic attraction, or size exclusion mechanisms (Efome et al., 2018; Zeng et al., 2019). As a result, different

membranes systems have emerged as an effective tool to treat wastewater in multiple ways. The membrane technologies particularly, direct membrane filtration, and less frequently, forward osmosis and dynamic membranes, were elucidated for initial concentration of organic and particulate matters in municipal wastewater before primary and secondary treatments, whereas ultrafiltration, nanofiltration, and RO are used for final processing of water and removal of specific organic and inorganic constituent (Sharma et al., 2021; Nascimento et al., 2020; Donato and Drioli, 2021). The organic wastes such as dyes from textile and dye manufacturing industries and the pesticides from agriculture-based wastewater provoke serious health and environmental hazards (Cheng et al., 2019; Kandambeth et al., 2017; Mitra et al., 2016), although the proper channelization of the organic waste towards anaerobic digestors facilitates the generation of biogas and fertilizers.

Additionally, the recovery and recycling of valuable products such as heavy metals and rare earth metals render economical and eco-friendly industrial processes (Nascimento et al., 2020; Verma and Sharma, 2017). The membranes systems fabricated from sustainable materials and solvents have shown excellent performance for removing organic compounds along with suitable solvent permeance (Table 4).

The utilization of green-synthesized nanoparticles is itself an effective approach to degrade harmful products from wastewater. For instance, the AgNPs (15–50 nm) synthesized using *Zanthoxylum armatum* leaves were effective in degrading mutagenic and thermal resistant organic dyes, including methyl orange, methyl red, Safranine O, and methylene blue via their catalytic reduction (Jyoti and Singh, 2016). Furthermore, the photocatalytic degradation of recalcitrant organic matter in petroleum refinery wastewater was elucidated using green synthesized TiO_2 nanoparticles as a catalyst in a membrane bioreactor (MBR) (de Oliveira et al., 2020).

Although the nanoparticles are effective alone, these nanoparticles and other inorganic materials, including GO, carbon quantum dots (CQD), and MOF/COF, can be used to decorate pristine membranes to enhance the permeability, selectivity, hydrophilicity and mechanical strength for different applications. For instance, the incorporation of reduced GO (1.6 wt%) in sodium alginate membranes enhanced the separation efficiency as well as water permeation (1699 g $m^{-2}h^{-1}$) as compared to pristine membranes (Cao et al., 2014).

The precise separation of organic molecules as small as 300 Da was stated with hydrophilic graphene quantum dots and cellulose composite membranes fabricated using an ionic liquid (1-ethyl-3-methylimidazolium acetate) as the common solvent for both quantum dots and cellulose (Colburn et al., 2018). Dual fillers nanocrystalline cellulose and halloysite were also studied to tailor forward osmosis membrane, which exhibited improved desalination performance and anti-fouling characteristics (Rezaei-DashtArzhandi et al., 2020). Besides this, several carbon or graphene quantum dots tailored membranes were studied, which divulged the improved robustness, waste rejection efficiency, and water flux compared to pristine membranes and antifouling characteristics (Bi et al., 2019; Verma et al., 2021; Zhang et al., 2017; Fathizadeh et al., 2019).

These particles are usually incorporated only within the dense-selective layer via interfacial polymerization process forming thin-film nanocomposite (TFN) membranes which minimize the cost while maximizing performance. However, the mechanism for bacterial inactivation (*E. coli* and *S. aureus*) and antifouling characteristics of the composite membranes are not well known; three processes, charge repulsion, physical or oxidative stress, supported the phenomenon up to some extent (Hui et al., 2016; Zhao et al., 2020). The other two ways of membrane customization involve the addition of decorating particles on the top layer using a coating agent or homogeneous integration throughout the matrix to form composite membranes (Verma et al., 2021).

Additionally, many green membranes are tailored via omission of hazardous solvents during membrane fabrication or replacement with eco-friendly and non-toxic solvents (DMSO, Polarclean®), which not only conferred the membranes with green characteristics but also improved solute rejection, permeability, wettability, and anti-fouling characteristics (Wu et al., 2019b; Xie et al., 2019; Marino et al., 2018). The solvents such as methyl lactate, ethyl lactate, tributyl citrate, and supercritical CO_2 possess the specific characteristics which make them acceptable for green membrane synthesis (Table 5). Furthermore, thorough elimination of the solvents also designed effective green membranes. For example, Xiao and his team (Ji et al., 2021) customized the solvent-free multilayered nanofiltration membranes for textile wastewater treatment by depositing the GO within the interfacial pores of PVDF followed by polymerization of polypyrrole (PPy) on the surface. As a result, the hydrophilic green membrane (MWCO 3580 Da, pore size 2.5–4.0 nm) displayed a very high potential for separating negative dyes from brine solution with high rejection efficiency (98.5%), offering a promising strategy to treat wastewater from dye manufacturing industries.

Further, the entire organic COF thin films are an emerging class of green membranes portraying their potential use in water purification and waste removal, along with other fields, including drug delivery, sensors, and energy storage (Wang et al., 2019b). The captivating features of these membranes, for instance, ultrathin layers, tunable porosity, large surface area, chemical functionality, and predictable structure, endorsed their excellent performance in permeability as well as selectivity. These membranes can also be used as free-standing or supported on substrates. However, the stand-alone membranes show a comparatively higher performance of permeance and separation owing to neither shielded performance in hybrid matrices nor other issues regarding poor adhesion or improper growth on the support (Wang et al., 2019b; Matsumoto et al., 2018).

COF membranes have been proved enormously efficient to separate various organic dyes, including brilliant blue, congo red, acid fuchsin, rhodamine B, rhodamine WT, thymolphthalein blue, methylene blue, reactive red, chrysoidine G, chromo black T, and alcian T from water with high rejection rate (90–99%) (Kandambeth et al., 2017; Dey et al., 2017; Matsumoto et al., 2018; Fan et al., 2018; Shinde et al., 2020). The extraordinary stability in water, organic solvents, and mineral acids rendered them superior to conventional nanofiltration membranes. These membrane systems have also been effectively used for the removal of the recalcitrant pesticides and herbicides; organophosphorus dimethoate (Donato and Drioli, 2021), 2,4-dichlorophenoxyacetic acid (Kashani et al., 2016), podophyllotoxin (Cheng et al., 2013), which do contaminate not only ground and surface water but also soil and food.

Besides, MOF composite membranes exhibit a wide range of liquid and gas separation capacity due to pore size tunability, chemical and structural stability, and high surface area to mass ratios (>6000 $m^2 g^{-1}$), which were regulated by organic linkers-inorganic metal ions interaction and pore surface functionalization through a variety of approaches (Efome et al., 2018; Qiu et al., 2014). ZHANG et al. designed MOF-based multifunctional thin-film nanocomposite (TFN) membranes that possessed an enormous potential for desalination, water purification, and wastewater treatment (Zhang et al., 2020). These green and ultrasensitive membranes were tailored *via* interfacial polymerization of three natural compounds: glucose, polydopamine (pDA), and Zr-based MOFs (UiO-66-NH_2 or UiO-66), which unleashed high dye rejection efficiency. The comparative study of three types of membranes: pDA-glucose, pDA-glucose/UiO-66, and pDA-glucose/UiO-66-NH_2, inferred the superior performance of pDA-glucose/UiO-66-NH_2 composite membranes for solvent permeance and dye rejection efficiency (Fig. 8). Fig. 8c ascribes the relative permeance (>15 $Lm^{-2}h^{-1}bar^{-1}$) of various polar solvents: methanol (MeOH), ethanol (EtOH), isopropanol (IPA), acetone, ethyl acetate (EA), and dimethylformamide (DMF) and rejection rates (>98%) of rose Bengal dye with these membranes. The membranes displayed high rejection efficiency for several organic dyes (Molecular weight 407–1017 Da) with ethanol and DMF solvents, as well as for inorganic salts in an aqueous solution (Fig. 8d and e). The authors mentioned that the solvent permeance with designed

Table 4
Performance of green membranes for water flux, organic solvent permeance, and solute rejection.

Membrane Composition	Solvent used for fabrication	Fabrication Method	Thickness (nm)	Rejected solute (MW g/mol)	Rejection Efficiency	Solvent flux/ permeance (L $m^{-2}h^{-1}$ bar^{-1})	Refs.
PVDF/GO/MWNTs	water	Intercalation	0.5–2.0	Direct Yellow (956.8) Methyl Orange (327.34) Na_2SO_4 (142.04) NaCl (58.44)	>99% >96% 83.5% 51.4%	Water: 11.3	Han et al. (2015)
PVC/PVC-*g*-PEGMA	NMP:DMAc: DMSO = 4:3:3	Intercalation	23–29	NaAlg (216.12)	94.7 ± 1.3%	Water: 891.54 ± 64.41	Xie et al. (2019)
PVDF/PVDF-*g*-PEGMA	DMAc/DMSO = 7:3	Intercalation	0.173	NaAlg (216.12)	87.00 ± 2.41%	Water: 735 ± 74	Wu et al. (2019b)
PET/Priamine/tannic acid	p-Cymene, water	Interfacial polymerization	30	styrene dimer (235.0)	90%	Acetone 13.7	Park et al. (2021b)
(a) Tp-Bpy covalent organic framework (COF) (b) Tp-Azo COF on Macroporous polyester-3329	Dichloromethane/ water	Interfacial synthesis	160 ± 10 150 ± 10	Congo red (696.7), Brilliant blue-G (854.0), rhodamine B (479.0) with Tp-Bye & Tp-Azo, respectively. Acid fuchsin (585.5),	CR (80%) BB (94% & (90%), & (97% & 99%) and RH (98% & 99%) with Tp-Bpy & Tp-Azo resp. (79%), AF	Water: 211; Acetonitrile: 339 Ethanol:174; Methanol:108	Dey et al. (2017)
TAPB-PDA COF/PES	water	Interfacial synthesis	0.1 ± 2.5	Rhodamine WT (567)	91%		Matsumoto et al. (2018)
Aluminium/COF-LZU1* (TFB/ PPD)	water	Solvothermal synthesis	400	13 water soluble dyes with diameter larger than 1.2 nm	>90%	Water: 760	Fan et al. (2018)
GO Reduced GO GO/PAM	water	Non-covalent interaction	0.85 (GO) 0.36 (rGO) 0.68 (GO/ PAM)	Rhodamine B (479.0)	85.03% (GO), 95.43% (GO/ PAM), 97.06% (rGO)	Water: 399.04 (GO), 188.89 (GO/PAM), 85.85 (rGO)	Cheng et al. (2019)
M-TpBD COF M-TpTD COF (self-standing)	water	Baking and knife-casting		Rhodamine B (479.0), Methylene blue (319.85), Congo Red (696.7), and vitamin B12 (1355) with M-TpBD & M-TpTD, respectively	RB (99% & 84%), MB (96% & 80%), CR (94% & 83%) and vit B12 (99% & 96%) with M-TpBD & M-TpTD resp.	Water: 120; Acetonitrile: 278; Acetone: 194; 2-butanone: 141; Methanol: 138; Ethanol: 86.5; DMAc: 61; Isopropyl alcohol: 47.9; n-butanol: 39;	Kandambeth et al. (2017)
PVDF/GO/PPy	Solvent-free	Vacuum filtration/ polymerization	Pore size 2.5–4.0 nm	Congo Red (696.7), Polyethylene glycol (1000, 2000, 4000, 6000 and 8000 Da), Acid orange 10 (452.4), Direct yellow (561.48)	>98.5%	Water: 9.0	Ji et al. (2021)
Microporous substrates/reduced GO	water	Vacuum filtration	22–53	Organic dyes, Ionic Salts	>99%, 20–60%	Water: 21.8	Han et al. (2013)
Glucose/polydopamine/UiO-66	hexane, water, tris HCl	Interfacial polymerization	214	Rhodamine B (479.0), Na_2SO_4 (142.04), $MgSO_4$ (120.37), $MgCl_2$ (95.21), NaCl (58.44)	>98%, 99.9%, 98.9%, 97.4%, 92.3%	Water: 39.3 Ethanol: 30.2	Zhang et al. (2020)
Reduced GO	water	Electro-spraying	31.4	Basic fuscin (337.86), Methylene blue (319.85), Methyl orange (327.34), Evans blue (960.8) Na_2SO_4 (142.04), NaCl (58.44) $MgSO_4$ (120.37), $MgCl_2$ (95.21)	98.88%, 98.97%, 100%, 99.99%, 63.13%, 27.86%, 41.82%, 15.00%	Water: 11.13–20.23	Chen et al. (2018)
PI/UiO-66 or ZIF-93	DMSO	Crosslinking	35	Sunset Yellow (452)	93%	Methanol:11	Paseta et al. (2019)
Bio-phenol (dopamine, tannic acid, vanillyl alcohol, eugenol, morin, and quercetin) coated supports PI, PAN, PSF, PVDF, PBI or polymethylsiloxane (PDMS))	Water: EtOH	Phase inversion/ polymerization		Polystyrene (390–1550)	5–100%	Acetone: 1–10	Fei et al. (2019)

(*continued on next page*)

Table 4 (*continued*)

Membrane Composition	Solvent used for fabrication	Fabrication Method	Thickness (nm)	Rejected solute (MW g/mol)	Rejection Efficiency	Solvent flux/ permeance (L $m^{-2}h^{-1}$ bar^{-1})	Refs.
PBI/PDA/Polypropylene	DMAc, Water	Phase inversion	Pore size 0.8–1.4 nm	Polystyrene (190–850)	≈100%	DMF:12	Zhao et al. (2019)
PES/Tannic acid/Fe_3^+	Water	Active layer formation via coordination reaction	3.44 ± 0.20	Orange GII (452.4) Congo red (696.7)	92% 97%	Water: 73.4	Fan et al. (2015)
Hydroxypropylcellulose (HPC)	Water	Phase inversion/ crosslinking	50	PEG200	–	Water:38 ± 5	Hanafia et al. (2017)
PVDF	ATBC (Citroflex®)	Phase inversion	Pore size 51–71 nm	–	–	Water:538	Kim et al. (2016)
PVDF, PAN or CA	DMSO2	Phase inversion		–	–	Water:1491	Liang et al. (2013)
PA/PE	Hexane, Water	Interfacial polymerization	<10	Styrene oligomer (≈1000)	>99%	Acetone: 20	Park et al. (2018)
SPAES/PE separator, TR-NFM or PET nonwoven	DMSO	sequential spraying and drying	50–150	Styrene oligomer (1595)	>99%	DMF:0.37	Kim et al. (2018a)
NaAlg/PAN	Water	Crosslinking	370	B12 (1355)	98 ± 2%	Methanol:1.27 ± 0.2	Aburabie et al. (2020)
NaAlg/crosslinked PAN	Water	Crosslinking	370	B12 (1355)	98 ± 1%	DMF:0.21 ± 0.1	Aburabie et al. (2020)
NaAlg/cellulose	Water	Crosslinking	370	B12 (1355)	95 ± 1%	Methanol:1.38 ± 0.1	Aburabie et al. (2020)
NaAlg/alumina support	Water	Crosslinking	370	B12 (1355)	80 ± 3%	NMP:0.11 ± 0.03	Aburabie et al. (2020)
NaAlg/alumina support	Water	Crosslinking	370	B12 (1355)	76 ± 2%	DMSO:0.15 ± 0.05	Aburabie et al. (2020)
NaAlg/alumina support	Water	Crosslinking	370	B12 (1355)	70 ± 1%	DMF0.25 ± 0.02	Aburabie et al. (2020)
NaAlg/alumina support	Water	Crosslinking	370	B12 (1355)	90 ± 2%	Methanol:1.6 ± 0.1	Aburabie et al. (2020)
Cellulose	(EMIM)OAc	Phase inversion	0.25	Bromothymol Blue (624.4)	94%	Ethanol:0.3	Sukma and Çulfaz-Emecen (2018)
Cellulose	(EMIM)OAc/ Acetone	Phase inversion	0.25	Bromothymol Blue (624.4)	69.8%	Ethanol:8.4	Sukma and Çulfaz-Emecen (2018)
Cellulose	[(EMIM)(DEP)]	Spinning	–	Congo Red (696)	>90%	Ethanol:19 ± 1	Falca et al. (2019)
Cellulose	[(EMIM)(DEP)]	Spinning	–	Congo Red (696)	>99%	Water:48 ± 3	Falca et al. (2019)
PVDF	PolarClean[#]	Phase inversion	–	Polystyrene	99.99%	Water: 988 ± 80	Jung et al. (2018b)
PES/nonwoven polyester	Cyrene	Gel casting	0.50			Water:2542.7	Milescu et al. (2019)
CA/nonwoven polypropylene	Methyl lactate 2-methyl THF	Phase inversion	0.25	Rose Bengal (1017)	92%	Water:3.5	Rasool et al. (2020)
CTA/nonwoven polypropylene	GVL or Methyl lactate	Phase inversion	0.25	Rose Bengal (1017)	>90%	Water 11.7–12.7	Rasool and Vankelecom (2019)
PBI/PLA/bamboo fiber	DMC, DMAc	Casting and phase inversion	0.1			Water:1068 ± 32	Le Phuong et al. (2019)

AF: acid fuchsin; AO10: Acid orange 10; ATBC Acetyl tributyl citrate; Azo:4,4′-azodianiline; BB; brilliant blue-G; BD: Benzidine; BF: Basic fuscin; Bpy:2,2′-bipyridine-5,5′-diamine; CA: cellulose acetate; CR: congo red; CTA: Cellulose triacetate; DMAc: N,N-dimethylacetamide; DMF: Dimethylformamide; DMSO: dimethyl sulfoxide; DMSO2: Dimethyl sulfone; DY24: Direct yellow 24; EB: evans blue; (EMIM)(Ac): 1-ethyl-3-methylimidazolium acetate; (EMIM)(DEP): 1-ethyl-3-ethylimidazolium diethyl phosphate; (EMIM)OAc: 1-ethyl-3-methylimidazolium acetate; GO: Graphene oxide; GVL: γ-Valerolactone; MB: methylene blue; MO: methyl orange; MWNT: multiwalled carbon nanotubes; NaAlg: Sodium alginate; NMP:1-methyl-2-pyrrolidinone; PAM: polyacrylamide; PAN: polyacrylonitrile; PBI: Polybenzimidazole; PDA: polydopamine; PEGMA: poly-(ethylene glycol) methyl ether methacrylate; PES: polyethersulfone; PET: polyethylene terephthalate; PI: Polyimide; PPD: para-phenylenediamine; PPy: polypyrrole; PS: polysulfone; PVC: polyvinyl chloride; PVDF: polyvinylidene fluoride; RB: rose Bengal; RH: rhodamine B; SPAES: sulfonated poly(arylene ether sulfone); TAPB (1,3,5-tris(4-aminophenyl)benzene); TB: thymolphthalein blue; TD: 4,4″-diamino-p-terphenyl; TFB:1,3,5-triformyl-benzene; Tp: 1,3,5-triformylphloroglucinol; TR-NFM: thermally rearranged nanofibrous membrane; Tta: 4,4′,4″-(1,3,5-triazine-2,4,6-triyl) trianiline; Ttba: 4,4′,4″-(1,3,5-triazine-2,4,6-triyl) tris(1,1′-biphenyl) trianiline; [#]Polarclean: (methyl5-(dimethylamino)-2-methyl-5-oxo pentanoate; *LZU stands for Lanzhou University.

membranes was achieved quickly at low pressure, which assured lesser energy than high energy-consuming membranes working at high pressure (Rundquist et al., 2012). Additionally, the membranes presented high selectivity for various inorganic salts (1000 mg L^{-1}), for instance, for Na_2SO_4 (99.9%), $MgSO_4$ (98.9%), $MgCl_2$ (97.4%) and NaCl (92.3%). The membranes' high salt rejection efficiency and water flux (20.9 L $m^{-2}h^{-1}bar^{-1}$) were not compromised even at higher concentrations of inorganic salts (3000 mg L^{-1}), as clearly shown in Fig. 9e. Moreover, the extraordinary performance of the anti-fouling membranes remained unaffected even after 10 days (Fig. 8f and g).

The chemically stable membranes were superior to state-of-the-art membranes comprised of unsustainable materials and conventional

Table 5
Characteristics of solvents used for green membranes synthesis.

Green Solvent	Characteristics	References
Methyl lactate	Biodegradable, water-miscible, readily dissolve cellulose acetate	Medina-Gonzalez et al. (2011)
Ethyl-lactate	Biodegradable, non-corrosive, non-carcinogenic, highly volatile	Pereira et al. (2011)
γ-butyrolactone	Water-soluble, able to dissolve polyether ether ketone (PEEK)	(Figoli et al., 2014; Bey et al., 2011)
Ionic liquids	Inflammable, high ionic conductivity, low toxicity	(Mallakpour and Rafiee, 2011; Xing et al., 2010)
Tributyl O-acetyl citrate	Reduced toxicity, compatibility with many polymers, particularly with PVDF	Cui et al. (2013)
Tributyl citrate	Non-volatile solvent for PVDF membranes fabrication	Liu et al. (2010)
Supercritical CO_2	Inflammable, relatively non-toxic	Wang et al. (2019c)

bio-based polymeric membranes. The synergistic effect of three purely green products overcome low solvent permeance, poor chemical stability, and reduced selectivity of traditional polymers. The fabrication of such green multifeatured sensitive membranes opened an avenue for constructing more unrivaled membranes with a plethora of combinations from natural compounds with compatible functionality. The application of MOF filters was also explored as a catalyst for water purification (Wang et al., 2020b). The nanocomposite filters fabricated by *in-situ* growth of MOFs on PAN matrix have the potential to deteriorate the organic pollutants by sulfate radical ($SO_4^{\bullet-}$)-based advanced oxidation process (SR-AOP). Here, the ZIF-67 (MOF) catalyzed the reaction of sulfate radical generation from peroxymonosulfate (PMS). The approach can be extended to other MOFs and for other separation applications as well.

Additionally, MOF composite membranes' strong adsorption feasibility for removing environmentally toxic heavy metal ions and health-hazardous, radioactive nuclides (^{60}C) have also been explored, owing to the chelation of metallic ions with the organic functional groups presenting in MOFs (Yuan et al., 2018, 2019).

Efome et al. (2018) described the use of MOF modified PAN and PVDF electrospun nanofibrous membranes to remove lead and mercury ions from aqueous solution with a permeance of as high as 870 L m^{-1} h^{-1} bar^{-1}. The membranes were competent to lower the lead ion concentration to drinking water standards (<10 μg L^{-1}) and were found to be reusable as no leaching of MOFs and lowering of adsorption efficiency in permeate was observed even after four cycles of filtration. Thus, the hydro-stability, reusability, and excellent filtration performance rendered these membranes efficient for treating contaminated water.

Correspondingly, the imprinting of membrane with specific ligand, preferably hydrophilic and of low molecular weight, results in the membrane's ion selectivity, which possesses great potential for recovery and removal of metal ions from wastewater (Mokhtar et al., 2018). Furthermore, the ion-imprinted chitosan-based membranes have shown a very good adsorbent efficiency for metal ions; for instance, glutaric acid-modified ion-imprinted chitosan-PVA membranes demonstrated a very good Pb(II) adsorption selectivity over Ni(II), Cu(II), and Zn(II) in aqueous solution (Lv et al., 2019). Zeng et al. (2020) also reported the Ni (II)-imprinted silica gel membranes applicable for industrial wastewater treatment. The membranes displaying Ni(II) selectivity over Cu(II) and Zn(II) presented high membrane flux along with lowered concentration of Ni(II) ions in permeate when used for the treatment of electroplating industry effluent onto the surface of ceramic membrane.

Recently, a novel ion-imprinted blended membrane was customized to remove Pt(IV) from aqueous solutions (Zeng et al., 2019). Pt(IV) complex and an amphiphilic copolymer poly(methyl methacrylate)-b-poly(4-vinylpyridine) (PMMA-b-P4VP) were blended with PVDF membrane to form reusable imprinted membranes which expressed the selectivity for Pt(IV) over Cu(II) and Ni(II) ions. The selective separation of platinum ions is highly required as it is highly toxic in its soluble form. For example, their halogenated salts may cause asthma and bronchitis on inhalational exposure and contact dermatitis following skin exposure. Therefore, continuous efforts have been made to develop appropriate methods, and the designed membranes revealed their potential application at the commercial level.

Further, the green silica-based ceramic hollow fiber membranes obtained from rice husk wastes displayed high efficiency in removing arsenic, which is highly toxic (Hubadillah et al., 2019). The hydrophobic membrane modified with fluoroalkylsilane grafting resulted in a flux of 51.3 kg m^{-2} h^{-1} for As(V) and 50.4 kg m^{-2} h^{-1} for As(III) *via* direct contact membrane distillation, and membranes possessed the potential to reject arsenic to the maximum contaminant level limit of 10 μg L^{-1}. The hybrid membranes formed from PVA and rice husk-derived silica have also demonstrated the efficiency to improve membrane flux (12.3 kg $m^{-2}h^{-1}$) without compromising the rejection efficiency (99.9%) for NaCl (3.5 wt%). The hybrid membranes usually establish brick-and-mortar morphology and improve performance by increased hydrophilicity, lower crystallinity, and active surface area (da Silva et al., 2020).

In addition, several green electrospun nanofibrous membranes have been fabricated from chitosan (biodegradable polysaccharide) and PVA (synthetic biodegradable polymers), which were reported as super-adsorbents for toxic metals like Pb(II) (Karim et al., 2019; Kumar et al., 2019), Cd(II) (Karim et al., 2019) and Cr(VI) (Kumar et al., 2019) in wastewater treatment. The nanofibrous composite microfiltration membranes also exhibited good adsorption efficiency for Cr(VI) and Cd (II) ions present in polluted water attributed to negatively charged hydrolyzed PVA-PAN membranes (Liu et al., 2020). Here, a two-nozzle electrospinning process was applied for nanofibrous membrane fabrication, which helped enhance adsorption efficiency per unit mass for free-standing membranes compared to substrate-based membranes. Along with heavy metals, removing some alkali metal ions is of great significance for water purification, for illustration, that of lithium ions in addition to Na^+, K^+, Mg^{2+}, and Ca^{2+} ions as it comprises 69% of the world reserve in salt brine. It also comprises a crucial element for eco-friendly lithium-ion batteries (Xiao et al., 2015; Cui et al., 2019), which gives momentum for their recovery. The selective methods are required to differentiate lithium ions from co-existing ions (Na^+, K^+, Mg^{2+}, and Ca^{2+}), and many green membrane separation systems have been employed for their separation and recovery.

Cui and his team (Cui et al., 2018, 2019) tailored two different types of green reusable ion-imprinted membranes using biodegradable cellulose acetate/chitosan and secondly, PVDF/GO as base membranes which manifested the lithium adsorption capacity of 20.08–27.10 mg/g with very high selectivity, i.e., $\beta_{Na/Li}$ = 1.780, $\beta_{K/Li}$ = 5.3780, $\beta_{Mg/Li}$ = 15.5620 and $\beta_{Ca/Li}$ = 21.9402).

Further, rare earth metals (REMs), including lanthanum (La), yttrium (Y), and scandium (Sc), have come into the limelight for various industrial applications due to their electrical, optical, and magnetic properties over the past decades. However, their increased use in military, high-tech manufacturing, petrochemical engineering, and clean energy generation has also enhanced the chances of their contamination in water (Donato and Drioli, 2021; Liu et al., 2017; Lu et al., 2018). Therefore, due to their toxic effects on the environment and human health, REMs removal from the water stream has been a global challenge that must be addressed instantly. Further, the need for recycling REMs dictates the use of membrane systems for their recovery from wastewater or other sources.

In the current scenario, ion-selective membranes played a pivot role in their isolation. The imprinted ion-selective membrane has appeared as a highly distinctive tool for their isolation from other resources and the separation of closely similar REMs from each other. The 'green' ion-imprinted microporous membranes have been designed and executed

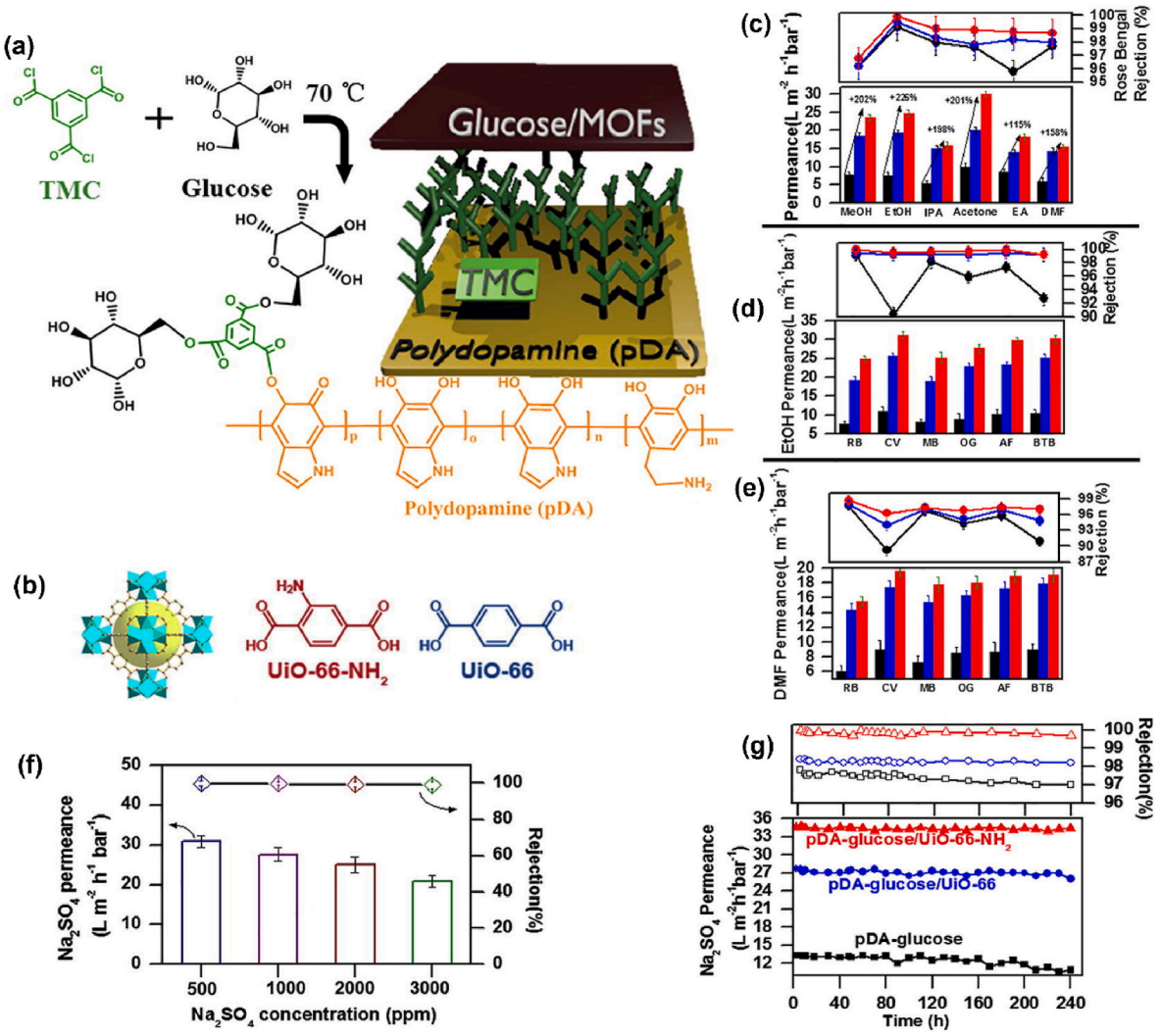

Fig. 8. **(a)** The synthetic pathway for membranes construction; Preparation of thin-film composite polydopamine membrane: I) Dissolving of dopamine hydrochloride in tris buffer solution (pH = 8.5). II) Immersion of polyimide (PI) into the dopamine solution (8 h at R.T.). III) Formation of composite polydopamine (pDA) membrane through *in situ* polymerization of dopamine on the surface of PI substrate. IV) washing with deionized (DI) water, and drying in air. Preparation of polydopamine-trimesoyl chloride membrane: I) Grafting of trimesoyl chloride (TMC) on the surface of composite pDA membrane by using a 0.2% TMC n-hexane solution. II) Rinsing the pDA-TMC membrane with n-hexane. Preparation of glucose-MOF/pDA-TMC membranes: I) Pouring of a glucose aqueous solution containing Zr-based metal organic frameworks (MOFs) onto the surface of pDA-TMC membrane. II) Resting of the glucose/MOF mixture on the pDA-TMC surface (5 min), curing (70 °C for 15 min), washing with DI water, and drying. **(b)** The structure of UiO-family MOFs. **(c)** Rose Bengal dye rejection and solvent permeance rates of pDA-glucose, pDA-glucose/UiO-66 and pDA-glucose/UiO-66-NH_2 thin film nanocomposite membranes with black, blue and red line/column, respectively. Rejection rate of various dyes in **(d)** ethanol (EtOH) and **(e)** dimethylformamide (DMF) solvents. **(f)** The performance of pDA-glucose/UiO-66-NH_2 membranes with different concentrations of Na_2SO_4. **(g)** The performance of membranes with 1000 ppm Na_2SO_4 aqueous solution concerning time. Reprinted with permission from (Zhang et al., 2020). Copyright 2020 Elsevier.

for the removal of dysprosium, Dy(III) (Liu et al., 2017; Zheng et al., 2018); gadolinium, Gd(III) (Zheng et al., 2019); neodymium, Nd(III) (Zheng et al., 2018); europium, Eu(III) (Lu et al., 2018), etc. Hence, green approaches are playing a substantial role in improving separation performance as well as sustainable development.

4.1.2. *Oil/water separation*

The oily discharge from the sewage of petrochemical, food processing, steel industries, oil-spilling during fuel transportation generates water contamination with oily substances and demands efficient and eco-friendly oil/water separation methods (Zhang et al., 2019; Shen et al., 2019). Nowadays, the green membranes comprised of super wetting materials have come into the limelight to treat oil-water emulsion and recover water and oily substances.

For instance, the super wetting materials, superhydrophobic-superoleophobic or superhydrophobic-superoleophobic substances, usually offer anti-fouling characteristics and excessive drop in surface oil adsorption, promoting facile oil/water separation (Zhao et al., 2021; Mahmud et al., 2020; Rafeie et al., 2017; Razmjou et al., 2017). First of all, Feng et al. (2004) customized the coating mesh films with super-hydrophobic (contact angle >150° with water) and super-oleophilic (contact angle 0° with diesel oil) surface for oil and water separation. The films prepared by an economical spray-and-dry method using a homogeneous emulsion with PTFE as a precursor and stainless-steel mesh (115 μm) as substrate presented applicability for oil wastewater treatment. Subsequently, many researchers used excellent repellency of super wetting substances to fabricate membrane systems for oil/water separation.

Shi et al. (2016) modified the inherent hydrophobic PVDF membranes to super-hydrophilic membranes by coating them with TiO_2 nanoparticles functionalized with silane coupling agent KH550. The membrane demonstrated high efficiency to separate several surfactants

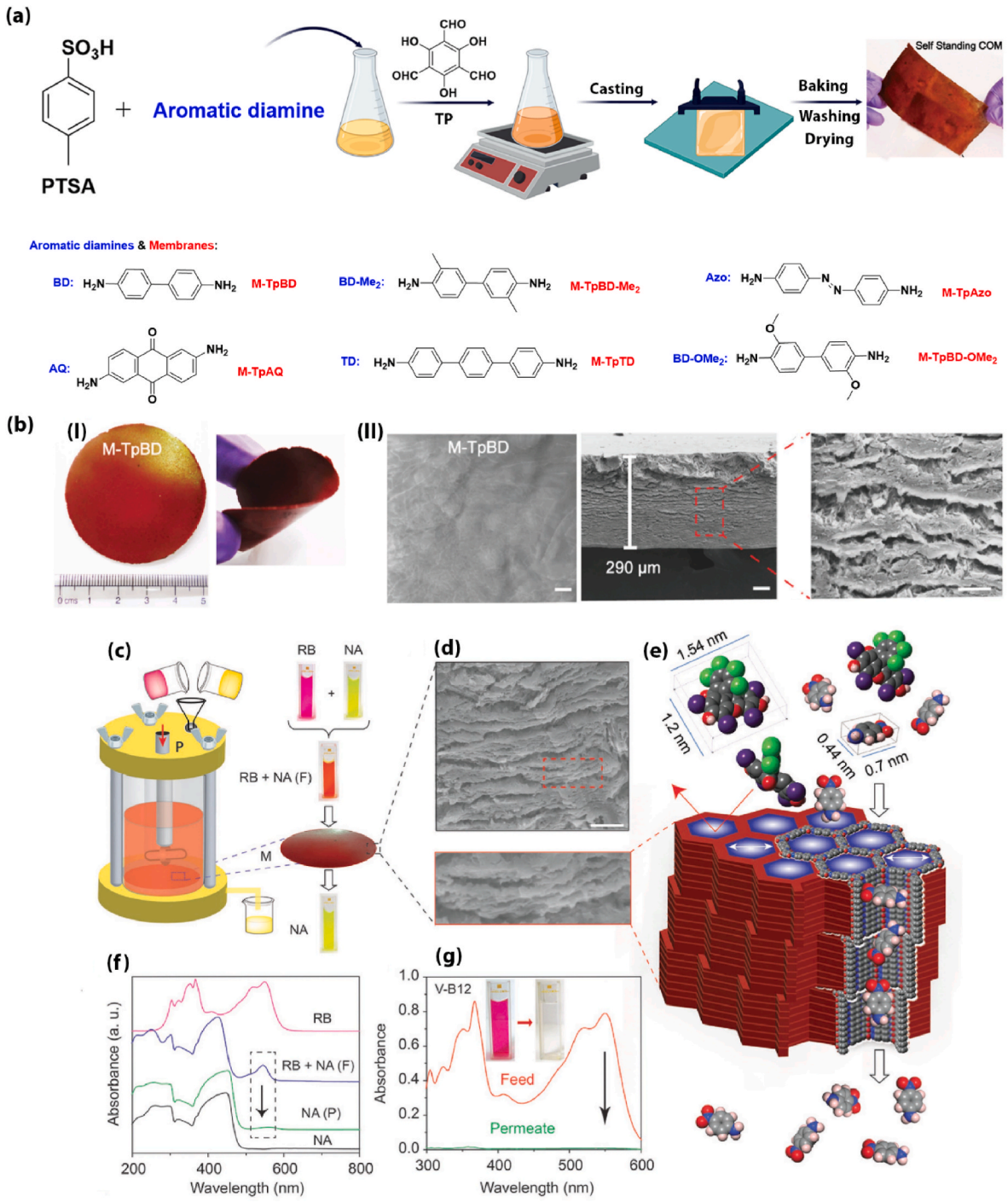

Fig. 9. Fabrication, characterization and applications of COF membranes (COMs) for selective molecular separation; **(a)** The fabrication of COM: Salt formation *via* mixing the aromatic diamine and *p*-toluene sulfonic acid (PTSA), making the dough from shaking the resultant salt and 1,3,5-triformylphloroglucinol (Tp), casting on the glass plate, baking at 60–120 °C in an oven for 12–72 h, and washing the COM with distilled water and acetone. **(b)** The M-TpBD COM pictures: **(I)** The membranes flexibility, **(II)** The SEM images demonstrating the defects and cracks free surfaces. **(c)** The nanofiltration assembly and separation of nitroaniline (NA) from its mixture with rose Bengal (RB), (F: feed and P: permeate). **(d)** The M-TpBD SEM cross-section after NA separation representing the stacked-layer sheets. **(e)** The molecular sieving mechanism through M-TpBD. UV–vis spectra demonstrating **(f)** the selective recovery of NA from the NA + RB mixture from water, and **(g)** the V–B12 filtration from water. Reprinted with permission from Ref. (Kandambeth et al., 2017). Copyright 2016 Willey.

stabilized oil-in-water emulsions. Additionally, the excellent antifouling and oil resistance properties of mussel-inspired membranes rendered them readily reusable.

Similarly, photoinduced TiO_2 coated single-walled carbon nanotube (SWCNT) composite ultrathin films presented the ultrahigh separation efficiency (99.99%) for wide droplet sized (100 nm- 3 µm) oil-in-water emulsions (Gao et al., 2014). The permeation flux of membranes was observed as high as 32 540 L $m^{-2}.h^{-1}.bar^{-1}$ for a surfactant-free petroleum ether-in-water emulsion whereas 15 690 and 17 560 L $m^{-2}.h^{-1}.bar^{-1}$ for surfactant-stabilized hexadecane-in-water and isooctane-in-water emulsions, respectively, which were 100 times better than commercial membranes with similar separation efficiency.

More recently, green super-wettable membranes were engineered by co-depositing proanthocyanidins (PC) and γ-amino-propyltriethoxysilane (APTES) on PVDF microfiltration membrane, which imparted super-hydrophilicity to the membrane surfaces. Here, PC was used for the first time in the membrane separation system, an eco-friendly and biocompatible material extracted mainly from grape seeds or French pine barks (Ferreira and Slade, 2002). Under submerged situations, membranes displayed super-oleophobic behavior allowing oil/water separation, rejecting 99.5% of the different types of oil (petroleum ether, dichloroethane, soybean oil, toluene, and red oil) (Zhao et al., 2021). In addition, the membranes show excellent salt rejection, anti-crude oil fouling and suitable chemical, pH (5–13), and mechanical stability. Thus, the membranes possessed great potential for application in wastewater treatment and to produce self-cleaning clothes as well. Eventually, the use of super wetting materials and nanoparticle modification in membrane systems facilitate the oil-water separation and reusability of the membranes attributed to self-cleaning and antifouling properties. The idea can be expanded to membrane manufacturing for filtration equipment and separation at a large scale.

4.1.3. Energy production from wastewater

Microbial fuel cell (MFC) is an eco-friendly technology to treat wastewater, fostering a way of generating energy. At this point, various biocompatible polymeric membranes have played a pivotal role in expediting H^+ (proton) transfer between two electrodes of MFCs (Shaari and Kamarudin, 2015; Seol et al., 2012). The biopolymers such as chitosan and alginate possess inherent hydrophilic nature and are flexible to acquire required superficial properties for MFCs, for instance, low proton conductivity and methanol permeability, similar to Nafion membranes (Shaari and Kamarudin, 2015). Further, the MMM of biopolymers bestow more advantages as compared to the pristine membrane. For example, Cabello et al. (2017) studied the impact of pectin as a green polymer electrolyte on the properties of chitosan-pectin membranes and observed improved methanol permeability for MMM (1.51×10^{-6} cm^2/s) as compared to pure chitosan membranes (4.24×10^{-6} cm^2/s).

Furthermore, the energy generation and remediation of wastewater can substantially be enhanced by synergistic relationship between MFC and algae or cyanobacteria; the latter support the bacterial growth at the anode, facilitate oxygen supply from photosynthesis and remove nitrogen and phosphorous from wastewater (Luo et al., 2017). Here again, the integration of membrane systems in the bioremediation of wastewater is highly beneficial for harvesting algal biomass, extracting lipids or unused nutrients, and downstream processing valuable products like biofuels. Recently, Kumar and his team (Kumar et al., 2020) presented a comprehensive review on the membrane-integrated green approach for simultaneous algal-based production of biofuels and value-added co--products from wastewater.

In addition to generating energy from wastewater, another way of saving energy and resources is to use green membranes for water purification, which are purely designed with live biomass instead of using bioderived polymers. Recently, Zodrow and his team (Eggensperger et al., 2020) demonstrated an exciting way for designing the living filtration membranes using a symbiotic culture of bacteria and yeast (SCOBY) which was formed by growing culture on green kombucha tea. The ultrafiltration membrane presented pure water flux of 135 ± 25 L $m^{-2}.h^{-1}.bar^{-1}$and high efficiency to reject polypropylene and gold nanoparticles (≈90%). Furthermore, the living microbial cells in the membranes provided the capacity to regenerate following any scratch due to the production of new cellulose fibers. depicts the restoring water permeability of membranes after an incision or puncture in a growing solution, which regained 110−250% of the original water flux within 10 days. The healing of the membranes was observed under a confocal microscope after staining cellulose fibers with calcoflour white. The cross-sectioned views of the membranes displayed an appropriate picture of fresh growth of microbes and renaissance of the membrane over the disrupted open area. Such green membranes do not require sophisticated equipment and can be customized from easily accessible and sustainable materials, which showed a new direction for fabricating inexpensive and eco-friendly membranes for water purification. The membrane systems play a substantial role in wastewater treatment and desalination processes. Hence, sustainable membrane technologies are imperative for water treatment as standalone or complementary processes, and advanced studies are highly recommended to overcome the factors affecting the economics and performance of membrane systems like membrane fouling, water flux, and sustainability.

4.2. Removal of therapeutics and pharmaceutical compounds

The membranes have played a pivotal role in separating and purifying various therapeutics and pharmaceutical compounds for the last few decades. Furthermore, the first step for monitoring therapeutics and pharmaceutical compounds in the biological systems necessitates their removal from complex matrices to concentrate the analytes. Here, green membranes are presented as eco-friendly and economical alternatives for conventional liquid-liquid extraction approaches (Tabani et al., 2018). Furthermore, the membrane systems are applicable for analyte extraction *via* different approaches with porous and non-porous membranes, which include dialysis (Boerma et al., 2015), electrodialysis (Lindenburg et al., 2013), and filtration (Mohammad et al., 2015) for porous membrane, whereas liquid membrane extraction (Khataei et al., 2018), gel-based electro-membrane extraction (Asadi et al., 2018) and polymer inclusion membranes based extraction (Almeida et al., 2017) using non-porous membranes.

The membranes support the preparation of drug-protein adducts (Boerma et al., 2015), facilitate the estimation of protein-drug binding (Garcia-Martínez et al., 2018; Kiebooms et al., 2014) as well as allow the regular drug concentration analysis in tissues with microanalysis (Ma et al., 2012; Wetterhall et al., 2014). Dahlin et al. used the refined microdialysis approach for protein biomarker sample collection in acute brain injury. However, offline analysis caused issues related to contamination and analyte degradation on storing and transferring. Those issues were later resolved by real-time analysis *via* coupling the microdialysis with LC-MS/MS while assessing the effects of *rhizome coptidis* on diabetic rats (Dahlin et al., 2014; Wang et al., 2015).

The online coupling of membrane systems with sophisticated analytic instruments resulted in the advancement of bioanalytical validation studies to determine unbound drugs in human plasma. Furthermore, it settled the challenges for the need for extensive sample volume and multiple sample preparatory steps (Garcia-Martínez et al., 2018). Thus, electro membrane extraction (EME) techniques have come into the limelight in the last decade. EME prevailed over microextraction owing to their speedy and efficient efficiency, which uses a small amount of organic solvent immobilized on the surface of a porous hollow fiber such as polypropylene to extract the target analyte.

In 2017, Tabani et al. introduced agarose gel as a green membrane in EME to extract different drugs with vast polarity ranging from logP value of 0.43–3.7, without using harmful organic solvents (Tabani et al., 2017). Later, polyacrylamide gel was also launched in the gel-EME method to recover basic drugs named pseudoephedrine, propranolol, and lidocaine, from breast milk and wastewater samples (Asadi et al., 2018).

The method was extended either by using the rotatory electrode for extraction and trace level quantification of drugs naloxone, naltrexone, and nalbuphine (Behpour et al., 2020) or coupling with dispersive liquid-liquid microextraction for the extraction of trimipramine and clomipramine drugs [269] from human urine samples permitting outstanding enrichment factors in the range of 260–370. Furthermore, the gel EME was also analyzed by impregnating agarose gel membranes with graphene nanomaterials which improved the drug recovery by increasing electrical conductivity and determining drugs propranolol and atenolol used for the treatment of cardiac diseases in complex

biological samples (Moghaddam et al., 2021).

Similarly, the extraction of morphine and codeine from complex biological samples was also studied by novel modification of gel-EME known as "inside" gel-EME to overcome the electroendosmosis phenomenon in which an aqueous media was entrapped within agarose gel membrane that behaved both as separation membrane as well as supported liquid acceptor phase (Rahimi et al., 2020). Hence, the different variants of membrane systems have been developed to remove therapeutics and pharmaceutical compounds from complex biological fluids.

Further, the upstream and downstream processing of biotechnological products such as antibiotics, enzymes or hormones, also involves membrane-based techniques such as ultrafiltration, microfiltration, chromatography, high-performance tangential flow filtration, electrophoretic extraction, and use of membrane reactors (Saxena et al., 2009). The membranes required for the separation and purification of therapeutics and pharmaceutical compounds usually possess organic solvent permeance, which is quite challenging due to the need for high chemical stability and excellent performance in harsh organic solvent environments (Donato and Drioli, 2021). The first thin-film composite (TFC) membranes for organic solvent nanofiltration (OSN) were designed almost a decade ago, using an ultrathin polyamide selective layer displayed on porous support formed by crosslinking of trimesoyl chloride (TMC) and m-phenylenediamine (MPD) *via* interfacial polymerization (Solomon et al., 2012).

Recently, several novel membranes have been designed for the removal of value-added products. For instance, the hydrophobic membranes for OSN were designed exclusively from green resources viz. priamine and tannic acid monomers derived from plants; p-Cymene and water as green solvents; and hydrophobic polyethylene terephthalate (PET) as solid support obtained from recycled plastic bottles (Park et al., 2021b).

The as-prepared TFC nanofiltration membranes (≈30 nm) exhibited high permeance for six solvents (Acetone, n-heptane, toluene, ethanol, methyl ethyl ketone, acetonitrile) and styrene (235 g mol^{-1}) dimer rejection with MWCO 236–795 g mol^{-1}. In addition, another biocompatible catechin/cellulose thin film composite (TFC) nanofiltration membranes were customized by interfacial polymerization exhibiting DMF permeance of 1.2 Lm^{-2} h^{-1} bar^{-1} with MWCO of 500 g/mol (Abdellah et al., 2018).

In contrast, Aburabie and his team (Aburabie et al., 2020) successfully tailored bio-based alginate composite membranes by polymer casting and crosslinking for DMF's permeance and methanol and DMSO organic solvents (0.8–1.8 L $m^{-2}.h^{-1}.bar^{-1}$) with nanofiltration of materials with MWCO 1200 g mol^{-1}. The alginate-based membranes were synthesized using green, inexpensive, and easy approaches; sodium alginate as a matrix, water as a solvent, aqueous calcium chloride solution as a crosslinker, and cellulose, alumina discs PAN, or cross-linked PAN as matrix support.

Recently, Kandambeth et al. prepared the novel self-standing crystalline COF membranes supporting organic solvent nanofiltration (OSN) by molecular precursors baking and knife casting (Fig. 9), as simple as making cakes and cookies, and revealed their extreme potential for removal of valuable drugs from organic solvents in the pharmaceutical industry (Kandambeth et al., 2017). The flexible, crack-free, and orderly porous membranes were prepared by mixing aromatic diamines, p-toluene sulfonic acid (PTSA), and water, followed by 1,3,5-triformylphloroglucinol (Tp) addition, and the solutions were then cast, baked, and exfoliated from glass surface (Fig. 9a). The green, inexpensive, and easily scalable membranes exhibited the excellent molecular sieving of nanoparticles (>1 nm). For example, the nitroaniline was selected over Rose Bengal (RB) with 99% rejection of RB (Fig. 9c–f), and vitamin B12 was utterly recovered, leaving colorless solution by M-TpBD (Fig. 9g).

The COF membranes demonstrate very high organic solvent permeance; for instance, acetonitrile permeance of M-TpTD (278 L $m^{-2}.h^{-1}.bar^{-1}$) was observed 2.5 times higher than state-of-the-art polyamide-based nanofiltration membranes (112 L $m^{-2}.h^{-1}.bar^{-1}$), whereas another membrane (M-TpBpy) designed by the same group *via* interfacial crystallization showed acetonitrile permeance as high as 339 L $m^{-2}.h^{-1}.bar^{-1}$[192, 198]. Furthermore, the organic solvent permeance of membranes spurs their use for active pharmaceutical ingredients (APIs) recovery from organic solvents. For instance, M-TpBD membranes efficiently showed the recovery of tetracycline (a well-known pharmaceutical and an organic contaminant of water) and curcumin dissolved in acetonitrile (food additive), in addition to the rejection of gram-negative *Escherichia coli* from contaminated water (Kandambeth et al., 2017).

The imprinting membranes that are prepared by introducing specific recognition sites with templates also give relevant input in removing therapeutics and pharmaceutical compounds *via* sensing or enantiomeric separations. In addition, membranes' selectivity and separation efficiency, mimicking the living systems, can be further intensified by integrating with other approaches such as nanofiltration, membrane crystallization, and distillation (Donato and Drioli, 2021).

For example, the molecularly imprinted nanofiltration membranes were devised *via* the phase inversion technique using the chemical and solvent stable polybenzimidazole polymer and the pharmaceutical genotoxic compound 2-aminopyrimidine (2AP) as template molecule (Székely et al., 2015). As-prepared imprinted membranes acted as shape-specific adsorbent and size-exclusion membranes and showed fourfold higher flux than pristine membranes with the same rejection performance.

The membranes divulge the adsorption of 2-AP *via* molecular recognition over 4-dimethylaminopyridine and recover roxithromycin, an active pharmaceutical ingredient (API) and permeate organic solvent. Similarly, many bioactive compounds, namely oleuropein, luteolin, and pinoresinol (biophenols) (Voros et al., 2019); diosgenin (able to reduce cholesterol in blood) (Dima et al., 2009), and artemisinin (anti-malarial drug) (Cui et al., 2016) was recovered in an organic solvent environment accompanied by the recovery of solvent using imprinted polymeric adsorption integrated membrane systems.

Oleuropein acquires an extreme therapeutic potential for several diseases, by being antioxidant, anti-cancerous, cardioprotective, anti-inflammatory, and anti-angiogenic. Scientists showed oleuropein recovery from olive leaves and recycling of recovered ethyl acetate to regulate the continuous process sustainably and economically using imprinted polymer for adsorption and nanofiltration membrane for concentrating the retentate and permeate (Didaskalou et al., 2017). Olive leaf extract is passed through chromatographic columns containing imprinted polymers with oleuropein-specific recognition sites for adsorption, desorbed in the second column by circulating the solvent ethyl acetate. Subsequently, polybenzimidazole-based OSN membranes were employed to concentrate (17.5 g/kg adsorbent per hour) the oleuropein with 99.7% purity and recover the solvent (97.5%), which is recirculated. Such green processes for recycling the solvent, recovering the valuable products, and valorizing the agricultural waste enlighten the path for sustainable development.

4.3. Removal of synthesized products and chemical contaminants

Fabricating membrane systems seems to be the most suitable method for the separation of synthesized products and chemical contaminants from the reaction mixtures due to high productivity and low energy requirement as compared to tedious and expensive traditional methods such as chromatography, distillation, and extraction. Moreover, the aforementioned techniques affect the overall productivity of the process (Roy and Singha, 2017).

Basically, removal of synthesized products and chemical contaminants from the reaction mixture becomes necessary to continue the process forward; for instance, the butanol recovery in acetone-butanol-ethanol (ABE) fermentation is mandatory to keep the fermentation process in progress. ABE fermentation is carried out to generate biofuel, a remedy for the energy crisis and environmental pollution. The process undergoes cessation when the butanol concentration rises above a

specified level (>60 wt%), which necessitates the continuous removal of butanol from fermented broth (Fadeev et al., 2000; Liu et al., 2011). In the current scenario, the vaporized organic compound butanol can be easily separated from the mixture without compromising the productivity, moving through the membrane using temperature and pressure gradient as the driving force in the pervaporation process.

Lan and Peng developed the nanocomposite membranes comprised of a polymer of intrinsic microporosity (PIM-1) and functionalized carbon black (CB) nanoparticles for butanol recovery (Lan and Peng, 2019). The functionalized nanoparticles supported membrane with a higher hydrophobicity, increased swelling resistance, and decent separation efficiency as compared to the pristine polymer membranes. The hybrid membranes were also promising systems for the fabrication of membrane reactors for the *in situ* butanol extraction from fermentation broth.

The MMMs usually impart the benefits of economy and flexibility in choosing polymers such that inorganic materials such as nanoparticles of MOFs or COFs guarantee a high selectivity and mechanical strength as well (Castro-Muñoz et al., 2019). Several nanocomposite green membranes have been customized for the dehydration of alcoholic beverages or reduction of alcohol content to make them more demanding and relatively healthier low-alcoholic beverages without compromising the content of other organoleptic compounds (Table 6).

Recently, Msahel et al. (2021) investigated the use of green synthesized MOF with biopolymer PLA to form a novel MMM for azeotropic separation of methanol/methyl tert-butyl ether (MeOH/MTBE) mixture by pervaporation and observed 22% improved selectivity as compared to the pristine PLA membrane. MTBE, synthesized by the chemical reaction between isobutylene and MeOH, was served to increase octane number of gasoline; therefore, it had to be free of unreacted MeOH to work efficiently. Consequently, the spherical MOFs (MIL-100 Fe) with a total pore volume of 0.96 $cm^3\ g^{-1}$ were synthesized with an environmentally safe and solvent-free manner employing microwave-assisted hydrothermal synthesis. The product improved the selectivity of methanol by creating preferential pathways and by altering membrane wettability, mechanical strength, and swelling degree. Furthermore, eco-friendly and cost-effective fabrication technology endorsed the plethora of possibilities for developing membrane separation systems. Synthesized products, such as pharmaceuticals, personal care products, and pesticides, were distinguished for modern society but could pose adverse effects on the environment and human health in the case there were not properly managed. Conventional treatment methods, such as activated carbon adsorption and advanced oxidation processes, have limitations in terms of efficiency, cost, and environmental impact. Green membranes have emerged as a promising alternative for the removal of synthesized products due to their high selectivity, permeability, and low energy consumption. One of the most common types of green membranes used for the removal of synthesized products is the MBR system. It combines biological treatment with membrane filtration potential to support a high-quality effluent. The biological treatment process, which involves the use of microorganisms to degrade contaminants, is enhanced by the membrane filtration process. The physical barrier formed accordingly could retain the microorganisms and prevent their washout. The MBR system has been shown to be effective in removal of a wide range of synthesized products, including antibiotics, hormones,

Table 6
Green nanocomposite membranes for dehydration/dealcoholization of fermented products *via* pervaporation process.

Green Polymer	Nanocomposite	Reaction mixture separated by pervaporation	Flux ($g\ m^{-2}\ h^{-1}$)/ Temperature (K)	Separation Factor/Feed composition (wt%)	Refs.
CS	IDD	IPA/H_2O	184/298	125/70:30 (IPA/H2O)	Han et al. (2014)
PDMS	SiO_2	EtOH/H_2O	807/333	13/5:95 (EtOH/H_2O)	Yan et al. (2015)
PDMS	ZIF-8	EtOH/H_2O	1229/333	10/5:95 (EtOH/H_2O)	Yan et al. (2015)
PDMS	SiO_2	n-BuOH/H_2O	1693/333	9/5:95 (n-BuOH/H_2O)	Yan et al. (2015)
PDMS	ZIF-8	n-BuOH/H_2O	1743/333	30/5:95 (n-BuOH/H_2O)	Yan et al. (2015)
Matrimid	$Cu_3(BTC)_2$	IPA/H_2O	400/323	245/90:10 (IPA/H_2O)	Sorribas et al. (2015)
Matrimid	Zeolite-4A	IPA/H_2O	21/303	>5000/10:90 (H_2O/IPA)	Khosravi et al. (2012)
PDMS	TMS-H-silica	IPA/H_2O	135/298	33/4:96 (IPA/H_2O)	Shirazi et al. (2012)
PDMS	TMS-H-silica	IPA/H_2O	405/323	32/4:96 (IPA/H_2O)	Shirazi et al. (2012)
PDMS	TMS-H-silica	EtOH/H_2O	117/303	28/4:96 (EtOH/H_2O)	Shirazi et al. (2012)
PDMS	TMS-H-silica	EtOH/H_2O	329/323	26/4:96 (EtOH/H_2O)	Shirazi et al. (2012)
PDMS	Fumed silica (A200)	EtOH/H_2O	200/313	19/5:95 (EtOH/H_2O)	Peng et al. (2011)
PDMS	Fumed silica	EtOH/H_2O	-/313	7/5:95 (EtOH/H_2O)	Peng et al. (2011)
PDMS	Carbon Black	EtOH/H_2O	-/308	7/5:95 (EtOH/H_2O)	Peng et al. (2011)
PDMS	Zeolite-Y	EtOH/H_2O	750/308	5/5:95 (EtOH/H_2O)	Peng et al. (2011)
PDMS	Silicalite-1 (a type of zeolite)	EtOH/H_2O	51/295.5	17/5:95 (EtOH/H_2O)	Peng et al. (2011)
PVA	H-ZSM5	EtOH/H_2O	182/323	46/15:85 (H_2O/EtOH)	Suhas et al. (2014)
PVA	PMA	IPA/H_2O	36/323	29 991/90:10 (IPA/H_2O)	Mali et al. (2011)
PVA	Silicalite-1	IPA/H_2O	69/323	2241/90:10 (IPA/H_2O)	Mali et al. (2011)
PBI	ZIF-8	IPA/H_2O	103/333	1686/15:85 (H_2O/IPA)	Shi et al. (2012)
PBI	ZIF-8	n-BuOH/H_2O	81/333	341.7/15:85 (H_2O/n-BuOH)	Shi et al. (2012)
PBI	ZIF-8	EtOH/H_2O	992/333	10/15:85 (H_2O/EtOH)	Shi et al. (2012)
PVA	5 wt % ZIF-8	IPA/H_2O	868/303	132/10:90 (H_2O/IPA)	Prasad et al. (2012)
PVA	7.5 wt % ZIF-8	IPA/H_2O	952/293	91/10:90 (H_2O/IPA)	Prasad et al. (2012)
PVA/PS	GOQDs	IPA/H2O	463.5/298	476.4/70:30 (IPA/H2O)	Lecaros et al. (2019)

CS: chitosan; GOQDs: graphene oxide quantum dots; H-ZSM5: zeolite socony mobil–5; IPA: Isopropyl alcohol; PBA: polybenzimidazole; PDMS: polydimethylsiloxane; PMA: phosphomolybdic acid; PVA: polyvinyl alcohol; THF: tetrahydrofuran; TMS-H-silica: trimethylsilanol hydrophobized silica; ZIF-8: zeolitic imidazolate framework; PS: polysulfone; Cu3(BTC)2: 1,3,5-benzene tricarboxylate; IDD: 4-isocyanato-40-(3,30-dimethyl-2,4-dioxo azetidino)diphenylmethane.

and personal care products. Another type of green membrane being widely used for the removal of synthesized products is the nanofiltration (NF) membrane. NF membranes conduct removal of small organic molecules, such as pharmaceuticals and pesticides through size exclusion and electrostatic interactions. NF membranes have shown high selectivity and efficiency in the removal of synthesized products, making them a promising option for water and wastewater treatment. Chemical contaminants, such as heavy metals, VOCs, and persistent organic pollutants (POPs), are present in various sources, including industrial effluents and contaminated soils. The removal of chemical contaminants is crucial to prevent their adverse effects on the environment and human health. Traditional treatment methods, such as chemical precipitation and adsorption, have limitations in terms of efficiency, cost, and environmental impact. Green membranes have shown great potential in the removal of chemical contaminants due to their high selectivity, permeability, and low energy consumption. One of the most common types of green membranes used for the removal of chemical contaminants is the RO membrane. RO membranes enable removal of various chemical contaminants, including heavy metals, VOCs, and POPs, based on size exclusion and electrostatic interactions mechanisms. RO membranes have shown high selectivity and efficiency in the removal of chemical contaminants, making them a promising option for water and wastewater treatment. Another green process repeatedly used for the removal of chemical contaminants is the membrane distillation (MD) process. MD utilize a temperature gradient to drive the separation of chemical contaminants from water, with exceptional. (Cevallos-Mendoza et al., 2022; Kim et al., 2018b; Heo et al., 2020).

4.4. Other applications

Membrane technology has gained much attention in the field of biomedical applications due to its unique properties such as permeability, selectivity, and stability. In recent years, there has been a growing interest in the development of green membranes, which are environmentally friendly, biocompatible, and biodegradable. Green synthesis, decoration, and fabrication of membranes are novel approaches that have been developed to enhance the properties of membranes. In this text, we will discuss the role of green membranes in various biomedical applications including drug delivery, gene delivery, tissue engineering, and biosensors. The green membranes based on naturally existing biological products possess multiple capabilities for legions of fields such as food industries, biomedical applications, sensing, gas separation, etc., in addition to the above-mentioned fields. Moreover, the use of biodegradable products surmounts the concerned obstacles of health and environmental safety, waste disposal, and energy crisis. Green membranes can be fabricated using various natural polymers, such as chitosan, cellulose, alginate, and gelatin, which particularly been well-known for supporting cell attachment and proliferation.

The membrane systems have been involved in the processing of different food products such as soybeans processing to tofu, yogurt, soy milk, cheese, or oil on the elimination of unwanted elements; the processing of dairy products to improve shelf-life, taste, and protein content; concentrating coconut water to healthy drinks and fermentation media; and processing of seaweeds to value-added products such as materials such as mannitol, carrageenan, alginate, and sorbitol (Tres et al., 2009; Firman et al., 2013; Van Meer et al., 2008; Rudin et al., 2021). Furthermore, green membranes have continuously and extensively been used in food industries as biodegradable thin films for food packaging.

Goh et al. prepared the biodegradable sandwich-designed composite thin films from PLA and reduced GO (PLA-rGO), which presented very good water and oxygen impermeability together with an excellent pertinency for food packaging. These thin films showed competency to extend the shelf life of air- and moisture-sensitive food products such as potato chips and edible oil (Goh et al., 2016).

Furthermore, the membrane systems have been an admirable tool for separating, concentrating, and purifying proteins, natural pigments, anthocyanins, polyphenols, and natural sweeteners from diverse sources such as plant extracts and agricultural food residues or fermented broth (Vedadghavami et al., 2018; Castro-Muñoz et al., 2020).

Aguero et al. (2017) examined separating proteins from whey, a byproduct of cheese manufacturing industries and the potential constituents for food or pharmaceutical industries, with economically integrated membrane systems compared to expensive chromatographic separation. The combination of pressure-driven membrane processes with charged membranes or an electrical field furnished great separation efficiency and avoided the concentration polarization problem of the conventional method.

Recently, Castro-Muñoz et al. (2020) provided an overview of membrane separation systems such as composite hydrophobic or organic solvent permeant membranes for better extraction and purification of natural sweeteners, *i.e.,* steviol glycosides obtained from *Stevia rebaudiana*. Natural sweeteners usually preclude the diseases such as *diabetes mellitus*, lipid metabolism disorders, and cancer by substituting sugar or its derivatives in food products. Furthermore, membrane technology has played a significant role in clarifying and concentrating juices, improving aroma retention and microbiological stability, preventing nutrient damage at a lower temperature, and reducing operational and transportation costs (Bhattacharjee et al., 2017). Hence, membranes perform a different role in making the food supply safer and more cost-effective.

The membrane systems are advantageous in various biomedical applications such as drug delivery, disease diagnosis, and tissue engineering. Here, the electrospun membranes comprised of PLA and polycaprolactone green polymers were proposed as excellent DDS due to their efficiency to release a molecule of interest in a controlled manner through fine fibrous structures, diameter 0.8 μm and 1.8 μm, respectively (Herrero-Herrero et al., 2018). Likewise, nano-channeled membranes are used as DDS. The membranes with uniform-sized nanochannels allow sustained drug release, whereas tunable sized and ligand-functionalized nanochannels permit controlled drug delivery based on stimuli such as pH control, light, or electrostatic balance (Zhang et al., 2018).

A sustained and controlled drug release is highly dependent on the type of diseases as chronic diseases such as graft rejection, autoimmune disorders, or hormone replacement require long-lasting drug release systems within the therapeutic range. In contrast, other diseases such as diabetes, asthma, or migraine need the drug supply only on-demand, under some specific circumstances. Furthermore, the microbial cellulose-based membranes usually offer their applicability in wound-dressing on account of their water holding capacity, flexibility, and biocompatibility. The guanidinium-based COF membranes (TpTGCl@PSF) also demonstrated inherent antimicrobial characteristics retarding the growth of both gram-positive and gram-negative bacteria and offering their suitability for such applications (Mitra et al., 2016).

The use of green membranes in tissue engineering has also shown promising results. Tissue engineering is an interdisciplinary field that aims to regenerate damaged or lost tissues by combining cells, biomaterials, and growth factors (Zarrintaj et al., 2018; Rahmati et al., 2021). One of the key challenges in tissue engineering is to create a 3D scaffold that can provide a suitable microenvironment for cells to grow and differentiate. Traditional scaffolds are made of synthetic polymers or ceramics, which often lack biological cues that can promote cell adhesion, proliferation, and differentiation. Green membranes, on the other hand, offer a unique combination of biocompatibility, biodegradability, and bioactivity, which make them an attractive candidate for tissue engineering applications. The membranes based on green materials have also been applied in tissue engineering (Yazdi et al., 2020b); for example, Xu et al. (2017) observed the magnificent mineralization of hydroxyapatite (regeneration membrane) on PLA/chitosan scaffolds, showing improved attachment and growth of preosteoblast

(MC3T3-E1) cells suited for bone tissue engineering. Many other research groups also divulged the impending applications of sustainable PLA fibrous membranes embellished with highly bioactive chitosan, graphene-based nanomaterials, and human amniotic membranes for wound healing and tissue engineering (Xu et al., 2017; Wang et al., 2013; Nguyen and Park, 2011; Au et al., 2012; Shalumon et al., 2012; Lee et al., 2015; Guazzo et al., 2018; Sara et al., 2020).

Additionally, the membranes, particularly ionophores and nanostructured based membranes, demonstrated their applications in separation and sensing of several ions or molecules, e.g., Na^+, K^+, Ca^{2+}, Li^+, Mg^{2+}, Cl^-, F^-, SCN− (Asadnia et al., 2016, 2017; Sanders et al., 2017), ion separations (Ahmadi et al., 2020), cancer biomarkers (Pan et al., 2017; Hasanzadeh et al., 2018), pharmaceutical products (Faridbod and Dorrani, 2015; Gomes Amorim et al., 2019) and exosomes (Su et al., 2019a; Marczak et al., 2021). The mechanism underlying such phenomena is grounded on assistance of the early disease diagnosis and precise biosensing. The ionic and molecular selective membranes have also shown their applicability in wearable devices such as tattoos, smartwatches, sweatbands, or fabric patches to monitor human health by analyzing specific ions or molecules in biological fluids such as blood, sweat, etc. urine, and tears (Wang et al., 2021; Huang et al., 2019). Hence, there are endless ever-increasing applications of membranes in the field of healthcare and biomedical to be explored.

The ion-selective membranes also play a significant role in flow batteries, a promising technology for renewable energy sources' sustainable and efficient use. For example, a single-cell membrane in the vanadium flow battery (VFB) restricts the vanadium ions to move into the anolyte/catholyte whilst allowing the proton transport to form an internal circuit (Schwenzer et al., 2011).

The most frequently used VFB nowadays is the Nafion-based family, but there is a need for an alternate due to their high cost. Several green approaches have been proposed to design high-performance, inexpensive and eco-friendly composite ion-exchange membranes to balance ion selectivity and proton conductivity in the current scenario. In addition to ionic separation, green membrane systems have correspondingly been employed in gaseous separation. For instance, Qiu et al. (2014) comprehensively reviewed the application of MOF membranes for the separation and purification of hydrogen and carbon dioxide and the efficient separation of propylene and propane, possessing similar physical properties.

The separation efficiency of microporous membranes depends not only on the size/shape of the separate molecules or their interaction with the matrix but also on several other factors such as the pore size distribution, limiting pore size, surface diffusion, capillary condensation, shape selectivity, molecular sieving, and preferential adsorption. A green flexible nanocomposite membrane was designed, which was efficient to capture air particulates as small as 2.5 μm, usually comprising inorganic (NO_3, SiO_2, and SO_4) and/or organic (elemental or organic carbon) matter (Cui et al., 2021). The air filters comprising of PVA and sodium lignosulfonate (LS) are assembled by combining biocompatible electrospinning and physical crosslinking methods, which displayed high tensile strength (25.8 ± 4.3 MPa), low-pressure drop (24.5 Pa), and sustained filtration efficiency (99.38–99.44%) even after 10 filtration cycles. The durable environmental-friendly membranes possess the usability in personal protection masks from outdoor air pollution.

Many biocompatible and photo-crosslinked electrospun nanofibrous membranes were tailored with chitosan, PVA, superhydrophobic silica, and AgNPs (CS/PVA@SiO_2/AgNPs) which possess not only high filtration efficiency but also antibacterial characteristics (Zhu et al., 2019b). Currently, due to the Covid-19 pandemic, membrane separation systems have been extensively used in personal protection masks and equipment kits to filter air particles and pathogens and avoid health investments (Buluş et al., 2020; Micah et al., 2023). Hence, applications of green membrane articulate the sustainable development and perpetual resolution for safer water and food supply, drug delivery, tissue engineering, the economic recovery of drugs and other organic molecules.

In a more specific view, one can consider the use of green membranes in DDS, which has progressively been on-demand in recent years due to their biocompatibility, biodegradability, and controlled release properties. Green membranes used in this field are mainly synthesized using a well-defined class of natural materials such as chitosan, cellulose, and alginate, which are non-toxic, renewable, and abundant. These materials have shown excellent potential for drug delivery due to their ability to encapsulate a wide range of drugs, including hydrophobic and hydrophilic drugs (Khan et al., 2019; Bagheri et al., 2019).

Chitosan-based membranes have been extensively used in DDS due to their excellent biocompatibility, biodegradability, and mucoadhesive properties. Chitosan is a natural polymer derived from chitin, which is found in the exoskeletons of crustaceans. Chitosan-based membranes have been used to deliver a wide range of drugs, including proteins, peptides, and small molecules (Mohebbi et al., 2019). The use of chitosan-based membranes in DDS has opened and enlightened new avenues in drug bioavailability, reduce toxicity, and provide controlled release of drugs. Green membranes are excellent for gene delivery due to their biocompatibility, biodegradability, and ability to protect nucleic acids from degradation. Chitosan-based membranes have been extensively used in gene delivery systems. Chitosan-based membranes have been shown to protect DNA and RNA from degradation and to facilitate the delivery of nucleic acids into cells. Chitosan-based membranes have been used to deliver genes such as green fluorescent protein, bone morphogenetic protein, and vascular endothelial growth factor. The use of chitosan-based membranes in gene delivery systems has been shown to increase gene expression, reduce immune responses, and provide sustained gene delivery (Saeedi et al., 2022; Rabiee et al., 2021b; Hamedi et al., 2022). In view of cell attachment and proliferation, chitosan membranes have been used to support the growth of osteoblasts, which are bone-forming cells, and promote bone regeneration *in vivo*.

Cellulose-based membranes have also been widely used in DDS. Cellulose is a natural polymer derived from plant cell walls and has excellent biocompatibility and biodegradability. Cellulose-based membranes have been used to deliver drugs such as doxorubicin, paclitaxel, and curcumin. The use of cellulose-based membranes in DDS has been shown to increase drug stability, provide controlled release of drugs, and reduce drug toxicity. Cellulose-based membranes have also been used in gene delivery systems. Cellulose-based membranes have been shown to protect DNA and RNA from degradation and to facilitate the delivery of nucleic acids into cells. Cellulose-based membranes have also been modified with functional groups such as carboxyl, amine, and sulfonic acid to enhance their gene delivery capabilities. Similar to chitosan, cellulose membranes have been used to support the growth of fibroblasts, which are cells producing extracellular matrix proteins, and promote wound healing *in vivo*.

Alginate-based membranes have also been extensively used in DDS. Alginate is a natural polymer derived from seaweed and has excellent biocompatibility and biodegradability. Alginate-based membranes have been used to deliver drugs such as insulin, doxorubicin, and vancomycin. The use of alginate-based membranes in DDS has been shown to increase drug stability, provide sustained release of drugs, and reduce drug toxicity. Green membranes have also been used in gene delivery systems due to their ability to protect DNA and RNA from degradation and to facilitate the delivery of nucleic acids into cells. Gene delivery is an emerging field that aims to deliver therapeutic genes into cells to treat genetic disorders and other diseases. Alginate membranes have been used to encapsulate pancreatic islet cells and protect them from immune rejection in diabetes treatment.

Other types of green membranes are also investigated. For instance, gelatin ones have been used to promote the differentiation of stem cells into cartilage and bone tissues. In addition to individual usage of green polymers, blends of biopolymers, e.g. chitosan and other biopolymers, have shown a great potential for biomedical engineering applications (Seidi et al., 2021). Moreover, green membranes can be decorated with

various bioactive molecules, such as growth factors, peptides, and drugs, to enhance their bioactivity and therapeutic potential. For example, chitosan membranes have been decorated with bone morphogenetic protein-2 (BMP-2), a growth factor that can stimulate bone formation, and used to promote bone regeneration *in vivo*. Cellulose membranes have been decorated with epidermal growth factor (EGF), a growth factor that can stimulate cell proliferation and migration, and used to promote wound healing in vitro. Alginate membranes have been decorated with insulin-like growth factor-1 (IGF-1), a growth factor that can stimulate cell proliferation and differentiation, and used to promote tissue regeneration *in vivo*. Gelatin membranes have been decorated with various peptides, such as RGD and YIGSR, which can enhance cell adhesion and migration, and used to promote tissue engineering in vitro and *in vivo* (Min et al., 2020; Frati et al., 2020; Miyagawa et al., 2020; Su et al., 2019b).

In addition to tissue engineering, green membranes also hold great potential for DDS and gene delivery systems. DDS based on green membranes have several advantages over conventional ones, such as improved biocompatibility, biodegradability, and targeting efficiency. Green membranes can be used to encapsulate drugs and release them in a controlled manner, which can minimize side effects and increase therapeutic efficacy. Moreover, green membranes can be functionalized with targeting ligands, such as antibodies or aptamers, which can selectively deliver drugs to specific cells or tissues. Gene delivery systems based on green membranes also offer several advantages over conventional gene delivery systems, such as improved biocompatibility, transfection efficiency, and safety. Green membranes can be used to encapsulate nucleic acids, such as plasmid DNA or siRNA, and deliver them to cells or tissues. Green membranes can protect nucleic acids from enzymatic degradation and facilitate their uptake by cells. Moreover, green membranes can be functionalized with targeting ligands, such as peptides or aptamers, which can enhance their specificity and selectivity (Zhu et al., 2015; Fahimmunisha et al., 2020; Jahangirian et al., 2017; Sivanesan et al., 2021; Kalantari et al., 2019; Fang et al., 2017; Yunas et al., 2020).

5. Conclusion and future direction

Membranes are emerging technologies for water desalination and/or purification with promising potential for highly efficient removal of organic, inorganic, pharmaceutical, and heavy metal contaminants. However, traditional membranes usually contain toxic substances along with fouling of contaminants that imposes some safety and environmental risks. Therefore, petroleum-based membranes should be replaced by non-toxic substances of desirable efficiency. Greener alternatives to the traditional membrane are recognized as the solution to this problem. In this regard, we reviewed green synthesized nano-membranes by focusing on metal and metal oxide, polymeric nanoparticles, metal-organic frameworks, and nanocomposites, highlighting their toxicity and biosafety issues. The use of synthesized green nanomaterials as a membrane seems inspiring for the removal of contaminants and aqueous metal ions. Nevertheless, it is not that easy to switch from a conventional to a green nano-membrane, as a consequence of some challenging features to be considered according to the regulations dictated by the green institutional agencies. First, sustainability, toxicity, and safety requirementsshould be considered when designing green nano-membranes in the quest of production at industrial and commercial scales. Second, although the fabrication of nano-membranes based on green synthesis methods is simple and environmentally friendly, the effects of reaction parameters and the stability of the prepared materials should be analyzed and optimized. Materials and operational factors affect the behavior of nanomaterials, their morphology and contaminant removal efficiency, which are interdependently correlated in a complex manner. Therefore, multi-objective optimization seems necessary after collecting several bundles of data. Third, cost-effectiveness analyses are centered on the green nano-membranes manufacturing. In this regard, preparation of green-synthesized nano-membranes should be economically compared with the corresponding conventional membranes.

The development of advanced membrane materials exhibiting enhanced mechanical, thermal, and chemical stability, and a performance competitive with or superior to conventional membranes has become increasingly important from both industrial and environmental angles. The use of natural components and materials in membrane technology offers several advantages over conventional materials like polymeric membranes. One of the most significant advantages of natural components and materials is their inherent biocompatibility and biodegradability, which makes them more environmentally friendly than conventional synthetic materials. Moreover, natural components and materials offer unique properties such as high porosity, surface area, and sometimes comparable mechanical strength, which make them suitable for myriad applications. For example, the use of natural materials such as cellulose, chitin, and silk fibroin in membrane technology has been shown to provide the user with excellent mechanical strength, biocompatibility, and biodegradability. Another advantage of using natural materials in membrane technology is their potential for functionalization and modification. For instance, natural materials such as chitosan and lignin can be modified to exhibit unique properties such as antibacterial activity and improved selectivity for specific ions. In addition, natural materials can be combined with other materials such as carbon nanotubes, graphene, and metal nanoparticles to enhance their properties and functionality. The future ahead of green or natural component-based membranes in water treatment and other applications looks bright, with numerous ongoing research efforts aimed at improving their performance and expanding their applications. One of the promising areas of research in this field is the development of advanced green nano-membranes that can selectively remove specific contaminants from water and other fluids. For example, researchers examined the use of natural materials such as zeolites, clays, and activated carbon in membrane technology to selectively remove heavy metals, organic pollutants, and other contaminants from water. Another area of research is the use of natural materials in the development of self-cleaning and anti-fouling membranes. Fouling is a common problem that occurs in membrane systems due to the accumulation of microorganisms, colloids, and other materials on the membrane surface, leading to reduced membrane performance and efficiency. Researchers are exploring the use of natural materials such as polyphenols and bio-inspired coatings in membrane technology to prevent fouling and improve membrane efficiency. The development of natural component-based membranes for other applications such as gas separation and energy storage is also an area of active research. For instance, researchers applied lignin and cellulose in the development of advanced membranes for gas separation and carbon capture applications. In addition, the use of natural materials in the development of advanced membranes for energy storage applications such as batteries and supercapacitors is gaining momentum.

In conclusion, some critical issues related to green-synthesized nano-based membranes' toxicity, biosafety, and mechanistic aspects should be carefully and consistently assessed. More detailed studies have yet been requested to reach a low-cost, recyclable green fabricated nano-membrane with high adsorption capacity and selectivity. In addition, it would be beneficial to analyze the efficacy and removal performance of the green nano-membrane under service.

Declaration of competing interest

The authors declare that they have no known competing financial interests or personal relationships that could have appeared to influence the work reported in this paper.

Data availability

No data was used for the research described in the article.

Acknowledgment

The authors would like to thanks BioRender.com for their professional services in designing the figures/schemes.

References

Abdellah, M.H., Pérez-Manríquez, L., Puspasari, T., Scholes, C.A., Kentish, S.E., Peinemann, K.-V., 2018. A catechin/cellulose composite membrane for organic solvent nanofiltration. J. Membr. Sci. 567, 139–145.
Abdollahzadeh, M., Hosseini, E., Ahmadi, H., Lim, S., Korayem, A.H., Razmjou, A., Asadnia, M., 2021. Low humid transport of anions in layered double hydroxides membranes using polydopamine coating. J. Membr. Sci. 624, 118974.
Aburabie, J.H., Puspasari, T., Peinemann, K.-V., 2020. Alginate-based membranes: paving the way for green organic solvent nanofiltration. J. Membr. Sci. 596, 117615.
Adatoz, E., Avci, A.K., Keskin, S., 2015. Opportunities and challenges of MOF-based membranes in gas separations. Separ. Purif. Technol. 152, 207–237.
Adyani, S.H., Soleimani, E., 2019. Green synthesis of Ag/Fe3O4/RGO nanocomposites by Punica Granatum peel extract: catalytic activity for reduction of organic pollutants. Int. J. Hydrogen Energy 44 (5), 2711–2730.
Agrawal, S., Ranjan, R., Lal, B., Rahman, A., Singh, S.P., Selvaratnam, T., Nawaz, T., 2021. Synthesis and water treatment applications of nanofibers by electrospinning. Processes 9 (10), 1779.
Aguado, S., Nicolas, C.-H., Moizan-Baslé, V., Nieto, C., Amrouche, H., Bats, N., Audebrand, N., Farrusseng, D., 2011. Facile synthesis of an ultramicroporous MOF tubular membrane with selectivity towards CO 2. New J. Chem. 35 (1), 41–44.
Aguero, R., Bringas, E., San Román, M., Ortiz, I., Ibanez, R., 2017. Membrane processes for whey proteins separation and purification. A review. Curr. Org. Chem. 21 (17), 1740–1752.
Ahmadi, H., Hosseini, E., Cha-Umpong, W., Abdollahzadeh, M., Korayem, A.H., Razmjou, A., Chen, V., Asadnia, M., 2020. Incorporation of natural lithium-ion trappers into graphene oxide nanosheets. Advanced Materials Technologies, 2000665.
Al Jabri, H., Saleem, M.H., Rizwan, M., Hussain, I., Usman, K., Alsafran, M., 2022. Zinc oxide nanoparticles and their biosynthesis: overview. Life 12 (4), 594.
Al Mayyahi, A., 2018. Thin-film composite (TFC) membrane modified by hybrid ZnO-graphene nanoparticles (ZnO-Gr NPs) for water desalination. J. Environ. Chem. Eng. 6 (1), 1109–1117.
Alharbi, F.A., Alarfaj, A.A., 2020. Green synthesis of silver nanoparticles from Neurada procumbens and its antibacterial activity against multi-drug resistant microbial pathogens. J. King Saud Univ. Sci. 32 (2), 1346–1352.
Ali, H.R., Nassar, H.N., El-Gendy, N.S., 2017. Green synthesis of α-Fe2O3 using Citrus reticulum peels extract and water decontamination from different organic pollutants. Energy Sources, Part A Recovery, Util. Environ. Eff. 39 (13), 1425–1434.
Alippilakkotte, S., Kumar, S., Sreejith, L., 2017. Fabrication of PLA/Ag nanofibers by green synthesis method using Momordica charantia fruit extract for wound dressing applications. Colloids Surf. A Physicochem. Eng. Asp. 529, 771–782.
Almeida, M.I.G., Cattrall, R.W., Kolev, S.D., 2017. Polymer inclusion membranes (PIMs) in chemical analysis-A review. Anal. Chim. Acta 987, 1–14.
Aminuzzaman, M., Ying, L.P., Goh, W.-S., Watanabe, A., 2018. Green synthesis of zinc oxide nanoparticles using aqueous extract of Garcinia mangostana fruit pericarp and their photocatalytic activity. Bull. Mater. Sci. 41 (2), 1–10.
Amir Razmjou, M.A., Hosseini, Ehsan, Asghar Habibnejad Korayem, Chen, Vicki, 2019. Design principles of ion selective nanostructured membranes for the extraction of lithium ions. Nat. Commun. 10 (1), 5793.
Amiri, M., Salavati-Niasari, M., Akbari, A., Gholami, T., 2017. Removal of malachite green (a toxic dye) from water by cobalt ferrite silica magnetic nanocomposite: herbal and green sol-gel autocombustion synthesis. Int. J. Hydrogen Energy 42 (39), 24846–24860.
Appapalam, S.T., Panchamoorthy, R., 2017. Aerva lanata mediated phytofabrication of silver nanoparticles and evaluation of their antibacterial activity against wound associated bacteria. J. Taiwan Inst. Chem. Eng. 78, 539–551.
Applerot, G., Lipovsky, A., Dror, R., Perkas, N., Nitzan, Y., Lubart, R., Gedanken, A., 2009. Enhanced antibacterial activity of nanocrystalline ZnO due to increased ROS-mediated cell injury. Adv. Funct. Mater. 19 (6), 842–852.
Asadi, S., Tabani, H., Nojavan, S., 2018. Application of polyacrylamide gel as a new membrane in electromembrane extraction for the quantification of basic drugs in breast milk and wastewater samples. J. Pharmaceut. Biomed. Anal. 151, 178–185.
Asadnia, M., Myers, M., Akhavan, N.D., O'Donnell, K., Umana-Membreno, G.A., Mishra, U., Nener, B., Baker, M., Parish, G., 2016. Mercury (II) selective sensors based on AlGaN/GaN transistors. Anal. Chim. Acta 943, 1–7.
Asadnia, M., Myers, M., Umana-Membreno, G.A., Sanders, T.M., Mishra, U.K., Nener, B. D., Baker, M.V., Parish, G., 2017. Ca2+ detection utilising AlGaN/GaN transistors with ion-selective polymer membranes. Anal. Chim. Acta 987, 105–110.
Ashour, R.M., Abdel-Magied, A.F., Wu, Q., Olsson, R.T., Forsberg, K., 2020. Green synthesis of metal-organic framework bacterial cellulose nanocomposites for separation applications. Polymers 12 (5), 1104.
Au, H.T., Pham, L.N., Vu, T.H.T., Park, J.S., 2012. Fabrication of an antibacterial non-woven mat of a poly (lactic acid)/chitosan blend by electrospinning. Macromol. Res. 20 (1), 51–58.
Aziz, N., Faraz, M., Sherwani, M.A., Fatma, T., Prasad, R., 2019. Illuminating the anticancerous efficacy of a new fungal chassis for silver nanoparticle synthesis. Front. Chem. 7, 65.
Bagheri, B., Zarrintaj, P., Surwase, S.S., Baheiraei, N., Saeb, M.R., Mozafari, M., Kim, Y. C., Park, O.O., 2019. Self-gelling electroactive hydrogels based on chitosan–aniline oligomers/agarose for neural tissue engineering with on-demand drug release. Colloids Surf. B Biointerfaces 184, 110549.
bakht Dalir, S.J., Djahaniani, H., Nabati, F., Hekmati, M., 2020. Characterization and the evaluation of antimicrobial activities of silver nanoparticles biosynthesized from Carya illinoinensis leaf extract. Heliyon 6 (3), e03624.
Basavaiah, K., Kahsay, M.H., RamaDevi, D., 2018. Green synthesis of magnetite nanoparticles using aqueous pod extract of Dolichos lablab L for an efficient adsorption of crystal violet. Emergent Materials 1 (3), 121–132.
Behpour, M., Tabani, H., Nojavan, S., 2020. Gel electromembrane extraction using rotating electrode: a new strategy for mass transfer enhancement of basic drugs from real human urine samples. J. Chromatogr. B 1152, 122258.
Bey, S., Criscuoli, A., Simone, S., Figoli, A., Benamor, M., Drioli, E., 2011. Hydrophilic PEEK-WC hollow fibre membrane contactors for chromium (VI) removal. Desalination 283, 16–24.
Bhattacharjee, C., Saxena, V., Dutta, S., 2017. Fruit juice processing using membrane technology: a review. Innovat. Food Sci. Emerg. Technol. 43, 136–153.
Bi, R., Zhang, R., Shen, J., Liu, Y.-n., He, M., You, X., Su, Y., Jiang, Z., 2019. Graphene quantum dots engineered nanofiltration membrane for ultrafast molecular separation. J. Membr. Sci. 572, 504–511.
Boerma, J.S., Elias, N.S., Vermeulen, N.P., Commandeur, J.N., 2015. Mini-dialysis tubes as tools to prepare drug-protein adducts of P450-dependent reactive drug metabolites. J. Pharmaceut. Biomed. Anal. 103, 17–25.
Bordbar, M., Negahdar, N., Nasrollahzadeh, M., Melissa Officinalis, L., 2018. Leaf extract assisted green synthesis of CuO/ZnO nanocomposite for the reduction of 4-nitrophenol and Rhodamine B. Separ. Purif. Technol. 191, 295–300.
Bremner, D.H., Molina, R., Martínez, F., Melero, J.A., Segura, Y., 2009. Degradation of phenolic aqueous solutions by high frequency sono-Fenton systems (US–Fe2O3/SBA-15–H2O2). Appl. Catal. B Environ. 90 (3–4), 380–388.
Brown, J., 2017. Impact of silver nanoparticles on wastewater treatment. In: Nanotechnologies for Environmental Remediation. Springer, pp. 255–267.
Buluş, E., Buluş, G.S., Yakuphanoglu, F., 2020. Production of polylactic acid-activated charcoal nanofiber membranes for COVID-19 pandemic by electrospinning technique and determination of filtration efficiency. Journal of Materials and Electronic Devices 4 (1), 21–26.
Cabello, S.P., Ochoa, N.A., Takara, E.A., Mollá, S., Compañ, V., 2017. Influence of Pectin as a green polymer electrolyte on the transport properties of Chitosan-Pectin membranes. Carbohydr. Polym. 157, 1759–1768.
Calderon, B., Smith, F., Aracil, I., Fullana, A., 2018. Green synthesis of thin shell carbon-encapsulated iron nanoparticles via hydrothermal carbonization. ACS Sustain. Chem. Eng. 6 (6), 7995–8002.
Cao, K., Jiang, Z., Zhao, J., Zhao, C., Gao, C., Pan, F., Wang, B., Cao, X., Yang, J., 2014. Enhanced water permeation through sodium alginate membranes by incorporating graphene oxides. J. Membr. Sci. 469, 272–283.
Carner, C.A., Croft, C.F., Kolev, S.D., Almeida, M.I.G., 2020. Green solvents for the fabrication of polymer inclusion membranes (PIMs). Separ. Purif. Technol. 239, 116486.
Castro-Muñoz, R., Galiano, F., Fíla, V., Drioli, E., Figoli, A., 2019. Mixed matrix membranes (MMMs) for ethanol purification through pervaporation: current state of the art. Rev. Chem. Eng. 35 (5), 565–590.
Castro-Muñoz, R., Díaz-Montes, E., Cassano, A., Gontarek, E., 2020. Membrane separation processes for the extraction and purification of steviol glycosides: an overview. Crit. Rev. Food Sci. Nutr. 1–23.
Celebioglu, A., Topuz, F., Yildiz, Z.I., Uyar, T., 2019. One-step green synthesis of antibacterial silver nanoparticles embedded in electrospun cyclodextrin nanofibers. Carbohydr. Polym. 207, 471–479.
Cevallos-Mendoza, J., Amorim, C.G., Rodríguez-Díaz, J.M., Montenegro, M.d.C.B., 2022. Removal of contaminants from water by membrane filtration: a review. Membranes 12 (6), 570.
Chang, J., Zuo, J., Zhang, L., O'Brien, G.S., Chung, T.-S., 2017. Using green solvent, triethyl phosphate (TEP), to fabricate highly porous PVDF hollow fiber membranes for membrane distillation. J. Membr. Sci. 539, 295–304.
Chen, X., Lu, W., Xu, T., Li, N., Qin, D., Zhu, Z., Wang, G., Chen, W., 2017. A bio-inspired strategy to enhance the photocatalytic performance of g-C3N4 under solar irradiation by axial coordination with hemin. Appl. Catal. B Environ. 201, 518–526.
Chen, L., Moon, J.-H., Ma, X., Zhang, L., Chen, Q., Chen, L., Peng, R., Si, P., Feng, J., Li, Y., 2018. High performance graphene oxide nanofiltration membrane prepared by electrospraying for wastewater purification. Carbon 130, 487–494.
Chen, B., Jin, Z., Pei, X., Li, J., Liu, C., Zhao, H., 2020. Liquid-like secondary amine containing POSS as reactive nanoadditive to improve the anticorrosion performance of epoxy coating. Mater. Lett. 261, 127103.
Cheng, H., Zhu, X., Yang, S., Wu, Y., Cao, Q., Ding, Z., 2013. A pH-controllable imprinted composite membrane for selective separation of podophyllotoxin and its analog. J. Appl. Polym. Sci. 128 (1), 363–370.
Cheng, M.-m., Huang, L.-j., Wang, Y.-x., Zhao, Y.-c., Tang, J.-g., Wang, Y., Zhang, Y., Hedayati, M., Kipper, M.J., Wickramasinghe, S.R., 2019. Synthesis of graphene oxide/polyacrylamide composite membranes for organic dyes/water separation in water purification. J. Mater. Sci. 54 (1), 252–264.

Chong, M.N., Jin, B., Chow, C.W., Saint, C., 2010. Recent developments in photocatalytic water treatment technology: a review. Water Res. 44 (10), 2997–3027.
Choudhury, P., Mondal, P., Majumdar, S., Saha, S., Sahoo, G.C., 2018. Preparation of ceramic ultrafiltration membrane using green synthesized CuO nanoparticles for chromium (VI) removal and optimization by response surface methodology. J. Clean. Prod. 203, 511–520.
Colburn, A., Wanninayake, N., Kim, D., Bhattacharyya, D., 2018. Cellulose-graphene quantum dot composite membranes using ionic liquid. J. Membr. Sci. 556, 293–302.
Cui, Z., Hassankiadeh, N.T., Lee, S.Y., Lee, J.M., Woo, K.T., Sanguineti, A., Arcella, V., Lee, Y.M., Drioli, E., 2013. Poly (vinylidene fluoride) membrane preparation with an environmental diluent via thermally induced phase separation. J. Membr. Sci. 444, 223–236.
Cui, J., Wu, Y., Meng, M., Lu, J., Wang, C., Zhao, J., Yan, Y., 2016. Bio-inspired synthesis of molecularly imprinted nanocomposite membrane for selective recognition and separation of artemisinin. J. Appl. Polym. Sci. 133 (19).
Cui, J., Zhang, Y., Wang, Y., Ding, J., Yu, P., Yan, Y., Li, C., Zhou, Z., 2018. Fabrication of lithium ion imprinted hybrid membranes with antifouling performance for selective recovery of lithium. New J. Chem. 42 (1), 118–128.
Cui, J., Zhou, Z., Xie, A., Liu, S., Wang, Q., Wu, Y., Yan, Y., Li, C., 2019. Facile synthesis of degradable CA/CS imprinted membrane by hydrolysis polymerization for effective separation and recovery of Li+. Carbohydr. Polym. 205, 492–499.
Cui, J., Lu, T., Li, F., Wang, Y., Lei, J., Ma, W., Zou, Y., Huang, C., 2021. Flexible and transparent composite nanofibre membrane that was fabricated via a "green" electrospinning method for efficient particulate matter 2.5 capture. J. Colloid Interface Sci. 582, 506–514.
da Silva, D.A.R.O., Zuge, L.C.B., de Paula Scheer, A., 2020. Preparation and characterization of a novel green silica/PVA membrane for water desalination by pervaporation. Separ. Purif. Technol. 247, 116852.
Dahlin, A.P., Purins, K., Clausen, F., Chu, J., Sedigh, A., Lorant, T., Enblad, P., Lewen, A., Hillered, L., 2014. Refined microdialysis method for protein biomarker sampling in acute brain injury in the neurointensive care setting. Anal. Chem. 86 (17), 8671–8679.
Dankovich, T.A., Gray, D.G., 2011. Bactericidal paper impregnated with silver nanoparticles for point-of-use water treatment. Environ. Sci. Technol. 45 (5), 1992–1998.
Datta, A., Patra, C., Bharadwaj, H., Kaur, S., Dimri, N., Khajuria, R., 2017. Green synthesis of zinc oxide nanoparticles using parthenium hysterophorus leaf extract and evaluation of their antibacterial properties. J. Biotechnol. Biomater. 7 (3), 271–276.
de Oliveira, C.P.M., Viana, M.M., Amaral, M.C.S., 2020. Coupling photocatalytic degradation using a green TiO2 catalyst to membrane bioreactor for petroleum refinery wastewater reclamation. J. Water Process Eng. 34, 101093.
Devatha, C., Thalla, A.K., Katte, S.Y., 2016. Green synthesis of iron nanoparticles using different leaf extracts for treatment of domestic waste water. J. Clean. Prod. 139, 1425–1435.
Dey, K., Pal, M., Rout, K.C., Kunjattu H, S., Das, A., Mukherjee, R., Kharul, U.K., Banerjee, R., 2017. Selective molecular separation by interfacially crystallized covalent organic framework thin films. J. Am. Chem. Soc. 139 (37), 13083–13091.
Didaskalou, C., Buyuktiryaki, S., Kecili, R., Fonte, C.P., Szekely, G., 2017. Valorisation of agricultural waste with an adsorption/nanofiltration hybrid process: from materials to sustainable process design. Green Chem. 19 (13), 3116–3125.
Dima, S.-O., Sarbu, A., Dobre, T., Bradu, C., Antohe, N., Radu, A.-L., Nicolescu, T.-V., Lungu, A., 2009. Molecularly imprinted membranes for selective separations. Mater. Plast. 46 (4), 372–378.
Divya, K., Kurian, L.C., Vijayan, S., Manakulam Shaikmoideen, J., 2016. Green synthesis of silver nanoparticles by Escherichia coli: analysis of antibacterial activity. Journal of Water and Environmental Nanotechnology 1 (1), 63–74.
Donato, L., Drioli, E., 2021. Imprinted membranes for sustainable separation processes. Front. Chem. Sci. Eng. 1–18.
Dubey, S., Kumar, J., Kumar, A., Sharma, Y.C., 2018. Facile and green synthesis of highly dispersed cobalt oxide (Co3O4) nano powder: characterization and screening of its eco-toxicity. Adv. Powder Technol. 29 (11), 2583–2590.
Efome, J.E., Rana, D., Matsuura, T., Lan, C.Q., 2018. Metal–organic frameworks supported on nanofibers to remove heavy metals. J. Mater. Chem. 6 (10), 4550–4555.
Eggensperger, C.G., Giagnorio, M., Holland, M.C., Dobosz, K.M., Schiffman, J.D., Tiraferri, A., Zodrow, K.R., 2020. Sustainable living filtration membranes. Environ. Sci. Technol. Lett. 7 (3), 213–218.
Elella, M.H.A., Goda, E.S., Abdallah, H.M., Shalan, A.E., Gamal, H., Yoon, K.R., 2021. Innovative bactericidal adsorbents containing modified xanthan gum/montmorillonite nanocomposites for wastewater treatment. Int. J. Biol. Macromol. 167, 1113–1125.
Eskandarloo, H., Kierulf, A., Abbaspourrad, A., 2017. Nano-and micromotors for cleaning polluted waters: focused review on pollutant removal mechanisms. Nanoscale 9 (37), 13850–13863.
Ezhilarasi, A.A., Vijaya, J.J., Kaviyarasu, K., Kennedy, L.J., Ramalingam, R.J., Al-Lohedan, H.A., 2018. Green synthesis of NiO nanoparticles using Aegle marmelos leaf extract for the evaluation of in-vitro cytotoxicity, antibacterial and photocatalytic properties. J. Photochem. Photobiol. B Biol. 180, 39–50.
Fadeev, A., Meagher, M., Kelley, S., Volkov, V., 2000. Fouling of poly [-1-(trimethylsilyl)-1-propyne] membranes in pervaporative recovery of butanol from aqueous solutions and ABE fermentation broth. J. Membr. Sci. 173 (1), 133–144.
Fahimmunisha, B.A., Ishwarya, R., AlSalhi, M.S., Devanesan, S., Govindarajan, M., Vaseeharan, B., 2020. Green fabrication, characterization and antibacterial potential of zinc oxide nanoparticles using Aloe socotrina leaf extract: a novel drug delivery approach. J. Drug Deliv. Sci. Technol. 55, 101465.
Falca, G., Musteata, V.-E., Behzad, A.R., Chisca, S., Nunes, S.P., 2019. Cellulose hollow fibers for organic resistant nanofiltration. J. Membr. Sci. 586, 151–161.
Fan, L., Ma, Y., Su, Y., Zhang, R., Liu, Y., Zhang, Q., Jiang, Z., 2015. Green coating by coordination of tannic acid and iron ions for antioxidant nanofiltration membranes. RSC Adv. 5 (130), 107777–107784.
Fan, H., Gu, J., Meng, H., Knebel, A., Caro, J., 2018. High-flux membranes based on the covalent organic framework COF-LZU1 for selective dye separation by nanofiltration. Angew. Chem. Int. Ed. 57 (15), 4083–4087.
Fang, R.H., Jiang, Y., Fang, J.C., Zhang, L., 2017. Cell membrane-derived nanomaterials for biomedical applications. Biomaterials 128, 69–83.
Faridbod, F., Dorrani, M., 2015. Clenbuterol determination in pharmaceutical formulation by potentiometric membrane sensor. Int. J. Electrochem. Sci. 10 (2), 1447–1458.
Fathizadeh, M., Tien, H.N., Khivantsev, K., Song, Z., Zhou, F., Yu, M., 2019. Polyamide/nitrogen-doped graphene oxide quantum dots (N-GOQD) thin film nanocomposite reverse osmosis membranes for high flux desalination. Desalination 451, 125–132.
Fei, F., Le Phuong, H.A., Blanford, C.F., Szekely, G., 2019. Tailoring the performance of organic solvent nanofiltration membranes with biophenol coatings. ACS applied polymer materials 1 (3), 452–460.
Feng, L., Zhang, Z., Mai, Z., Ma, Y., Liu, B., Jiang, L., Zhu, D., 2004. A super-hydrophobic and super-oleophilic coating mesh film for the separation of oil and water. Angew. Chem. 116 (15), 2046–2048.
Ferreira, D., Slade, D., 2002. Oligomeric proanthocyanidins: naturally occurring O-heterocycles. Nat. Prod. Rep. 19 (5), 517–541.
Figoli, A., Marino, T., Simone, S., Di Nicolo, E., Li, X.-M., He, T., Tornaghi, S., Drioli, E., 2014. Towards non-toxic solvents for membrane preparation: a review. Green Chem. 16 (9), 4034–4059.
Firman, L.R., Ochoa, N.A., Marchese, J., Pagliero, C.L., 2013. Deacidification and solvent recovery of soybean oil by nanofiltration membranes. J. Membr. Sci. 431, 187–196.
Fortunato, E., Barquinha, P., Pimentel, A., Goncalves, A., Marques, A., Pereira, L., Martins, R., 2005. Recent advances in ZnO transparent thin film transistors. Thin Solid Films 487 (1–2), 205–211.
Frati, C., Graiani, G., Barbani, N., Madeddu, D., Falco, A., Quaini, F., Lazzeri, L., Cascone, M.G., Rosellini, E., 2020. Reinforced alginate/gelatin sponges functionalized by avidin/biotin-binding strategy: a novel cardiac patch. J. Biomater. Appl. 34 (7), 975–987.
Fu, Y., Qin, L., Huang, D., Zeng, G., Lai, C., Li, B., He, J., Yi, H., Zhang, M., Cheng, M., 2019. Chitosan functionalized activated coke for Au nanoparticles anchoring: green synthesis and catalytic activities in hydrogenation of nitrophenols and azo dyes. Appl. Catal. B Environ. 255, 117740.
Fu, W., Chen, J., Li, C., Jiang, L., Qiu, M., Li, X., Wang, Y., Cui, L., 2021. Enhanced flux and fouling resistance forward osmosis membrane based on a hydrogel/MOF hybrid selective layer. J. Colloid Interface Sci. 585, 158–166.
Galiano, F., Briceño, K., Marino, T., Molino, A., Christensen, K.V., Figoli, A., 2018. Advances in biopolymer-based membrane preparation and applications. J. Membr. Sci. 564, 562–586.
Ganguly, S., Das, P., Bose, M., Das, T.K., Mondal, S., Das, A.K., Das, N.C., 2017. Sonochemical green reduction to prepare Ag nanoparticles decorated graphene sheets for catalytic performance and antibacterial application. Ultrason. Sonochem. 39, 577–588.
Gao, S.J., Shi, Z., Zhang, W.B., Zhang, F., Jin, J., 2014. Photoinduced superwetting single-walled carbon nanotube/TiO2 ultrathin network films for ultrafast separation of oil-in-water emulsions. ACS Nano 8 (6), 6344–6352.
Garcia-Martínez, S., Rico, E., Casal, E., Grisaleña, A., Alcaraz, E., King, N., Leal, N., Navarro, I., Campanero, M.Á., 2018. Bionalytical validation study for the determination of unbound ambrisentan in human plasma using rapid equilibrium dialysis followed by ultra performance liquid chromatography coupled to mass spectrometry. J. Pharmaceut. Biomed. Anal. 150, 427–435.
Gargiulo, N., Peluso, A., Caputo, D., 2020. MOF-based adsorbents for atmospheric emission control: a review. Processes 8 (5), 613.
Ghosh, A., Das, G., 2020. Green synthesis of Sn (II)-BDC MOF: preferential and efficient adsorption of anionic dyes. Microporous Mesoporous Mater. 297, 110039.
Goh, K., Heising, J.K., Yuan, Y., Karahan, H.E., Wei, L., Zhai, S., Koh, J.-X., Htin, N.M., Zhang, F., Wang, R., 2016. Sandwich-architectured poly (lactic acid)–graphene composite food packaging films. ACS Appl. Mater. Interfaces 8 (15), 9994–10004.
Gomes Amorim, C., Araújo, A., da Conceição Montenegro, M., 2019. Use of cucurbit [6] uril as ionophore in ion selective electrodes for etilefrine determination in pharmaceuticals. Electroanalysis 31 (11), 2171–2178.
Goutam, S.P., Saxena, G., Singh, V., Yadav, A.K., Bharagava, R.N., Thapa, K.B., 2018. Green synthesis of TiO2 nanoparticles using leaf extract of Jatropha curcas L. for photocatalytic degradation of tannery wastewater. Chem. Eng. J. 336, 386–396.
Guazzo, R., Gardin, C., Bellin, G., Sbricoli, L., Ferroni, L., Ludovichetti, F.S., Piattelli, A., Antoniac, I., Bressan, E., Zavan, B., 2018. Graphene-based nanomaterials for tissue engineering in the dental field. Nanomaterials 8 (5), 349.
Gulbagca, F., Ozdemir, S., Gulcan, M., Sen, F., 2019. Synthesis and characterization of Rosa canina-mediated biogenic silver nanoparticles for anti-oxidant, antibacterial, antifungal, and DNA cleavage activities. Heliyon 5 (12), e02980.
Guo, X., Kong, L., Ruan, Y., Diao, Z., Shih, K., Su, M., Chen, D., 2020. Green and facile synthesis of cobalt-based metal–organic frameworks for the efficient removal of Congo red from aqueous solution. J. Colloid Interface Sci. 578, 500–509.
Hamedi, H., Moradi, S., Hudson, S.M., Tonelli, A.E., King, M.W., 2022. Chitosan based bioadhesives for biomedical applications: a review. Carbohydr. Polym., 119100
Hamid, A., Khan, M., Hayat, A., Raza, J., Zada, A., Ullah, A., Raziq, F., Li, T., Hussain, F., 2020. Probing the physio-chemical appraisal of green synthesized PbO nanoparticles in PbO-PVC nanocomposite polymer membranes. Spectrochim. Acta Mol. Biomol. Spectrosc., 118303

Han, Y., Xu, Z., Gao, C., 2013. Ultrathin graphene nanofiltration membrane for water purification. Adv. Funct. Mater. 23 (29), 3693–3700.
Han, Y.-J., Wang, K.-H., Lai, J.-Y., Liu, Y.-L., 2014. Hydrophilic chitosan-modified polybenzoimidazole membranes for pervaporation dehydration of isopropanol aqueous solutions. J. Membr. Sci. 463, 17–23.
Han, Y., Jiang, Y., Gao, C., 2015. High-flux graphene oxide nanofiltration membrane intercalated by carbon nanotubes. ACS Appl. Mater. Interfaces 7 (15), 8147–8155.
Hanafia, A., Faur, C., Deratani, A., Guenoun, P., Garate, H., Quemener, D., Pochat-Bohatier, C., Bouyer, D., 2017. Fabrication of novel porous membrane from biobased water-soluble polymer (hydroxypropylcellulose). J. Membr. Sci. 526, 212–220.
Hasanzadeh, M., Rahimi, S., Solhi, E., Mokhtarzadeh, A., Shadjou, N., Soleymani, J., Mahboob, S., 2018. Probing the antigen-antibody interaction towards ultrasensitive recognition of cancer biomarker in adenocarcinoma cell lysates using layer-by-layer assembled silver nano-cubics with porous structure on cysteamine caped GQDs. Microchem. J. 143, 379–392.
Heo, J., Kim, S., Her, N., Park, C.M., Yu, M., Yoon, Y., 2020. Removal of contaminants of emerging concern by FO, RO, and UF membranes in water and wastewater. Contaminants of emerging concern in water and wastewater 139–176.
Herrero-Herrero, M., Gómez-Tejedor, J.-A., Vallés-Lluch, A., 2018. PLA/PCL electrospun membranes of tailored fibres diameter as drug delivery systems. Eur. Polym. J. 99, 445–455.
Homaeigohar, S., Boccaccini, A.R., 2020. Antibacterial biohybrid nanofibers for wound dressings. Acta Biomater. 107, 25–49.
Hosseinpour-Mashkani, S.M., Sobhani-Nasab, A., 2017. Green synthesis and characterization of NaEuTi 2 O 6 nanoparticles and its photocatalyst application. J. Mater. Sci. Mater. Electron. 28 (5), 4345–4350.
Hu, Z., Cai, L., Liang, J., Guo, X., Li, W., Huang, Z., 2019. Green synthesis of expanded graphite/layered double hydroxides nanocomposites and their application in adsorption removal of Cr (VI) from aqueous solution. J. Clean. Prod. 209, 1216–1227.
Huang, D., Hu, C., Zeng, G., Cheng, M., Xu, P., Gong, X., Wang, R., Xue, W., 2017. Combination of Fenton processes and biotreatment for wastewater treatment and soil remediation. Sci. Total Environ. 574, 1599–1610.
Huang, H., Su, S., Wu, N., Wan, H., Wan, S., Bi, H., Sun, L., 2019. Graphene-based sensors for human health monitoring. Front. Chem. 7, 399.
Hubadillah, S.K., Othman, M.H.D., Ismail, A., Rahman, M.A., Jaafar, J., Iwamoto, Y., Honda, S., Dzahir, M.I.H.M., Yusop, M.Z.M., 2018. Fabrication of low cost, green silica based ceramic hollow fibre membrane prepared from waste rice husk for water filtration application. Ceram. Int. 44 (9), 10498–10509.
Hubadillah, S.K., Othman, M.H.D., Kadir, S.H.S.A., Jamalludin, M.R., Harun, Z., Abd Aziz, M.H., Rahman, M.A., Jaafar, J., Nomura, M., Honda, S., 2019. Removal of as (III) and as (V) from water using green, silica-based ceramic hollow fibre membranes via direct contact membrane distillation. RSC Adv. 9 (6), 3367–3376.
Hui, L., Huang, J., Chen, G., Zhu, Y., Yang, L., 2016. Antibacterial property of graphene quantum dots (both source material and bacterial shape matter). ACS Appl. Mater. Interfaces 8 (1), 20–25.
Ishwarya, R., Vaseeharan, B., Kalyani, S., Banumathi, B., Govindarajan, M., Alharbi, N.S., Kadaikunnan, S., Al-Anbr, M.N., Khaled, J.M., Benelli, G., 2018. Facile green synthesis of zinc oxide nanoparticles using Ulva lactuca seaweed extract and evaluation of their photocatalytic, antibiofilm and insecticidal activity. J. Photochem. Photobiol. B Biol. 178, 249–258.
Ismail, M., Khan, M., Khan, S.B., Khan, M.A., Akhtar, K., Asiri, A.M., 2018a. Green synthesis of plant supported CuAg and CuNi bimetallic nanoparticles in the reduction of nitrophenols and organic dyes for water treatment. J. Mol. Liq. 260, 78–91.
Ismail, M., Khan, M., Khan, S.A., Qayum, M., Khan, M.A., Anwar, Y., Akhtar, K., Asiri, A. M., Khan, S.B., 2018b. Green synthesis of antibacterial bimetallic Ag–Cu nanoparticles for catalytic reduction of persistent organic pollutants. J. Mater. Sci. Mater. Electron. 29 (24), 20840–20855.
Ismail, M., Gul, S., Khan, M., Khan, M.A., Asiri, A.M., Khan, S.B., 2019. Green synthesis of zerovalent copper nanoparticles for efficient reduction of toxic azo dyes Congo red and methyl orange. Green Process. Synth. 8 (1), 135–143.
Jahangirian, H., Lemraski, E.G., Webster, T.J., Rafiee-Moghaddam, R., Abdollahi, Y., 2017. A review of drug delivery systems based on nanotechnology and green chemistry: green nanomedicine. Int. J. Nanomed. 12, 2957.
Jain, S., Mehata, M.S., 2017. Medicinal plant leaf extract and pure flavonoid mediated green synthesis of silver nanoparticles and their enhanced antibacterial property. Sci. Rep. 7 (1), 1–13.
Ji, D., Xiao, C., Zhao, J., Chen, K., Zhou, F., Gao, Y., Zhang, T., Ling, H., 2021. Green preparation of polyvinylidene fluoride loose nanofiltration hollow fiber membranes with multilayer structure for treating textile wastewater. Sci. Total Environ. 754, 141848.
Jiang, S., Ladewig, B.P., 2020. Green synthesis of polymeric membranes: recent advances and future prospects. Current Opinion in Green and Sustainable Chemistry 21, 1–8.
Jin, X., Liu, Y., Tan, J., Owens, G., Chen, Z., 2018. Removal of Cr (VI) from aqueous solutions via reduction and absorption by green synthesized iron nanoparticles. J. Clean. Prod. 176, 929–936.
Jun, B.-M., Al-Hamadani, Y.A., Son, A., Park, C.M., Jang, M., Jang, A., Kim, N.C., Yoon, Y., 2020. Applications of metal-organic framework based membranes in water purification: a review. Separ. Purif. Technol. 247, 116947.
Jung, K.-W., Choi, B.H., Lee, S.Y., Ahn, K.-H., Lee, Y.J., 2018a. Green synthesis of aluminum-based metal organic framework for the removal of azo dye Acid Black 1 from aqueous media. J. Ind. Eng. Chem. 67, 316–325.
Jung, J.T., Wang, H.H., Kim, J.F., Lee, J., Kim, J.S., Drioli, E., Lee, Y.M., 2018b. Tailoring nonsolvent-thermally induced phase separation (N-TIPS) effect using triple spinneret to fabricate high performance PVDF hollow fiber membranes. J. Membr. Sci. 559, 117–126.
Jyoti, K., Singh, A., 2016. Green synthesis of nanostructured silver particles and their catalytic application in dye degradation. Journal of Genetic Engineering and Biotechnology 14 (2), 311–317.
Kalantari, K., Afifi, A.M., Jahangirian, H., Webster, T.J., 2019. Biomedical applications of chitosan electrospun nanofibers as a green polymer–Review. Carbohydr. Polym. 207, 588–600.
Kandambeth, S., Biswal, B.P., Chaudhari, H.D., Rout, K.C., Kunjattu H, S., Mitra, S., Karak, S., Das, A., Mukherjee, R., Kharul, U.K., 2017. Selective molecular sieving in self-standing porous covalent-organic-framework membranes. Adv. Mater. 29 (2), 1603945.
Karim, M.R., Aijaz, M.O., Alharth, N.H., Alharbi, H.F., Al-Mubaddel, F.S., Awual, M.R., 2019. Composite nanofibers membranes of poly (vinyl alcohol)/chitosan for selective lead (II) and cadmium (II) ions removal from wastewater. Ecotoxicol. Environ. Saf. 169, 479–486.
Karthiga Devi, G., Senthil Kumar, P., Sathish Kumar, K., 2016. Green synthesis of novel silver nanocomposite hydrogel based on sodium alginate as an efficient biosorbent for the dye wastewater treatment: prediction of isotherm and kinetic parameters. Desalination Water Treat. 57 (57), 27686–27699.
Karthik, K., Shashank, M., Revathi, V., Tatarchuk, T., 2019. Facile microwave-assisted green synthesis of NiO nanoparticles from Andrographis paniculata leaf extract and evaluation of their photocatalytic and anticancer activities. Mol. Cryst. Liq. Cryst. 673, 70–80.
Kashani, T., Jahanshahi, M., Rahimpour, A., Peyravi, M., 2016. Nanopore molecularly imprinted polymer membranes for environmental usage: selective separation of 2, 4-dichlorophenoxyacetic acid as a toxic herbicide from water. Polym.-Plast. Technol. Eng. 55 (16), 1700–1712.
Kataria, N., Garg, V., 2018. Green synthesis of Fe3O4 nanoparticles loaded sawdust carbon for cadmium (II) removal from water: regeneration and mechanism. Chemosphere 208, 818–828.
Khan, M.S.J., Khan, S.B., Kamal, T., Asiri, A.M., 2019. Agarose biopolymer coating on polyurethane sponge as host for catalytic silver metal nanoparticles. Polym. Test. 78, 105983.
Khan, S.A., Jain, M., Pandey, A., Pant, K.K., Ziora, Z.M., Blaskovich, M.A., Shetti, N.P., Aminabhavi, T.M., 2022. Leveraging the potential of silver nanoparticles-based materials towards sustainable water treatment. J. Environ. Manag. 319, 115675.
Khani, R., Roostaei, B., Bagherzade, G., Moudi, M., 2018. Green synthesis of copper nanoparticles by fruit extract of Ziziphus spina-christi (L.) Willd.: application for adsorption of triphenylmethane dye and antibacterial assay. J. Mol. Liq. 255, 541–549.
Khataei, M.M., Yamini, Y., Nazaripour, A., Karimi, M., 2018. Novel generation of deep eutectic solvent as an acceptor phase in three-phase hollow fiber liquid phase microextraction for extraction and preconcentration of steroidal hormones from biological fluids. Talanta 178, 473–480.
Khodadadi, B., Bordbar, M., Yeganeh-Faal, A., Nasrollahzadeh, M., 2017. Green synthesis of Ag nanoparticles/clinoptilolite using Vaccinium macrocarpon fruit extract and its excellent catalytic activity for reduction of organic dyes. J. Alloys Compd. 719, 82–88.
Khosravi, T., Mosleh, S., Bakhtiari, O., Mohammadi, T., 2012. Mixed matrix membranes of Matrimid 5218 loaded with zeolite 4A for pervaporation separation of water–isopropanol mixtures. Chem. Eng. Res. Des. 90 (12), 2353–2363.
Kiebooms, J.A.L., Wauters, J., Bussche, J.V., Vanhaecke, L., 2014. Validated ultra high performance liquid chromatography-tandem mass spectrometry method for quantitative analysis of total and free thyroid hormones in bovine serum. J. Chromatogr. A 1345, 164–173.
Kim, J.F., Jung, J.T., Wang, H.H., Lee, S.Y., Moore, T., Sanguineti, A., Drioli, E., Lee, Y. M., 2016. Microporous PVDF membranes via thermally induced phase separation (TIPS) and stretching methods. J. Membr. Sci. 509, 94–104.
Kim, J.H., Cook, M., Park, S.H., Moon, S.J., Kim, J.F., Livingston, A.G., Lee, Y.M., 2018a. A compact and scalable fabrication method for robust thin film composite membranes. Green Chem. 20 (8), 1887–1898.
Kim, S., Chu, K.H., Al-Hamadani, Y.A., Park, C.M., Jang, M., Kim, D.-H., Yu, M., Heo, J., Yoon, Y., 2018b. Removal of contaminants of emerging concern by membranes in water and wastewater: a review. Chem. Eng. J. 335, 896–914.
Klink, M.J., Laloo, N., Leudjo Taka, A., Pakade, V.E., Monapathi, M.E., Modise, J.S., 2022. Synthesis, characterization and antimicrobial activity of zinc oxide nanoparticles against selected waterborne bacterial and yeast pathogens. Molecules 27 (11), 3532.
Kugarajah, V., Ojha, A.K., Ranjan, S., Dasgupta, N., Ganesapillai, M., Dharmalingam, S., Elmoll, A., Hosseini, S.A., Muthulakshmi, L., Vijayakumar, S., 2021. Future applications of electrospun nanofibers in pressure driven water treatment: a brief review and research update. J. Environ. Chem. Eng. 9 (2), 105107.
Kumar, S., Krishnakumar, B., Sobral, A.J., Koh, J., 2019. Bio-based (chitosan/PVA/ZnO) nanocomposites film: thermally stable and photoluminescence material for removal of organic dye. Carbohydr. Polym. 205, 559–564.
Kumar, R., Ghosh, A.K., Pal, P., 2020. Synergy of biofuel production with waste remediation along with value-added co-products recovery through microalgae cultivation: a review of membrane-integrated green approach. Sci. Total Environ. 698, 134169.
Lan, Y., Peng, P., 2019. Preparation of polymer of intrinsic microporosity composite membranes and their applications for butanol recovery. J. Appl. Polym. Sci. 136 (1), 46912.
Landaburu-Aguirre, J., García-Pacheco, R., Molina, S., Rodríguez-Sáez, L., Rabadán, J., García-Calvo, E., 2016. Fouling prevention, preparing for re-use and membrane recycling. Towards circular economy in RO desalination. Desalination 393, 16–30.

Lawler, W., Bradford-Hartke, Z., Cran, M.J., Duke, M., Leslie, G., Ladewig, B.P., Le-Clech, P., 2012. Towards new opportunities for reuse, recycling and disposal of used reverse osmosis membranes. Desalination 299, 103–112.
Le, A.-T., Le, T.T., Tran, H.H., Dang, D.A., Tran, Q.H., Vu, D.L., 2012. Powerful colloidal silver nanoparticles for the prevention of gastrointestinal bacterial infections. Adv. Nat. Sci. Nanosci. Nanotechnol. 3 (4), 045007.
Le Phuong, H.A., Izzati Ayob, N.A., Blanford, C.F., Mohammad Rawi, N.F., Szekely, G., 2019. Nonwoven membrane supports from renewable resources: bamboo fiber reinforced poly (lactic acid) composites. ACS Sustain. Chem. Eng. 7 (13), 11885–11893.
Lecaros, R.L.G., Deseo, K.M., Hung, W.-S., Tayo, L.L., Hu, C.-C., An, Q.-F., Tsai, H.-A., Lee, K.-R., Lai, J.-Y., 2019. Influence of integrating graphene oxide quantum dots on the fine structure characterization and alcohol dehydration performance of pervaporation composite membrane. J. Membr. Sci. 576, 36–47.
Lee, Y.-R., Fu, S.-J., Lin, C.-C., 2015. Preparation of HA-mineralized CS/PLA composites nanofiber GBR mats. In: 1st Global Conference on Biomedical Engineering & 9th Asian-Pacific Conference on Medical and Biological Engineering. Springer, pp. 28–31.
Lee, J., Boo, C., Ryu, W.-H., Taylor, A.D., Elimelech, M., 2016. Development of omniphobic desalination membranes using a charged electrospun nanofiber scaffold. ACS Appl. Mater. Interfaces 8 (17), 11154–11161.
Lee, Y.-J., Chang, Y.-J., Lee, D.-J., Hsu, J.-P., 2018. Water stable metal-organic framework as adsorbent from aqueous solution: a mini-review. J. Taiwan Inst. Chem. Eng. 93, 176–183.
Li, J., Gong, J.-L., Zeng, G.-M., Zhang, P., Song, B., Cao, W.-C., Liu, H.-Y., Huan, S.-Y., 2018. Zirconium-based metal organic frameworks loaded on polyurethane foam membrane for simultaneous removal of dyes with different charges. J. Colloid Interface Sci. 527, 267–279.
Liang, H.-Q., Wu, Q.-Y., Wan, L.-S., Huang, X.-J., Xu, Z.-K., 2013. Polar polymer membranes via thermally induced phase separation using a universal crystallizable diluent. J. Membr. Sci. 446, 482–491.
Lin, H., Maggard, P.A., 2008. Synthesis and structures of a new series of silver-vanadate hybrid solids and their optical and photocatalytic properties. Inorg. Chem. 47 (18), 8044–8052.
Lindenburg, P.W., Ramautar, R., Hankemeier, T., 2013. The potential of electrophoretic sample pretreatment techniques and new instrumentation for bioanalysis, with a focus on peptidomics and metabolomics. Bioanalysis 5 (22), 2785–2801.
Liu, M., Xu, Z.-l., Chen, D.-g., Wei, Y.-m., 2010. Preparation and characterization of microporous PVDF membrane by thermally induced phase separation from a ternary polymer/solvent/non-solvent system. Desalination Water Treat. 17 (1–3), 183–192.
Liu, G., Wei, W., Wu, H., Dong, X., Jiang, M., Jin, W., 2011. Pervaporation performance of PDMS/ceramic composite membrane in acetone butanol ethanol (ABE) fermentation–PV coupled process. J. Membr. Sci. 373 (1–2), 121–129.
Liu, E., Xu, X., Zheng, X., Zhang, F., Liu, E., Li, C., 2017. An ion imprinted macroporous chitosan membrane for efficiently selective adsorption of dysprosium. Separ. Purif. Technol. 189, 288–295.
Liu, S., Low, Z.-X., Hegab, H.M., Xie, Z., Ou, R., Yang, G., Simon, G.P., Zhang, X., Zhang, L., Wang, H., 2019a. Enhancement of desalination performance of thin-film nanocomposite membrane by cellulose nanofibers. J. Membr. Sci. 592, 117363.
Liu, X., Han, Q., Zhang, Y., Wang, X., Cai, S., Wang, C., Yang, R., 2019b. Green and facile synthesis of Rh/GO nanocomposites for high catalytic performance. Appl. Surf. Sci. 471, 929–934.
Liu, X., Jiang, B., Yin, X., Ma, H., Hsiao, B.S., 2020. Highly permeable nanofibrous composite microfiltration membranes for removal of nanoparticles and heavy metal ions. Separ. Purif. Technol. 233, 115976.
Loeb, S., 1965. Desalination research in California. Science 147 (3663), 1241–1242.
Lu, J., Wu, Y., Lin, X., Gao, J., Dong, H., Chen, L., Qin, Y., Wang, L., Yan, Y., 2018. Anti-fouling and thermosensitive ion-imprinted nanocomposite membranes based on graphene oxide and silicon dioxide for selectively separating europium ions. J. Hazard Mater. 353, 244–253.
Luo, S., Berges, J.A., He, Z., Young, E.B., 2017. Algal-microbial community collaboration for energy recovery and nutrient remediation from wastewater in integrated photobioelectrochemical systems. Algal Res. 24, 527–539.
Lv, X., Liu, Y., Zhang, J., Zhao, M., Zhu, K., 2019. Study on the adsorption behavior of glutaric acid modified Pb (II) imprinted chitosan-based composite membrane to Pb (II) in aqueous solution. Mater. Lett. 251, 172–175.
M Izzah Binti Mohammad, A.R., Liang, K., Asadnia, M., Chen, V., 2019. MOF-based enzymatic microfluidic biosensor via surface patterning and biomineralization. ACS Appl. Mater. Interfaces 11 (2), 1807–1820.
Ma, R.-H., Yang, J., Qi, L.-W., Xin, G.-Z., Wang, C.-Z., Yuan, C.-S., Wen, X.-D., Li, P., 2012. In vivo microdialysis with LC–MS for analysis of spinosin and its interaction with cyclosporin A in rat brain, blood and bile. J. Pharmaceut. Biomed. Anal. 61, 22–29.
Mahmoodi, N.M., Keshavarzi, S., Oveisi, M., Rahimi, S., Hayati, B., 2019a. Metal-organic framework (ZIF-8)/inorganic nanofiber (Fe2O3) nanocomposite: green synthesis and photocatalytic degradation using LED irradiation. J. Mol. Liq. 291, 111333.
Mahmoodi, N.M., Taghizadeh, M., Taghizadeh, A., 2019b. Activated carbon/metal-organic framework composite as a bio-based novel green adsorbent: preparation and mathematical pollutant removal modeling. J. Mol. Liq. 277, 310–322.
Mahmoodi, N.M., Oveisi, M., Taghizadeh, A., Taghizadeh, M., 2019c. Novel magnetic amine functionalized carbon nanotube/metal-organic framework nanocomposites: from green ultrasound-assisted synthesis to detailed selective pollutant removal modelling from binary systems. J. Hazard Mater. 368, 746–759. https://doi.org/10.1016/j.jhazmat.2019.01.107.
Mahmud, M., Ejeian, F., Azadi, S., Myers, M., Pejcic, B., Abbasi, R., Razmjou, A., Asadnia, M., 2020. Recent progress in sensing nitrate, nitrite, phosphate, and ammonium in aquatic environment. Chemosphere, 127492.
Mali, M.G., Magalad, V.T., Gokavi, G.S., Aminabhavi, T.M., Raju, K., 2011. Pervaporation separation of isopropanol–water mixtures using mixed matrix blend membranes of poly (vinyl alcohol)/poly (vinyl pyrrolidone) loaded with phosphomolybdic acid. J. Appl. Polym. Sci. 121 (2), 711–719.
Mallakpour, S., Rafiee, Z., 2011. Ionic liquids as environmentally friendly solvents in macromolecules chemistry and technology, Part I. J. Polym. Environ. 19 (2), 447–484.
Marczak, S., Ramshani, Z., Hill, R., Go, D.B., Chang, H.-C., Senapati, S., 2021. Simultaneous Isolation and Preconcentration of Exosomes by Ion Concentration Polarization Method and Apparatus. Google Patents.
Marino, T., Blasi, E., Tornaghi, S., Di Nicolò, E., Figoli, A., 2018. Polyethersulfone membranes prepared with Rhodiasolv® Polarclean as water soluble green solvent. J. Membr. Sci. 549, 192–204.
Matsumoto, M., Valentino, L., Stiehl, G.M., Balch, H.B., Corcos, A.R., Wang, F., Ralph, D. C., Mariñas, B.J., Dichtel, W.R., 2018. Lewis-acid-catalyzed interfacial polymerization of covalent organic framework films. Chem 4 (2), 308–317.
Medina-Gonzalez, Y., Aimar, P., Lahitte, J.-F., Remigy, J.-C., 2011. Towards green membranes: preparation of cellulose acetate ultrafiltration membranes using methyl lactate as a biosolvent. Int. J. Sustain. Eng. 4 (1), 75–83.
Micah, A.E., Bhangdia, K., Cogswell, I.E., Lasher, D., Lidral-Porter, B., Maddison, E.R., Nguyen, T.N.N., Patel, N., Pedroza, P., Solorio, J., 2023. Global investments in pandemic preparedness and COVID-19: development assistance and domestic spending on health between 1990 and 2026. Lancet Global Health 11 (3), e385–e413.
Milescu, R.A., McElroy, C.R., Farmer, T.J., Williams, P.M., Walters, M.J., Clark, J.H., 2019. Fabrication of PES/PVP water filtration membranes using Cyrene®, a safer bio-based polar aprotic solvent. Adv. Polym. Technol. 2019.
Min, Q., Yu, X., Liu, J., Zhang, Y., Wan, Y., Wu, J., 2020. Controlled delivery of insulin-like growth factor-1 from bioactive glass-incorporated alginate-poloxamer/silk fibroin hydrogels. Pharmaceutics 12 (6), 574.
Mitra, S., Kandambeth, S., Biswal, B.P., Khayum, M., A, Choudhury, C.K., Mehta, M., Kaur, G., Banerjee, S., Prabhune, A., Verma, S., 2016. Self-exfoliated guanidinium-based ionic covalent organic nanosheets (iCONs). J. Am. Chem. Soc. 138 (8), 2823–2828.
Miyagawa, T., Chen, Z.-Y., Chang, C.-Y., Chen, K.-H., Wang, Y.-K., Liu, G.-S., Tseng, C.-L., 2020. Topical application of hyaluronic Acid-RGD Peptide-Coated Gelatin/Epigallocatechin-3 Gallate (EGCG) nanoparticles inhibits corneal neovascularization via inhibition of VEGF production. Pharmaceutics 12 (5), 404.
Moghaddam, A.Z., Goharjoo, M., Ghiamati, E., Khodaei, K., Tabani, H., 2021. Gel electro-membrane extraction of propranolol and atenolol from blood serum samples: effect of graphene-based nanomaterials on extraction efficiency of gel membrane. Talanta 222, 121557.
Mohammad, A.W., Teow, Y., Ang, W., Chung, Y., Oatley-Radcliffe, D., Hilal, N., 2015. Nanofiltration membranes review: recent advances and future prospects. Desalination 356, 226–254.
Mohebbi, S., Nezhad, M.N., Zarrintaj, P., Jafari, S.H., Gholizadeh, S.S., Saeb, M.R., Mozafari, M., 2019. Chitosan in biomedical engineering: a critical review. Curr. Stem Cell Res. Ther. 14 (2), 93–116.
Mokhtar, M., Dickson, S.E., Kim, Y., Mekky, W., 2018. Preparation and characterization of ion selective membrane and its application for Cu2+ removal. J. Ind. Eng. Chem. 60, 475–484.
Mondal, P., Purkait, M.K., 2018. Green synthesized iron nanoparticles supported on pH responsive polymeric membrane for nitrobenzene reduction and fluoride rejection study: optimization approach. J. Clean. Prod. 170, 1111–1123.
Moradnia, F., Fardood, S.T., Ramazani, A., Gupta, V.K., 2020. Green synthesis of recyclable MgFeCrO4 spinel nanoparticles for rapid photodegradation of direct black 122 dye. J. Photochem. Photobiol. Chem. 392, 112433.
Msahel, A., Galiano, F., Pilloni, M., Russo, F., Hafiane, A., Castro-Muñoz, R., Kumar, V.B., Gedanken, A., Ennas, G., Porat, Z.e., 2021. Exploring the effect of iron metal-organic framework particles in polylactic acid membranes for the azeotropic separation of organic/organic mixtures by pervaporation. Membranes 11 (1), 65.
Nascimento, T.A., Fdz-Polanco, F., Peña, M., 2020. Membrane-based technologies for the up-concentration of municipal wastewater: a review of pretreatment intensification. Separ. Purif. Rev. 49 (1), 1–19.
Nasrollahzadeh, M., Baran, T., Baran, N.Y., Sajjadi, M., Tahsili, M.R., Shokouhimehr, M., 2020. Pd nanocatalyst stabilized on amine-modified zeolite: antibacterial and catalytic activities for environmental pollution remediation in aqueous medium. Separ. Purif. Technol. 239, 116542.
Nasrollahzadeh, M., Sajjadi, M., Iravani, S., Varma, R.S., 2021. Green-synthesized nanocatalysts and nanomaterials for water treatment: current challenges and future perspectives. J. Hazard Mater. 401, 123401.
Naushad, M., Ahamad, T., Alothman, Z.A., Ala'a, H., 2019. Green and eco-friendly nanocomposite for the removal of toxic Hg (II) metal ion from aqueous environment: adsorption kinetics & isotherm modelling. J. Mol. Liq. 279, 1–8.
Nava, O., Luque, P., Gómez-Gutiérrez, C., Vilchis-Nestor, A., Castro-Beltrán, A., Mota-González, M., Olivas, A., 2017a. Influence of Camellia sinensis extract on Zinc Oxide nanoparticle green synthesis. J. Mol. Struct. 1134, 121–125.
Nava, O., Soto-Robles, C., Gómez-Gutiérrez, C., Vilchis-Nestor, A., Castro-Beltrán, A., Olivas, A., Luque, P., 2017b. Fruit peel extract mediated green synthesis of zinc oxide nanoparticles. J. Mol. Struct. 1147, 1–6.
Nguyen, T.T.T., Park, J.-S., 2011. Fabrication and characterization of electrospun CS (core)/PLA (shell) nanofibers. Journal of Chitin and Chitosan 16 (4), 282–288.

Ni, P., Fox, J.T., 2020. Metal organic frameworks synthesized with green chemistry for the removal of silicic acid from aqueous solutions. Separ. Purif. Technol., 118118
Nilavukkarasi, M., Vijayakumar, S., Kumar, S.P., 2020. Biological synthesis and characterization of silver nanoparticles with Capparis zeylanica L. leaf extract for potent antimicrobial and anti proliferation efficiency. Materials Science for Energy Technologies 3, 371–376.
Nthunya, L.N., Derese, S., Gutierrez, L., Verliefde, A.R., Mamba, B.B., Barnard, T.G., Mhlanga, S.D., 2019a. Green synthesis of silver nanoparticles using one-pot and microwave-assisted methods and their subsequent embedment on PVDF nanofibre membranes for growth inhibition of mesophilic and thermophilic bacteria. New J. Chem. 43 (10), 4168–4180.
Nthunya, L.N., Gutierrez, L., Verliefde, A.R., Mhlanga, S.D., 2019b. Enhanced flux in direct contact membrane distillation using superhydrophobic PVDF nanofibre membranes embedded with organically modified SiO2 nanoparticles. J. Appl. Chem. Biotechnol. 94 (9), 2826–2837.
Nunes, S.P., Culfaz-Emecen, P.Z., Ramon, G.Z., Visser, T., Koops, G.H., Jin, W., Ulbricht, M., 2020. Thinking the future of membranes: perspectives for advanced and new membrane materials and manufacturing processes. J. Membr. Sci. 598, 117761.
Omran, B., Nassar, H., Fatthallah, N., Hamdy, A., El-Shatoury, E., El-Gendy, N.S., 2018. Characterization and antimicrobial activity of silver nanoparticles mycosynthesized by Aspergillus brasiliensis. J. Appl. Microbiol. 125 (2), 370–382.
Oveisi, M., Mahmoodi, N.M., Asli, M.A., 2019. Facile and green synthesis of metal-organic framework/inorganic nanofiber using electrospinning for recyclable visible-light photocatalysis. J. Clean. Prod. 222, 669–684.
Ozkan, Z., Cakirgoz, M., Kaymak, E., Erdim, E., 2018. Rapid decolorization of textile wastewater by green synthesized iron nanoparticles. Water Sci. Technol. 77 (2), 511–517.
Padhi, D.K., Panigrahi, T.K., Parida, K., Singh, S., Mishra, P., 2017. Green synthesis of Fe3O4/RGO nanocomposite with enhanced photocatalytic performance for Cr (VI) reduction, phenol degradation, and antibacterial activity. ACS Sustain. Chem. Eng. 5 (11), 10551–10562.
Pan, L.-H., Kuo, S.-H., Lin, T.-Y., Lin, C.-W., Fang, P.-Y., Yang, H.-W., 2017. An electrochemical biosensor to simultaneously detect VEGF and PSA for early prostate cancer diagnosis based on graphene oxide/ssDNA/PLLA nanoparticles. Biosens. Bioelectron. 89, 598–605.
Pandey, S., Goswami, G.K., Nanda, K.K., 2012. Green synthesis of biopolymer–silver nanoparticle nanocomposite: an optical sensor for ammonia detection. Int. J. Biol. Macromol. 51 (4), 583–589.
Park, S.H., Kim, Y.J., Kwon, S.J., Shin, M.G., Nam, S.E., Cho, Y.H., Park, Y.I., Kim, J.F., Lee, J.-H., 2018. Polyethylene battery separator as a porous support for thin film composite organic solvent nanofiltration membranes. ACS Appl. Mater. Interfaces 10 (50), 44050–44058.
Park, S.-H., Alammar, A., Fulop, Z., Pulido, B.A., Nunes, S.P., Szekely, G., 2021a. Hydrophobic thin film composite nanofiltration membranes derived solely from sustainable sources. Green Chem. 23 (3), 1175–1184.
Park, S.-H., Alammar, A., Fulop, Z., Pulido, B.A., Nunes, S.P., Szekely, G., 2021b. Hydrophobic thin film composite nanofiltration membranes derived solely from sustainable sources. Green Chem.
Parkerson, Z.J., Le, T., Das, P., Mahmoodi, S.N., Esfahani, M.R., 2020. Cu-MOF-Polydopamine-Incorporated functionalized nanofiltration membranes for water treatment: effect of surficial adhesive modification techniques. ACS ES&T Water.
Parthiban, E., Manivannan, N., Ramanibai, R., Mathivanan, N., 2019. Green synthesis of silver-nanoparticles from Annona reticulata leaves aqueous extract and its mosquito larvicidal and anti-microbial activity on human pathogens. Biotechnology Reports 21, e00297.
Paseta, L., Navarro, M., Coronas, J., Téllez, C., 2019. Greener processes in the preparation of thin film nanocomposite membranes with diverse metal-organic frameworks for organic solvent nanofiltration. J. Ind. Eng. Chem. 77, 344–354.
Peng, P., Shi, B., Lan, Y., 2011. Preparation of PDMS—silica nanocomposite membranes with silane coupling for recovering ethanol by pervaporation. Separ. Sci. Technol. 46 (3), 420–427.
Peng, Y., Zhang, Y., Huang, H., Zhong, C., 2018. Flexibility induced high-performance MOF-based adsorbent for nitroimidazole antibiotics capture. Chem. Eng. J. 333, 678–685.
Pereira, C.S., Silva, V.M., Rodrigues, A.E., 2011. Ethyl lactate as a solvent: properties, applications and production processes–a review. Green Chem. 13 (10), 2658–2671.
Policicchio, A., Filosa, R., Abate, S., Desiderio, G., Colavita, E., 2017. Activated carbon and metal organic framework as adsorbent for low-pressure methane storage applications: an overview. J. Porous Mater. 24, 905–922.
Prasad, C.V., Yeriswamy, B., Sudhakar, H., Sudhakara, P., Subha, M., Song, J., Rao, K.C., 2012. Preparation and characterization of nanoparticle-filled, mixed-matrix membranes for the pervaporation dehydration of isopropyl alcohol. J. Appl. Polym. Sci. 125 (5), 3351–3360.
Pugazhendhi, A., Prabakar, D., Jacob, J.M., Karuppusamy, I., Saratale, R.G., 2018. Synthesis and characterization of silver nanoparticles using Gelidium amansii and its antimicrobial property against various pathogenic bacteria. Microb. Pathog. 114, 41–45.
Punia, P., Bharti, M.K., Chalia, S., Dhar, R., Ravelo, B., Thakur, P., Thakur, A., 2021. Recent advances in synthesis, characterization, and applications of nanoparticles for contaminated water treatment-a review. Ceram. Int. 47 (2), 1526–1550.
Qasim, M., Udomluck, N., Chang, J., Park, H., Kim, K., 2018. Antimicrobial activity of silver nanoparticles encapsulated in poly-N-isopropylacrylamide-based polymeric nanoparticles. Int. J. Nanomed. 13, 235.
Qian, Q., Asinger, P.A., Lee, M.J., Han, G., Mizrahi Rodriguez, K., Lin, S., Benedetti, F.M., Wu, A.X., Chi, W.S., Smith, Z.P., 2020. MOF-based membranes for gas separations. Chem. Rev. 120 (16), 8161–8266.
Qiu, S., Xue, M., Zhu, G., 2014. Metal–organic framework membranes: from synthesis to separation application. Chem. Soc. Rev. 43 (16), 6116–6140.
Qiu, Q., Chen, S., Li, Y., Yang, Y., Zhang, H., Quan, Z., Qin, X., Wang, R., Yu, J., 2020. Functional nanofibers embedded into textiles for durable antibacterial properties. Chem. Eng. J. 384, 123241.
Rabiee, N., Bagherzadeh, M., Ghadiri, A.M., Fatahi, Y., Aldhaher, A., Makvandi, P., Dinarvand, R., Jouyandeh, M., Saeb, M.R., Mozafari, M., 2021a. Turning toxic nanomaterials into a safe and bioactive nanocarrier for Co-delivery of DOX/pCRISPR. ACS Appl. Bio Mater.
Rabiee, N., Bagherzadeh, M., Ghadiri, A.M., Kiani, M., Ahmadi, S., Jajarmi, V., Fatahi, Y., Aldhaher, A., Tahriri, M., Webster, T.J., 2021b. Calcium-based nanomaterials and their interrelation with chitosan: optimization for pCRISPR delivery. Journal of nanostructure in chemistry 1–14.
Rafeie, M., Welleweerd, M., Hassanzadeh-Barforoushi, A., Asadnia, M., Olthuis, W., Ebrahimi Warkiani, M., 2017. An easily fabricated three-dimensional threaded lemniscate-shaped micromixer for a wide range of flow rates. Biomicrofluidics 11 (1), 014108.
Raghavendra, V.B., Shankar, S., Govindappa, M., Pugazhendhi, A., Sharma, M., Nayaka, S.C., 2022. Green synthesis of zinc oxide nanoparticles (ZnO NPs) for effective degradation of dye, polyethylene and antibacterial performance in waste water treatment. J. Inorg. Organomet. Polym. Mater. 1–17.
Rahimi, A., Nojavan, S., Tabani, H., 2020. Inside gel electromembrane extraction: a novel green methodology for the extraction of morphine and codeine from human biological fluids. J. Pharmaceut. Biomed. Anal. 184, 113175.
Rahmati, M., Mills, D.K., Urbanska, A.M., Saeb, M.R., Venugopal, J.R., Ramakrishna, S., Mozafari, M., 2021. Electrospinning for tissue engineering applications. Prog. Mater. Sci. 117, 100721.
Rajakumaran, R., Boddu, V., Kumar, M., Shalaby, M.S., Abdallah, H., Chetty, R., 2019. Effect of ZnO morphology on GO-ZnO modified polyamide reverse osmosis membranes for desalination. Desalination 467, 245–256.
Rajesh, K., Ajitha, B., Reddy, Y.A.K., Suneetha, Y., Reddy, P.S., 2018. Assisted green synthesis of copper nanoparticles using Syzygium aromaticum bud extract: physical, optical and antimicrobial properties. Optik 154, 593–600.
Rajiv, P., Bavadharani, B., Kumar, M.N., Vanathi, P., 2017. Synthesis and characterization of biogenic iron oxide nanoparticles using green chemistry approach and evaluating their biological activities. Biocatal. Agric. Biotechnol. 12, 45–49.
Rambabu, K., Bharath, G., Banat, F., Show, P.L., 2021. Green synthesis of zinc oxide nanoparticles using Phoenix dactylifera waste as bioreductant for effective dye degradation and antibacterial performance in wastewater treatment. J. Hazard Mater. 402, 123560.
Rasheed, T., Bilal, M., Iqbal, H.M., Li, C., 2017. Green biosynthesis of silver nanoparticles using leaves extract of Artemisia vulgaris and their potential biomedical applications. Colloids Surf. B Biointerfaces 158, 408–415.
Rasool, M.A., Vankelecom, I., 2019. Use of γ-valerolactone and glycerol derivatives as bio-based renewable solvents for membrane preparation. Green Chem. 21 (5), 1054–1064.
Rasool, M.A., Van Goethem, C., Vankelecom, I.F., 2020. Green preparation process using methyl lactate for cellulose-acetate-based nanofiltration membranes. Separ. Purif. Technol. 232, 115903.
Razmjou, A., Asadnia, M., Ghaebi, O., Yang, H.-C., Ebrahimi Warkiani, M., Hou, J., Chen, V., 2017. Preparation of iridescent 2D photonic crystals by using a mussel-inspired spatial patterning of ZIF-8 with potential applications in optical switch and chemical sensor. ACS Appl. Mater. Interfaces 9 (43), 38076–38080.
Razmjou, A., Eshaghi, G., Orooji, Y., Hosseini, E., Korayem, A.H., Mohagheghian, F., Boroumand, Y., Noorbakhsh, A., Asadnia, M., Chen, V., 2019. Lithium ion-selective membrane with 2D subnanometer channels. Water Res. 159, 313–323.
Rethinam, S., Basaran, B., Vijayan, S., Mert, A., Bayraktar, O., Aruni, A.W., 2020. Electrospun nano-bio membrane for bone tissue engineering application-a new approach. Mater. Chem. Phys. 249, 123010.
Rezaei-DashtArzhandi, M., Sarrafzadeh, M.H., Goh, P.S., Lau, W.J., Ismail, A.F., Wong, K. C., Mohamed, M.A., 2020. Enhancing the desalination performance of forward osmosis membrane through the incorporation of green nanocrystalline cellulose and halloysite dual nanofillers. J. Appl. Chem. Biotechnol. 95 (9), 2359–2370.
Roy, S., Singha, N.R., 2017. Polymeric nanocomposite membranes for next generation pervaporation process: strategies, challenges and future prospects. Membranes 7 (3), 53.
Roy, K., Ghosh, C.K., Sarkar, C.K., 2017. Degradation of toxic textile dyes and detection of hazardous Hg2+ by low-cost bioengineered copper nanoparticles synthesized using Impatiens balsamina leaf extract. Mater. Res. Bull. 94, 257–262.
Rudin, N.A., Achimugu, S., Saha, A.K., 2021. Application of cell membrane principles in molecular separation process with membrane technology on food science. Proceeding International Conference on Science and Engineering 4, 306–310.
Rundquist, E.M., Pink, C.J., Livingston, A.G., 2012. Organic solvent nanofiltration: a potential alternative to distillation for solvent recovery from crystallisation mother liquors. Green Chem. 14 (8), 2197–2205.
Saad, M., Tahir, H., Ali, D., 2017. Green synthesis of Ag-Cr-AC nanocomposites by Azadirachta indica and its application for the simultaneous removal of binary mixture of dyes by ultrasonicated assisted adsorption process using Response Surface Methodology. Ultrason. Sonochem. 38, 197–213.
Saeed, M., Akram, N., Naqvi, S.A.R., Usman, M., Abbas, M.A., Adeel, M., Nisar, A., 2019. Green and eco-friendly synthesis of Co3O4 and Ag-Co3O4: characterization and photo-catalytic activity. Green Process. Synth. 8 (1), 382–390.

Saeedi, M., Vahidi, O., Moghbeli, M., Ahmadi, S., Asadnia, M., Akhavan, O., Seidi, F., Rabiee, M., Saeb, M.R., Webster, T.J., 2022. Customizing nano-chitosan for sustainable drug delivery. J. Contr. Release 350, 175–192.
Sagle, A., Freeman, B., 2004. Fundamentals of membranes for water treatment. The future of desalination in Texas 2 (363), 137.
Saleem, H., Trabzon, L., Kilic, A., Zaidi, S.J., 2020. Recent advances in nanofibrous membranes: production and applications in water treatment and desalination. Desalination 478, 114178.
Samuel, M.S., Selvarajan, E., Mathimani, T., Santhanam, N., Phuong, T.N., Brindhadevi, K., Pugazhendhi, A., 2020. Green synthesis of cobalt-oxide nanoparticle using jumbo Muscadine (Vitis rotundifolia): characterization and photo-catalytic activity of acid Blue-74. J. Photochem. Photobiol. B Biol. 211, 112011.
Sanders, T.M., Myers, M., Asadnia, M., Umana-Membreno, G.A., Baker, M., Fowkes, N., Parish, G., Nener, B., 2017. Description of ionophore-doped membranes with a blocked interface. Sensor. Actuator. B Chem. 250, 499–508.
Santhoshkumar, J., Kumar, S.V., Rajeshkumar, S., 2017. Synthesis of zinc oxide nanoparticles using plant leaf extract against urinary tract infection pathogen. Resource-Efficient Technologies 3 (4), 459–465.
Sara, L.M., Thomas, K., Nicola, H., Olena, P., Carsten, F., Martin, B., Constanca, F., Birgit, G., Oleksandr, G., 2020. Human Amniotic Membrane: a review on tissue engineering, application, and storage. J. Biomed. Mater. Res. B Appl. Biomater.
Sargazi, G., Afzali, D., Mostafavi, A., Shadman, A., Rezaee, B., Zarrintaj, P., Saeb, M.R., Ramakrishna, S., Mozafari, M., 2019. Chitosan/polyvinyl alcohol nanofibrous membranes: towards green super-adsorbents for toxic gases. Heliyon 5 (4), e01527.
Saxena, A., Tripathi, B.P., Kumar, M., Shahi, V.K., 2009. Membrane-based techniques for the separation and purification of proteins: an overview. Adv. Colloid Interface Sci. 145 (1–2), 1–22.
Schwenzer, B., Zhang, J., Kim, S., Li, L., Liu, J., Yang, Z., 2011. Membrane development for vanadium redox flow batteries. ChemSusChem 4 (10), 1388–1406.
Seetharaman, P., Chandrasekaran, R., Gnanasekar, S., Mani, I., Sivaperumal, S., 2017. Biogenic gold nanoparticles synthesized using Crescentia cujete L. and evaluation of their different biological activities. Biocatal. Agric. Biotechnol. 11, 75–82.
Seidi, F., Yazdi, M.K., Jouyandeh, M., Dominic, M., Naeim, H., Nezhad, M.N., Bagheri, B., Habibzadeh, S., Zarrintaj, P., Saeb, M.R., 2021. Chitosan-based blends for biomedical applications. Int. J. Biol. Macromol. 183, 1818–1850.
Senthil, B., Devasena, T., Prakash, B., Rajasekar, A., 2017. Non-cytotoxic effect of green synthesized silver nanoparticles and its antibacterial activity. J. Photochem. Photobiol. B Biol. 177, 1–7.
Seol, J.-H., Won, J.-H., Lee, M.-S., Yoon, K.-S., Hong, Y.T., Lee, S.-Y., 2012. A proton conductive silicate-nanoencapsulated polyimide nonwoven as a novel porous substrate for a reinforced sulfonated poly (arylene ether sulfone) composite membrane. J. Mater. Chem. 22 (4), 1634–1642.
Shaari, N., Kamarudin, S., 2015. Chitosan and alginate types of bio-membrane in fuel cell application: an overview. J. Power Sources 289, 71–80.
Shalumon, K., Sathish, D., Nair, S., Chennazhi, K., Tamura, H., Jayakumar, R., 2012. Fabrication of aligned poly (lactic acid)-chitosan nanofibers by novel parallel blade collector method for skin tissue engineering. J. Biomed. Nanotechnol. 8 (3), 405–416.
Shanker, U., Jassal, V., Rani, M., 2017. Green synthesis of iron hexacyanoferrate nanoparticles: potential candidate for the degradation of toxic PAHs. J. Environ. Chem. Eng. 5 (4), 4108–4120.
Sharma, D., Rajput, J., Kaith, B., Kaur, M., Sharma, S., 2010. Synthesis of ZnO nanoparticles and study of their antibacterial and antifungal properties. Thin Solid Films 519 (3), 1224–1229.
Sharma, M., Behl, K., Nigam, S., Joshi, M., 2018a. TiO2-GO nanocomposite for photocatalysis and environmental applications: a green synthesis approach. Vacuum 156, 434–439.
Sharma, K., Maiti, K., Kim, N.H., Hui, D., Lee, J.H., 2018b. Green synthesis of glucose-reduced graphene oxide supported Ag-Cu2O nanocomposites for the enhanced visible-light photocatalytic activity. Compos. B Eng. 138, 35–44.
Sharma, R., Verma, N., Lugani, Y., Kumar, S., Asadnia, M., 2021. Conventional and advanced techniques of wastewater monitoring and treatment. In: Green Sustainable Process for Chemical and Environmental Engineering and Science. Elsevier, pp. 1–48.
Shen, K., Cheng, C., Zhang, T., Wang, X., 2019. High performance polyamide composite nanofiltration membranes via reverse interfacial polymerization with the synergistic interaction of gelatin interlayer and trimesoyl chloride. J. Membr. Sci. 588, 117192.
Shi, G.M., Yang, T., Chung, T.S., 2012. Polybenzimidazole (PBI)/zeolitic imidazolate frameworks (ZIF-8) mixed matrix membranes for pervaporation dehydration of alcohols. J. Membr. Sci. 415, 577–586.
Shi, H., He, Y., Pan, Y., Di, H., Zeng, G., Zhang, L., Zhang, C., 2016. A modified mussel-inspired method to fabricate TiO2 decorated superhydrophilic PVDF membrane for oil/water separation. J. Membr. Sci. 506, 60–70.
Shinde, D.B., Cao, L., Wonanke, A.D., Li, X., Kumar, S., Liu, X., Hedhili, M.N., Emwas, A.-H., Addicoat, M., Huang, K.-W., 2020. Pore engineering of ultrathin covalent organic framework membranes for organic solvent nanofiltration and molecular sieving. Chem. Sci. 11 (21), 5434–5440.
Shirazi, Y., Ghadimi, A., Mohammadi, T., 2012. Recovery of alcohols from water using polydimethylsiloxane–silica nanocomposite membranes: characterization and pervaporation performance. J. Appl. Polym. Sci. 124 (4), 2871–2882.
Shivalingam, C., Mohan, L., Ganapathy, D., Shanmugam, R., Pitchiah, S., Ramadoss, R., Sundramoorthy, A.K., 2022. Current overview on the role of nanoparticles in water desalination technology. Curr. Anal. Chem. 18 (9), 989–998.
Singh, S., Kumar, V., Romero, R., Sharma, K., Singh, J., 2019. Applications of nanoparticles in wastewater treatment. In: Nanobiotechnology in Bioformulations. Springer, pp. 395–418.
Sivachidambaram, M., Vijaya, J.J., Kaviyarasu, K., Kennedy, L.J., Al-Lohedan, H.A., Ramalingam, R.J., 2017. A novel synthesis protocol for Co 3 O 4 nanocatalysts and their catalytic applications. RSC Adv. 7 (62), 38861–38870.
Sivanesan, I., Gopal, J., Muthu, M., Shin, J., Mari, S., Oh, J., 2021. Green synthesized chitosan/chitosan nanoforms/nanocomposites for drug delivery applications. Polymers 13 (14), 2256.
Solomon, M.F.J., Bhole, Y., Livingston, A.G., 2012. High flux membranes for organic solvent nanofiltration (OSN)—interfacial polymerization with solvent activation. J. Membr. Sci. 423, 371–382.
Soltani, R., Pelalak, R., Pishnamazi, M., Marjani, A., Shirazian, S., 2021a. A water-stable functionalized NiCo-LDH/MOF nanocomposite: green synthesis, characterization, and its environmental application for heavy metals adsorption. Arab. J. Chem. 14 (4), 103052.
Soltani, R., Pelalak, R., Pishnamazi, M., Marjani, A., Albadarin, A.B., Sarkar, S.M., Shirazian, S., 2021b. A novel and facile green synthesis method to prepare LDH/MOF nanocomposite for removal of Cd (II) and Pb (II). Sci. Rep. 11 (1), 1–15.
Sorribas, S., Kudasheva, A., Almendro, E., Zornoza, B., de la Iglesia, Ó., Téllez, C., Coronas, J., 2015. Pervaporation and membrane reactor performance of polyimide based mixed matrix membranes containing MOF HKUST-1. Chem. Eng. Sci. 124, 37–44.
Sravanthi, K., Ayodhya, D., Swamy, P.Y., 2018. Green synthesis, characterization of biomaterial-supported zero-valent iron nanoparticles for contaminated water treatment. Journal of Analytical Science and Technology 9 (1), 3.
Su, W., Li, H., Chen, W., Qin, J., 2019a. Microfluidic strategies for label-free exosomes isolation and analysis. TrAC, Trends Anal. Chem. 118, 686–698.
Su, J., Satchell, S.C., Wertheim, J.A., Shah, R.N., 2019b. Poly (ethylene glycol)-crosslinked gelatin hydrogel substrates with conjugated bioactive peptides influence endothelial cell behavior. Biomaterials 201, 99–112.
Subhapriya, S., Gomathipriya, P., 2018. Green synthesis of titanium dioxide (TiO2) nanoparticles by Trigonella foenum-graecum extract and its antimicrobial properties. Microb. Pathog. 116, 215–220.
Sudha, A., Jeyakanthan, J., Srinivasan, P., 2017. Green synthesis of silver nanoparticles using Lippia nodiflora aerial extract and evaluation of their antioxidant, antibacterial and cytotoxic effects. Resource-Efficient Technologies 3 (4), 506–515.
Suhas, D.P., Aminabhavi, T.M., Raghu, A.V., 2014. Mixed matrix membranes of H-ZSM5-loaded poly (vinyl alcohol) used in pervaporation dehydration of alcohols: influence of silica/alumina ratio. Polym. Eng. Sci. 54 (8), 1774–1782.
Sukma, F.M., Çulfaz-Emecen, P.Z., 2018. Cellulose membranes for organic solvent nanofiltration. J. Membr. Sci. 545, 329–336.
Sun, H., Tang, B., Wu, P., 2018. Hydrophilic hollow zeolitic imidazolate framework-8 modified ultrafiltration membranes with significantly enhanced water separation properties. J. Membr. Sci. 551, 283–293.
Suresh, J., Pradheesh, G., Alexramani, V., Sundrarajan, M., Hong, S.I., 2018. Green synthesis and characterization of zinc oxide nanoparticle using insulin plant (Costus pictus D. Don) and investigation of its antimicrobial as well as anticancer activities. Adv. Nat. Sci. Nanosci. Nanotechnol. 9 (1), 015008.
Sureshkumar, M., Siswanto, D.Y., Lee, C.-K., 2010. Magnetic antimicrobial nanocomposite based on bacterial cellulose and silver nanoparticles. J. Mater. Chem. 20 (33), 6948–6955.
Székely, G., Valtcheva, I.B., Kim, J.F., Livingston, A.G., 2015. Molecularly imprinted organic solvent nanofiltration membranes–Revealing molecular recognition and solute rejection behaviour. React. Funct. Polym. 86, 215–224.
Tabani, H., Asadi, S., Nojavan, S., Parsa, M., 2017. Introduction of agarose gel as a green membrane in electromembrane extraction: an efficient procedure for the extraction of basic drugs with a wide range of polarities. J. Chromatogr. A 1497, 47–55.
Tabani, H., Nojavan, S., Alexovič, M., Sabo, J., 2018. Recent developments in green membrane-based extraction techniques for pharmaceutical and biomedical analysis. J. Pharmaceut. Biomed. Anal. 160, 244–267.
Tabani, H., Dorabadizare, F., Pedersen-Bjergaard, S., 2023. Gel electro-membrane extraction: an overview on recent strategies for extraction efficiency enhancement. TrAC, Trends Anal. Chem., 116990
Taghizadeh, M., Taghizadeh, A., Vatanpour, V., Ganjali, M.R., Saeb, M.R., 2020. Deep eutectic solvents in membrane science and technology: fundamental, preparation, application, and future perspective. Separ. Purif. Technol., 118015
Tang, S., Zheng, J., 2018. Antibacterial activity of silver nanoparticles: structural effects. Advanced healthcare materials 7 (13), 1701503.
Toyao, T., Saito, M., Horiuchi, Y., Mochizuki, K., Iwata, M., Higashimura, H., Matsuoka, M., 2013. Efficient hydrogen production and photocatalytic reduction of nitrobenzene over a visible-light-responsive metal–organic framework photocatalyst. Catal. Sci. Technol. 3 (8), 2092–2097.
Tres, M.V., Mohr, S., Corazza, M.L., Di Luccio, M., Oliveira, J.V., 2009. Separation of n-butane from soybean oil mixtures using membrane processes. J. Membr. Sci. 333 (1–2), 141–146.
Ulubayram, K., Calamak, S., Shahbazi, R., Eroglu, I., 2015. Nanofibers based antibacterial drug design, delivery and applications. Curr. Pharmaceut. Des. 21 (15), 1930–1943.
Van Meer, G., Voelker, D.R., Feigenson, G.W., 2008. Membrane lipids: where they are and how they behave. Nat. Rev. Mol. Cell Biol. 9 (2), 112–124.
Vatanpour, V., Mansourpanah, Y., Khadem, S.S.M., Zinadini, S., Dizge, N., Ganjali, M.R., Mirsadeghi, S., Rezapour, M., Saeb, M.R., Karimi-Male, H., 2021. Nanostructured polyethersulfone nanocomposite membranes for dual protein and dye separation: lower antifouling with lanthanum (III) vanadate nanosheets as a novel nanofiller. Polym. Test. 94, 107040.

Vazquez-Muñoz, R., Meza-Villezcas, A., Fournier, P., Soria-Castro, E., Juarez-Moreno, K., Gallego-Hernández, A., Bogdanchikova, N., Vazquez-Duhalt, R., Huerta-Saquero, A., 2019. Enhancement of antibiotics antimicrobial activity due to the silver nanoparticles impact on the cell membrane. PLoS One 14 (11), e0224904.
Vedadghavami, A., Minoei, F., Hosseini, S.S., 2018. Practical techniques for improving the performance of polymeric membranes and processes for protein separation and purification. Iran. J. Chem. Chem. Eng. (Int. Engl. Ed.) 37 (2), 1–23.
Verma, N., Sharma, R., 2017. Bioremediation of toxic heavy metals: a patent review. Recent Pat. Biotechnol. 11 (3), 171–187.
Verma, N., Sharma, R., Asadnia, M., 2021. Role of quantum dots in separation processes. In: Quantum Dots – Properties and Applications, Inamuddin Ed. Materials Research Foundations, pp. 251–279.
Vijayakumar, S., Mahadevan, S., Arulmozhi, P., Sriram, S., Praseetha, P., 2018. Green synthesis of zinc oxide nanoparticles using Atalantia monophylla leaf extracts: characterization and antimicrobial analysis. Mater. Sci. Semicond. Process. 82, 39–45.
Voros, V., Drioli, E., Fonte, C., Szekely, G., 2019. Process intensification via continuous and simultaneous isolation of antioxidants: an upcycling approach for olive leaf waste. ACS Sustain. Chem. Eng. 7 (22), 18444–18452.
Wang, T., Ji, X., Jin, L., Feng, Z., Wu, J., Zheng, J., Wang, H., Xu, Z.-W., Guo, L., He, N., 2013. Fabrication and characterization of heparin-grafted poly-L-lactic acid–chitosan core–shell nanofibers scaffold for vascular gasket. ACS Appl. Mater. Interfaces 5 (9), 3757–3763.
Wang, Q., Zhang, J., Pi, Z., Zheng, Z., Xing, J., Song, F., Liu, S., Liu, Z., 2015. Application of online microdialysis coupled with liquid chromatography-tandem mass spectrometry method in assessing neuroprotective effect of Rhizoma coptidis on diabetic rats. Anal. Methods 7 (1), 45–52.
Wang, K., Tao, X., Xu, J., Yin, N., 2016. Novel chitosan–MOF composite adsorbent for the removal of heavy metal ions. Chem. Lett. 45 (12), 1365–1368.
Wang, L., Wu, Y., Xie, J., Wu, S., Wu, Z., 2018. Characterization, antioxidant and antimicrobial activities of green synthesized silver nanoparticles from Psidium guajava L. leaf aqueous extracts. Mater. Sci. Eng. C 86, 1–8.
Wang, X., Liu, W., Fu, H., Yi, X.-H., Wang, P., Zhao, C., Wang, C.-C., Zheng, W., 2019a. Simultaneous Cr (VI) reduction and Cr (III) removal of bifunctional MOF/Titanate nanotube composites. Environ. Pollut. 249, 502–511.
Wang, H., Zeng, Z., Xu, P., Li, L., Zeng, G., Xiao, R., Tang, Z., Huang, D., Tang, L., Lai, C., 2019b. Recent progress in covalent organic framework thin films: fabrications, applications and perspectives. Chem. Soc. Rev. 48 (2), 488–516.
Wang, H.H., Jung, J.T., Kim, J.F., Kim, S., Drioli, E., Lee, Y.M., 2019c. A novel green solvent alternative for polymeric membrane preparation via nonsolvent-induced phase separation (NIPS). J. Membr. Sci. 574, 44–54.
Wang, Y., He, L., Li, Y., Jing, L., Wang, J., Li, X., 2020a. Ag NPs supported on the magnetic Al-MOF/PDA as nanocatalyst for the removal of organic pollutants in water. J. Alloys Compd. 828, 154340.
Wang, C., Cheng, P., Yao, Y., Yamauchi, Y., Yan, X., Li, J., Na, J., 2020b. In-situ fabrication of nanoarchitectured MOF filter for water purification. J. Hazard Mater. 392, 122164.
Wang, R., Zhai, Q., An, T., Gong, S., Cheng, W., 2021. Stretchable gold fiber-based wearable textile electrochemical biosensor for lactate monitoring in sweat. Talanta 222, 121484.
Wang, Y., Wang, S., Wang, T., Song, T., Wu, X., Guo, L., Xie, W., Qiu, P., Dong, Q., Li, Q., 2023. A green nanocomposite membrane for concrete moisturizing, with excellent barrier properties and aging resistance. Mater. Today Commun. 35, 105553.
Weng, X., Guo, M., Luo, F., Chen, Z., 2017. One-step green synthesis of bimetallic Fe/Ni nanoparticles by eucalyptus leaf extract: biomolecules identification, characterization and catalytic activity. Chem. Eng. J. 308, 904–911.
Wetterhall, M., Bergquist, J., Hillered, L., Hjort, K., Dahlin, A.P., 2014. Identification of human cerebrospinal fluid proteins and their distribution in an in vitro microdialysis sampling system. Eur. J. Pharmaceut. Sci. 57, 34–40.
Wongpreecha, J., Polpanich, D., Suteewong, T., Kaewsaneha, C., Tangboriboonrat, P., 2018. One-pot, large-scale green synthesis of silver nanoparticles-chitosan with enhanced antibacterial activity and low cytotoxicity. Carbohydr. Polym. 199, 641–648.
Wu, Z., Su, X., Lin, Z., Owens, G., Chen, Z., 2019a. Mechanism of as (V) removal by green synthesized iron nanoparticles. J. Hazard Mater. 379, 120811.
Wu, Q., Tiraferri, A., Wu, H., Xie, W., Liu, B., 2019b. Improving the performance of PVDF/PVDF-g-PEGMA ultrafiltration membranes by partial solvent substitution with green solvent dimethyl sulfoxide during fabrication. ACS Omega 4 (22), 19799–19807.
Xia, Q.-C., Yang, W.-J., Fan, F., Ji, M., Wang, Y., Wang, Z.-Y., Cao, X.-L., Xing, W., Sun, S.-P., 2020. Encapsulated polyethyleneimine enables synchronous nanostructure construction and in situ functionalization of nanofiltration membranes. Nano Lett. 20 (11), 8185–8192.
Xiao, J.-L., Sun, S.-Y., Song, X., Li, P., Yu, J.-G., 2015. Lithium ion recovery from brine using granulated polyacrylamide–MnO2 ion-sieve. Chem. Eng. J. 279, 659–666.
Xie, W., Li, T., Chen, C., Wu, H., Liang, S., Chang, H., Liu, B., Drioli, E., Wang, Q., Crittenden, J.C., 2019. Using the green solvent dimethyl sulfoxide to replace traditional solvents partly and fabricating PVC/PVC-g-PEGMA blended ultrafiltration membranes with high permeability and rejection. Ind. Eng. Chem. Res. 58 (16), 6413–6423.
Xie, W., Li, T., Tiraferri, A., Drioli, E., Figoli, A., Crittenden, J.C., Liu, B., 2020. Toward the next generation of sustainable membranes from green chemistry principles. ACS Sustain. Chem. Eng.
Xing, D.Y., Peng, N., Chung, T.-S., 2010. Formation of cellulose acetate membranes via phase inversion using ionic liquid,[BMIM] SCN, as the solvent. Ind. Eng. Chem. Res. 49 (18), 8761–8769.
Xu, T., Yang, H., Yang, D., Yu, Z.-Z., 2017. Polylactic acid nanofiber scaffold decorated with chitosan islandlike topography for bone tissue engineering. ACS Appl. Mater. Interfaces 9 (25), 21094–21104.
Xu, Y., Xiao, Y., Zhang, W., Lin, H., Shen, L., Li, R., Jiao, Y., Liao, B.-Q., 2021. Plant polyphenol intermediated metal-organic framework (MOF) membranes for efficient desalination. J. Membr. Sci. 618, 118726.
Yan, H., Li, J., Fan, H., Ji, S., Zhang, G., Zhang, Z., 2015. Sonication-enhanced in situ assembly of organic/inorganic hybrid membranes: evolution of nanoparticle distribution and pervaporation performance. J. Membr. Sci. 481, 94–105.
Yang, W., Wang, J., Yang, Q., Pei, H., Hu, N., Suo, Y., Li, Z., Zhang, D., Wang, J., 2018. Facile fabrication of robust MOF membranes on cloth via a CMC macromolecule bridge for highly efficient Pb (II) removal. Chem. Eng. J. 339, 230–239.
Yaqoob, A.A., Parveen, T., Umar, K., Mohamad Ibrahim, M.N., 2020. Role of nanomaterials in the treatment of wastewater: a review. Water 12 (2), 495.
Yazdi, M.E.T., Amiri, M.S., Akbari, S., Sharifalhoseini, M., Nourbakhsh, F., Mashreghi, M., Abbasi, M.R., Modarres, M., Es-haghi, A., 2020a. Green synthesis of silver nanoparticles using helichrysum graveolens for biomedical applications and wastewater treatment. BioNanoScience 10 (4), 1121–1127.
Yazdi, M.K., Vatanpour, V., Taghizadeh, A., Taghizadeh, M., Ganjali, M.R., Munir, M.T., Habibzadeh, S., Saeb, M.R., Ghaedi, M., 2020b. Hydrogel membranes: a review. Mater. Sci. Eng. C 114, 111023.
Ye, Y., Zhang, D., Li, J., Liu, T., Pu, J., Zhao, H., Wang, L., 2019. One-step synthesis of superhydrophobic polyhedral oligomeric silsesquioxane-graphene oxide and its application in anti-corrosion and anti-wear fields. Corrosion Sci. 147, 9–21.
Yi, Y., Tu, G., Tsang, P.E., Xiao, S., Fang, Z., 2019. Green synthesis of iron-based nanoparticles from extracts of Nephrolepis auriculata and applications for Cr (VI) removal. Mater. Lett. 234, 388–391.
Yin, I.X., Zhang, J., Zhao, I.S., Mei, M.L., Li, Q., Chu, C.H., 2020a. The antibacterial mechanism of silver nanoparticles and its application in dentistry. Int. J. Nanomed. 2555–2562.
Yin, B., Sun, L., Tang, S., Zhou, H., 2020b. Preparation of metal–organic framework/polyvinylidene fluoride mixed matrix membranes for water treatment. Ind. Eng. Chem. Res. 59 (44), 19689–19697.
Yuan, G., Tu, H., Liu, J., Zhao, C., Liao, J., Yang, Y., Yang, J., Liu, N., 2018. A novel ion-imprinted polymer induced by the glycylglycine modified metal-organic framework for the selective removal of Co (II) from aqueous solutions. Chem. Eng. J. 333, 280–288.
Yuan, G., Tian, Y., Li, M., Zeng, Y., Tu, H., Liao, J., Yang, J., Yang, Y., Liu, N., 2019. Removal of Co (II) from aqueous solution with functionalized metal–organic frameworks (MOFs) composite. J. Radioanal. Nucl. Chem. 322 (2), 827–838.
Yunas, J., Mulyanti, B., Hamidah, I., Mohd Said, M., Pawinanto, R.E., Wan Ali, W.A.F., Subandi, A., Hamzah, A.A., Latif, R., Yeop Majlis, B., 2020. Polymer-based MEMS electromagnetic actuator for biomedical application: a review. Polymers 12 (5), 1184.
Yusuf, M., 2019. Silver nanoparticles: synthesis and applications. Handbook of Ecomaterials 2343.
Zare, M., Namratha, K., Alghamdi, S., Mohammad, Y.H.E., Hezam, A., Zare, M., Drmosh, Q.A., Byrappa, K., Chandrashekar, B.N., Ramakrishna, S., 2019. Novel green biomimetic approach for synthesis of ZnO-Ag nanocomposite; antimicrobial activity against food-borne pathogen, biocompatibility and solar photocatalysis. Sci. Rep. 9 (1), 1–15.
Zarei, F., Marjani, A., Soltani, R., 2019. Novel and green nanocomposite-based adsorbents from functionalised mesoporous KCC-1 and chitosan-oleic acid for adsorption of Pb (II). Eur. Polym. J. 119, 400–409.
Zarrintaj, P., Manouchehri, S., Ahmadi, Z., Saeb, M.R., Urbanska, A.M., Kaplan, D.L., Mozafari, M., 2018. Agarose-based biomaterials for tissue engineering. Carbohydr. Polym. 187, 66–84.
Zayan, S., Elshazly, A., Elkady, M., 2020. In situ polymerization of polypyrrole@ aluminum fumarate metal–organic framework hybrid nanocomposites for the application of wastewater treatment. Polymers 12 (8), 1764.
Zeng, J., Lv, C., Liu, G., Zhang, Z., Dong, Z., Liu, J., Wang, Y., 2019. A novel ion-imprinted membrane induced by amphiphilic block copolymer for selective separation of Pt (IV) from aqueous solutions. J. Membr. Sci. 572, 428–441.
Zeng, J., Zeng, J., Zhou, H., Liu, G., Yuan, Z., Jian, J., 2020. Ion-imprinted silica gel and its dynamic membrane for nickel ion removal from wastewaters. Front. Chem. Sci. Eng. 1–11.
Zhang, C., Wei, K., Zhang, W., Bai, Y., Sun, Y., Gu, J., 2017. Graphene oxide quantum dots incorporated into a thin film nanocomposite membrane with high flux and antifouling properties for low-pressure nanofiltration. ACS Appl. Mater. Interfaces 9 (12), 11082–11094.
Zhang, Z., Wen, L., Jiang, L., 2018. Bioinspired smart asymmetric nanochannel membranes. Chem. Soc. Rev. 47 (2), 322–356.
Zhang, Y., Ye, L., Zhang, B., Chen, Y., Zhao, W., Yang, G., Wang, J., Zhang, H., 2019. Characteristics and performance of PVDF membrane prepared by using NaCl coagulation bath: relationship between membrane polymorphous structure and organic fouling. J. Membr. Sci. 579, 22–32.
Zhang, Y., Cheng, X., Jiang, X., Urban, J.J., Lau, C.H., Liu, S., Shao, L., 2020. Robust natural nanocomposites realizing unprecedented ultrafast precise molecular separations. Mater. Today 36, 40–47.
Zhao, D., Kim, J.F., Ignacz, G., Pogany, P., Lee, Y.M., Szekely, G., 2019. Bio-inspired robust membranes nanoengineered from interpenetrating polymer networks of polybenzimidazole/polydopamine. ACS Nano 13 (1), 125–133.
Zhao, X., Gao, W., Zhang, H., Qiu, X., Luo, Y., 2020. Graphene quantum dots in biomedical applications: recent advances and future challenges. Handbook of nanomaterials in analytical chemistry 493–505.

Zhao, Y., Yang, X., Yan, L., Bai, Y., Li, S., Sorokin, P., Shao, L., 2021. Biomimetic nanoparticle-engineered superwettable membranes for efficient oil/water separation. J. Membr. Sci. 618, 118525.
Zheng, X., Zhang, Y., Zhang, F., Li, Z., Yan, Y., 2018. Dual-template docking oriented ionic imprinted bilayer mesoporous films with efficient recovery of neodymium and dysprosium. J. Hazard Mater. 353, 496–504.
Zheng, X., Zhang, Y., Bian, T., Zhang, Y., Zhang, F., Yan, Y., 2019. Selective extraction of gadolinium using free-standing imprinted mesoporous carboxymethyl chitosan films with high capacity. Cellulose 26 (2), 1209–1219.
Zhu, Z., Si, T., Xu, R.X., 2015. Microencapsulation of indocyanine green for potential applications in image-guided drug delivery. Lab Chip 15 (3), 646–649.
Zhu, W., Lei, J., Li, Y., Dai, L., Chen, T., Bai, X., Wang, L., Duan, T., 2019a. Procedural growth of fungal hyphae/Fe3O4/graphene oxide as ordered-structure composites for water purification. Chem. Eng. J. 355, 777–783.
Zhu, M., Xiong, R., Huang, C., 2019b. Bio-based and photocrosslinked electrospun antibacterial nanofibrous membranes for air filtration. Carbohydr. Polym. 205, 55–62.
Zodrow, K., Brunet, L., Mahendra, S., Li, D., Zhang, A., Li, Q., Alvarez, P.J., 2009. Polysulfone ultrafiltration membranes impregnated with silver nanoparticles show improved biofouling resistance and virus removal. Water Res. 43 (3), 715–723.